

DESIGN AND OPTIMIZATION OF COMPACT ON-METAL
ULTRA HIGH FREQUENCY RFID TAG ANTENNAS

CHIANG SHAO MING

MASTER OF ENGINEERING SCIENCE

LEE KONG CHIAN FACULTY OF ENGINEERING AND
SCIENCE
UNIVERSITI TUNKU ABDUL RAHMAN
SEPTEMBER 2021

**DESIGN AND OPTIMIZATION OF COMPACT ON-METAL
ULTRA HIGH FREQUENCY RFID TAG ANTENNAS**

By

CHIANG SHAO MING

A dissertation submitted to the Institute of Postgraduate Studies and Research,
Lee Kong Chian Faculty of Engineering and Science,
Universiti Tunku Abdul Rahman,
in partial fulfillment of the requirements for the degree of Master of
Engineering Science
September 2021

ABSTRACT

Design and Optimization of Compact on-metal Ultra High Frequency RFID Tag Antennas

Chiang Shao Ming

In this dissertation, two compact UHF RFID tag antennas have been proposed for metal-mountable applications. Lumped components have been incorporated into the flexible tag antenna structures for achieving tuning flexibility in a broad range. The dipolar patch antenna has been selected for both the tag designs. In the first project, the concept of inductive channel is introduced for tuning the resonant frequency of a bowtie dipolar tag antenna, which has a compact physical size of $50 \text{ mm} \times 50 \text{ mm} \times 3.38 \text{ mm}$ ($0.1447\lambda \times 0.1447\lambda \times 0.0098\lambda$), for applying on metal surfaces. The narrow inductive channel, which is embedded with an external lumped inductor, is loaded on top of the dipolar antenna for achieving arbitrary tuning capability in a broad range. It has been found that the top-loading patch can enhance the fields of the dipole, and the inductive channel can regulate the current flows on the top-loading patch. By adjusting the channel width as well as the external inductance, the resonant frequency can be effectively adjusted without affecting the read performances of the tag much. Here, an equivalent circuit has also been constructed for analyzing the impedance characteristics of the proposed tag antenna. The proposed tag antenna can achieve a measured maximum reading distance of nearly 19 m at an effective isotropic radiated power of 3.28 W. It can be arbitrarily tuned to operate at any frequency in the UHF band by simply adjusting the lumped inductor's value,

without changing the antenna structure. The proposed antenna is found to be insensitive to variation in the backing metal plate, and its operating frequency does not fluctuate with the plate size. In the second project, a novel UHF RFID tag antenna, which has a compact physical size of $35 \text{ mm} \times 30 \text{ mm} \times 3.118 \text{ mm}$ ($0.107\lambda \times 0.092\lambda \times 0.0095\lambda$), is proposed for metal mountable applications. The tag structure itself is designed using a pair of dipolar patches that are being fed by two T-shaped feedlines. Here, one pair of lumped capacitors are inserted across the narrow gap between the patches for introducing additional capacitance to bring down the resonant frequency and miniaturize the antenna size. The proposed tag antenna has a simple structure and it can be made on the single surface of a flexible PET substrate. Also, the tag resonant frequency can be easily tuned by adjusting the lumped capacitances. Experimental results show that the proposed tag antenna can achieve a far read distance of 11.1 m when it is placed on a metal plate, being tested with an effective isotropic radiated power of 3.28 W. Even though the tag size is small, it can still maintain good read performance. For both the projects, it has been demonstrated that lumped components can be introduced into the antenna structures for providing additional reactance for miniaturizing the antenna size. By adjusting the values of the lumped components, the resonant frequency of the proposed tag antennas can be arbitrarily. With the introduction of the external lumped components, the antenna structures of the proposed tag antennas can be kept intact without the need of modification for achieving frequency, as a result, the Q -factor of the antennas can be maintained for achieving high radiation efficiencies. All of the proposed tag antennas have been simulated and analyzed. Experiments have also been conducted to prove the working principles. Good agreement is found between

the simulation and measurement.

ACKNOWLEDGEMENTS

First of all, I would like to express my sincere gratitude to my supervisor, Prof. Ts. Dr. Lim Eng Hock, and co-supervisor, Dr. Chee Pei Song for providing their guidance and support so that I can have an in-depth understanding of antenna theory and complete my research projects on time.

Next, I would like to thank Dr. Lee Yong Hong and Dr. Bong Fwee Leong for solving my problems and providing technical assistance so that I was able to become familiar with all aspects of tag design more rapidly. Besides, I would also like to thank the seniors and friends of the research group for sharing their valuable personal experiences.

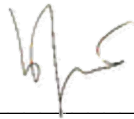
Special thanks to the Taiwanese company, SAG (SECUTITAG ASSEMBLY GROUP), for providing me with the opportunity to obtain a master's degree in engineering, and for funding this research project. I am very grateful to Mr. Peter Yan and Mr. Sam Liang for providing technical support at SAG to make the research smoother. I would also like to express my greatest gratitude to UTAR for providing me with research resources to realize my research project.

Thanks again to the research supervisor, Prof. Ts. Dr. Lim Eng Hock, for his meticulous care and encouragements, when I went to study abroad alone. Finally, I would like to thank my family for their support and consistent love, which has allowed me to venture abroad.

APPROVAL SHEET

This dissertation entitled “**DESIGN AND OPTIMIZATION OF COMPACT ON-METAL ULTRA HIGH FREQUENCY RFID TAG ANTENNAS**” was prepared by CHIANG SHAO MING and submitted as partial fulfillment of the requirement for the degree of Master of Engineering Science at Universiti Tunku Abdul Rahman.

Approved by:



(Prof. Ts. Dr. Lim Eng Hock)

Date: 11 Oct 2021

Supervisor

Department of Electrical and Electronic Engineering
Lee Kong Chian Faculty of Engineering and Science
Universiti Tunku Abdul Rahman



(Dr. Chee Pei Song)

Date: 11 Oct 2021

Co-supervisor

Department of Mechatronics and Biomedical Engineering
Lee Kong Chian Faculty of Engineering and Science
Universiti Tunku Abdul Rahman

LEE KONG CHIAN FACULTY OF ENGINEERING AND SCIENCE
UNIVERSITI TUNKU ABDUL RAHMAN

Date: 27 Sept. 2021

SUBMISSION OF DISSERTATION

It is hereby certified that **CHIANG SHAO MING** (ID No: **20UEM00187**) has completed this dissertation entitled “**DESIGN AND OPTIMIZATION OF COMPACT ON-METAL ULTRA HIGH FREQUENCY RFID TAG ANTENNAS**” under the supervision of Prof. Ts. Dr. Lim Eng Hock (Supervisor) from the Department of Electrical and Electronic Engineering, Lee Kong Chian Faculty of Engineering and Science (FES), and Dr. Chee Pei Song (Co-Supervisor) from the Department of Mechatronics and Biomedical Engineering, Lee Kong Chian Faculty of Engineering and Science (FES).

I understand that University will upload softcopy of my dissertation in pdf format into UTAR Institutional Repository, which may be made accessible to UTAR community and public.

Yours truly,

Chiang Shao Ming

(CHIANG SHAO MING)

DECLARATION

I hereby declare that the dissertation is based on my original work except for citations and quotations which have been duly acknowledged. I also declare that it has not been previously and concurrently submitted for any other degree or award at UTAR or other institutions.

Chiang Shao Ming

(CHIANG SHAO MING)

Date: *11 Oct, 2021*

TABLE OF CONTENTS

	Page
ABSTRACT	ii
ACKNOWLEDGEMENTS	ii
APPROVAL SHEET	vi
SUBMISSION OF DISSERTATION	vii
DECLARATION	viii
LIST OF TABLES	xi
LIST OF FIGURES	xii
LIST OF ABBREVIATIONS	xix
CHAPTER	
1 INTRODUCTION	1
1.1 Background	1
1.2 Working Principle of RFID System	4
1.3 Types of RFID Tag	6
1.4 Spectrum of RFID Systems	8
1.5 Problem Statements	11
1.6 Objectives	12
1.7 Dissertation Outline	13
2 LITERATURE REVIEW AND METHODOLOGY	39
2.1 Introduction	39
2.2 Passive Metal-Mountable UHF RFID Tag Antennas	40
2.2.1 Conventional Dipole Antenna	40
2.2.2 Separation of Antennas by Air Layers	41
2.2.3 Planar Antenna with FSS/AMC/EBG Structure	43
2.2.4 Planar Inverted Antenna	45
2.2.5 Folded-patch Antenna	47
2.3 Miniaturization Techniques for UHF RFID Tag Antenna	48

2.3.1	Meandering	48
2.3.2	Meandered Slotlines/Slotting on Radiator	50
2.3.3	Shorting Elements	52
2.3.4	High Dielectric Substrate	54
2.4	Impedance Matching	56
2.5	Research Methodology	57
2.6	Measurement Process of UHF RFID Tag Antenna	61
3	DIPOLAR TAG ANTENNA WITH A TOP-LOADING INDUCTIVE CHANNEL WITH BROADRANGE FREQUENCY TUNING CAPABILITY	65
3.1	Introduction	65
3.2	Configuration and Design Procedure	68
3.3	Equivalent Circuit Model and Parametric Analysis	76
3.4	Results and Discussion	83
3.5	Conclusion	95
4	CAPACITORS-LOADED DIPOLAR PATCH ANTENNA FOR UHF TAG MINIATURIZATION	96
4.1	Introduction	96
4.2	Antenna Configuration and Design Process	98
4.3	Parametric Analysis	103
4.4	Results and Discussion	112
4.5	Conclusion	123
5	SUMMARY AND DISCUSSION	125
5.1	Summary	125
5.2	Future Works	127
6	REFERENCES	128

LIST OF TABLES

Table		Page
Table 1.1:	Comparison of Barcode and RFID systems.	4
Table 1.2:	Comparison of radio frequency ranges and characteristics of different RFID systems.	10
Table 3.1:	Optimized parameters of the proposed design.	70
Table 3.2:	Parameters of the proposed equivalent circuit model.	78
Table 3.3:	Comparison of UHF tag antennas made of dipolar patch.	94
Table 4.1:	Optimized parameters of the proposed design.	99
Table 4.2:	Tuning sensitivity of the design parameters.	112
Table 4.3:	Comparison of other metal-mountable UHF tag antennas.	122

LIST OF FIGURES

Figure		Page
Figure 1.1:	Typical AIDC technologies.	3
Figure 1.2:	Architecture of the RFID system.	6
Figure 1.3:	Working principle of the RFID system.	6
Figure 1.4:	Operating spectrum of the RFID system.	9
Figure 1.5:	Spectrum distribution map of the world.	10
Figure 2.1:	Low-profile three-arm folded dipole antenna.	41
Figure 2.2:	(a) Top layer, (b) bottom layer, (c) lateral view of the broadband tag antenna with an air layer.	42
Figure 2.3:	Dipole antenna with AMC patch.	44
Figure 2.4:	The lateral and top view of the EBG structure.	44
Figure 2.5:	Structure of the dual PIFA array shown in (a) and (b).	46
Figure 2.6:	Inlay and prototype of the folded-patch antenna.	47
Figure 2.7:	Fabricated prototype of a meandered dipole.	49

Figure 2.8:	(a) Configuration of the meandered dipole. (b) Geometry of the meandered-loop antenna.	49
Figure 2.9:	Dipole patch antenna with meandered slotline.	50
Figure 2.10:	Dipole patch antenna with inductive slits and shorting vias.	51
Figure 2.11:	Flexible folded-patch antenna with serrated edges.	52
Figure 2.12:	Configuration of the RFID metal tag antenna with shorting vias.	53
Figure 2.13:	Structural configuration of the dual-layer antenna.	53
Figure 2.14:	(a) Configuration of the miniature coplanar-fed folded patch antenna, (b) Effects of stub width w_1 on resistance and reactance.	54
Figure 2.15:	(a) Prototype of the tag with a diameter of 34 mm and a thickness of 5 mm, (b) Prototype of the tag with a diameter of 32 mm and a thickness of 1.5 mm.	56
Figure 2.16:	Equivalent circuit model of the RFID tag antenna.	57
Figure 2.17:	Design process of the UHF RFID tag antenna.	60
Figure 2.18:	Setup of the UHF RFID measurement system.	64

Figure 2.19:	Actual measurement setup in anechoic cabinet.	64
Figure 3.1:	Configuration of the proposed tag antenna shown in (a) top view and (b) side view.	69
Figure 3.2:	Components of the prototype.	71
Figure 3.3:	Structural evolution of the antenna design. (a) <i>Configuration A</i> . (b) <i>Configuration B</i> . (c) <i>Configuration C</i> .	73
Figure 3.4:	Comparison of antenna impedances for (a) <i>Configuration A</i> and <i>Configuration B</i> . (b) <i>Configuration B</i> and <i>Configuration C</i> .	74
Figure 3.5:	Current distributions of (a) <i>Configuration A</i> and (b) <i>Configuration C</i> .	75
Figure 3.6:	Electric field distributions of (a) <i>Configuration A</i> and (b) <i>Configuration C</i> .	75
Figure 3.7:	Magnetic field distributions of (a) <i>Configuration A</i> and (b) <i>Configuration C</i> .	76
Figure 3.8:	Equivalent circuit model for the proposed tag antenna.	77
Figure 3.9:	Simulated and modeled input impedances of the proposed tag antenna.	79
Figure 3.10:	Effects of varying inductance L_p on the (a) power transmission coefficient, (b) input impedance.	81

Figure 3.11:	Effects of varying channel width w_c on the (a) power transmission coefficient, (b) input impedance.	82
Figure 3.12:	(a) The prototype is placed on the center of the metal plate. (b) Measurement setup in the anechoic cabinet.	84
Figure 3.13:	(a) Measured and simulated realized gains and the measured tag sensitivity when the tag is placed on a 20 cm \times 20 cm aluminium plate. (b) Measured realized gains when the inductive channel is loaded with a lumped inductor with different values.	86
Figure 3.14:	Plane definition for measuring the read patterns.	87
Figure 3.15:	Measured read patterns of the proposed tag antenna in the (a) xy -plane, (b) xz - and yz -planes at 868 MHz.	88
Figure 3.16:	Measured read distances of the proposed tag antenna on the metal plate with different (a) plate length L and (b) plate width W .	90
Figure 3.17:	Samples of different household containers (a) with the tag antenna mounted on the bottom, (b) with the tag antenna mounted on the body.	92
Figure 3.18:	Measured result of read distances for different household containers (a) with the	

	tag antenna mounted on the bottom, (b) with the tag antenna mounted on the body.	93
Figure 4.1:	(a) Antenna configuration. (b) Prototype of proposed tag antenna.	100
Figure 4.2:	Input impedances for the cases with and without the loading lumped capacitors.	101
Figure 4.3:	Current distributions for the case (a) without and (b) with the loading capacitors.	102
Figure 4.4:	Electric field distributions for the case (a) without and (b) with the loading lumped capacitors.	103
Figure 4.5:	Magnetic field distributions for the case (a) without and (b) with the loading lumped capacitors.	103
Figure 4.6:	Current distribution for the cases (a) without capacitor, (b) with single capacitor, and (c) with two capacitors in simulation.	105
Figure 4.7:	Antenna impedances for the cases in Fig. 4.6.	106
Figure 4.8:	Effects of varying capacitance C_l on the (a) power transmission coefficient, (b) input impedance.	107
Figure 4.9:	Electric field distributions for the case with the loading lumped capacitors.	108

Figure 4.10:	Effects of varying the gap width g_c on the (a) power transmission coefficient, (b) input impedance.	109
Figure 4.11:	Simulated current distribution on the stub.	110
Figure 4.12:	Effects of varying width of stubs s_w on the (a) power transmission coefficient, (b) input impedance.	111
Figure 4.13:	Measurement setup in the anechoic chamber.	113
Figure 4.14:	Measured and simulated realized gains and the measured tag sensitivity when the tag is placed on a 20 cm \times 20 cm aluminium plate.	114
Figure 4.15:	Plane definition for measuring the read distance and realized gain in anechoic chamber.	115
Figure 4.16:	Measured read patterns of the proposed tag antenna in the (a) xy -plane, (b) xz - and yz -planes at 910 MHz.	116
Figure 4.17:	Measured read distances of the proposed tag antenna on the metal plate with different (a) plate length L and (b) plate width W .	118
Figure 4.18:	Samples of different household containers (a) with the tag antenna mounted on the bottom, (b) with the tag antenna mounted on the body.	119

Figure 4.19: Measured read distances for different household containers (a) with the tag antenna mounted on the bottom, (b) with the tag antenna mounted on the body.

120

LIST OF ABBREVIATIONS

AIDC	Automatic Identification and Data Capture
AMC	Artificial Magnetic Conductor
EBG	Electromagnetic Bandgap
EIRP	Effective Isotropic Radiated Power
EM	Electromagnetic Wave
FSS	Frequency Selective Surface
HF	High Frequency
HIS	High Impedance Surface
LF	Low Frequency
LTCC	Low Temperature Co-fired Ceramic
OCR	Optical Character Recognition
PCB	Printed Circuit Board
PDMS	Polydimethylsiloxane
PET	Polyethylene Terephthalate
PIFA	Planar Inverted F Antenna

PMC	Perfect Magnetic Conductor
RFID	Radio Frequency IDentification
SMD	Surface Mount Device
TUT	Tag Under Test
UHF	Ultra-High Frequency

CHAPTER 1

INTRODUCTION

1.1 Background

In the information age, the collection and integration of data no longer require human involvement. Instead, the data can be captured by a computer system for analysis through the Automatic Identification and Data Capture (AIDC) methods (Smith and Offodile, 2002). Typical AIDC technologies include bar codes, radio frequency identification (RFID), biometrics (Jain et al., 2007), smart card, and optical character recognition (OCR), as shown in Figure 1.1. The popularity of the RFID systems has risen rapidly in the past two decades. Before this, commodity management was commonly used by the barcode system to read and collect data. Due to its low manufacturing cost, where the bar code can be simply printed on a piece of paper or plastic, the bar code system has been widely used in the retail industry. Despite its low cost, the barcode technology is still facing some problems, such as insufficient reading distance and poor data access capabilities. However, the gradual maturity of RFID technology has greatly improved the disadvantages of the traditional bar code systems. Table 1.1 summarizes the advantages of RFID over barcodes, which detailed analysis is given as follows:

- a) Electromagnetic energy is the communication medium for RFID. The Bar code system needs to read a barcode by line-of-sight (White et al., 2007) and use light as a medium for communication, which means that there can be no

obstacles between the scanner and the barcode, where the read distance is quite restricted. Besides, the barcode is usually placed on the surface of an object, which is susceptible to environmental pollution or physical damage, making the barcode label unable to be read in certain circumstances. On the other hand, the RFID uses radio waves to communicate, even if the tag is shielded, it can still be read effectively as long as it is within the range of interrogation area.

- b) RFID can have long distance reading and arbitrary orientation. Light sources such as infrared light is needed to sense a barcode and it must be aligned at a close distance to ensure that the light source of the scanner can focus on the barcode for scanning. On the other hand, the RFID tags use electromagnetic waves to return data to the reader. The read range depends on the radiation pattern of the tag antenna. Nowadays, most RFID tags have no limit on the reading direction and can reach at least 3 meters.
- c) The RFID has excellent access characteristics. Since the RFID tag has its microchip, the data storage capacity is relatively much larger than the bar code, and the tag can be read and written at the same time. The two-dimensional bar code only provides the relevant binary code to identify the information, and the editing of the data can only be modified by the back-end computer system. The real-time data cannot be stored in a barcode.
- d) A barcode has to be aligned with the scanner and it can only be read one at a time. In contrast, RFID has a very high data transmission rate, even when multiple tags are crossing into the interrogation area, all of them can be identified and accessed at the same time. This provides real-time updates of data, thereby improving overall data visibility.

Combining the advantages, in recent years, the RFID systems have been used in various fields such as logistics, transportation, manufacturing, and medical care. Besides, in terms of security, RFID tags have an encryption mechanism to protect the information security, and bar codes are easily forged and changed physically, so the RFID system has a higher security level. The main problem faced by RFID systems in the past was that the manufacturing cost was too high and it was not suitable for a single object. At first, the cost was reduced by simplifying the label structure and mass manufacturing. Now, with the advancement of technology, the RFID tags can be manufactured through new printing technologies (Virtanen et al., 2010) and metamaterials such as graphene (Kopyt et al., 2016), instead of traditional metals. The costs have been greatly reduced.

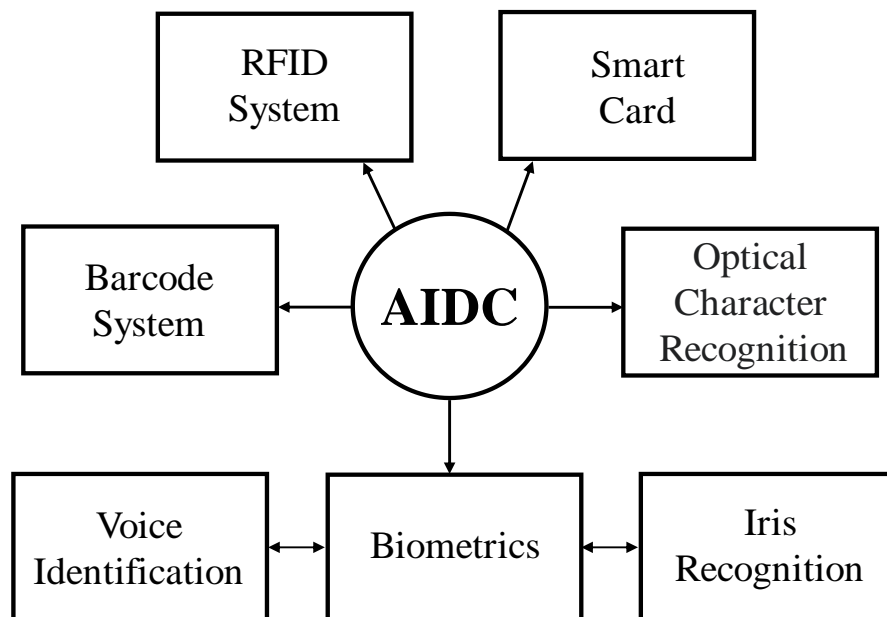


Figure 1.1: Typical AIDC technologies.

Table 1.1: Comparison of Barcode and RFID systems.

Items	Barcode	RFID
Communication medium	Line-of-sight	EM Wave
Read distance	Few centimeters	More than 3 meters
Read direction	Specific direction	Unlimited
Capability of read and write	Only read	Can read and write
Amount of data access	Less	Much larger
Identification rate	Can only identify one tag at a time.	Can identify multiple tags at a time.

1.2 Working Principle of RFID System

The RFID system consists of three main parts: host, interrogator, and transponder. The host is usually a workstation or a computer, which analyzes and processes the data to be written in the back end of the system. The interrogator consists of a reader and a reading antenna. The reader uses the reading antenna to transmit and receive bidirectional electromagnetic waves to exchange data with the transponder (Tag). Usually, a conventional transponder consists of a tag antenna and a chip. The working principle of the RFID system is now explained in detail, and the corresponding architecture is shown in Figure 1.2. First, when the transponder enters the interrogation area, the reader transmits RF energy through its antenna, which is received by the tag antenna and it excites the chip on the tag. Then, the data stored on the chip will be sent back to the

reading antenna via the tag antenna. After being received, it will be preliminarily demodulated on the reader, and the information will be sent to the computer system for further processing.

The propagation mechanism between the reader and the tag can be divided into two types: reactive near-field and radiative far-field. The differences between the two communication fields are narrated and shown in Figure 1.3:

- a) Reactive near-field: The physical mechanism of the near-field communication operation is inductive coupling (Chawla and Ha, 2007). Current passing through the reader coil will generate a dynamic magnetic field. When the tag approaches the reader at a close distance, the antenna coil inside the tag will generate an induced current to drive the chip and return the signal to the reader. Due to the limited magnetic field energy, there is usually only a communication distance of less than one wavelength, and the corresponding operating frequency bands are like LF and HF.
- b) Radiative far-field: In the far-field communication, the reader sends RF power coupled with the antenna to generate a current to excite the chip. Eliminating the power consumption on the circuit and the chip, the response signal is reflected to the reader with the same high-frequency carrier. This mechanism is called backscattering (Rao et al., 2005a). This type of far-field communication allows UHF tags to read at least three meters away.

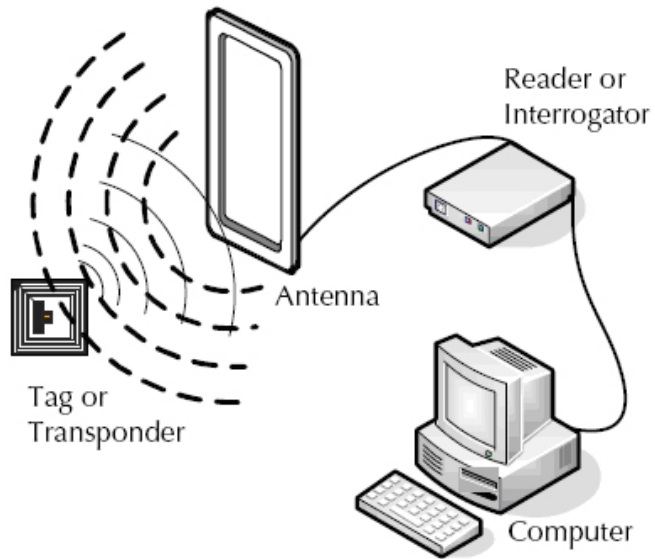


Figure 1.2: Architecture of the RFID system.

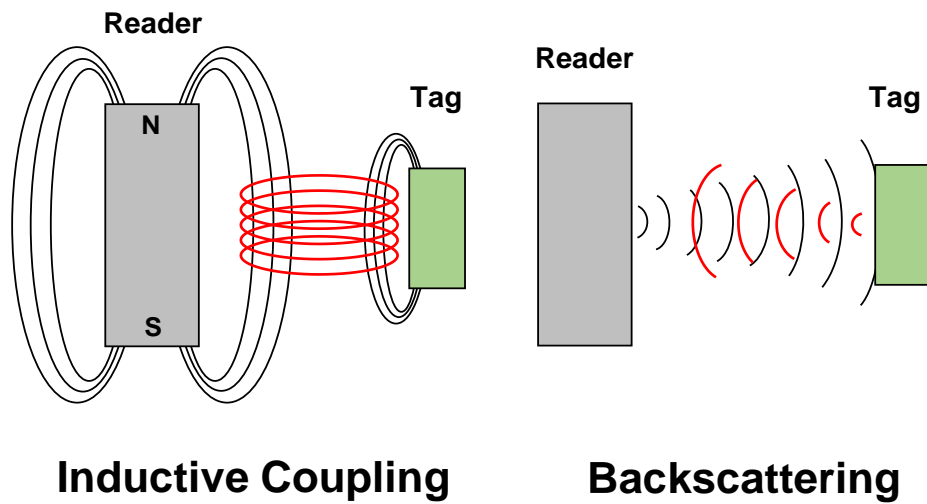


Figure 1.3: Working principle of the RFID system.

1.3 Types of RFID Tag

According to the power supply, RFID tags can be divided into three categories: active tags, semi-passive tags, and passive tags. Each tag is described in detail:

- a) Active tags: The tag itself has a power supply inside, so it is called an active tag. The built-in battery can supply the chip and the energy required to generate the signal. Therefore, the read distance of the active tag is much longer than the other two, and the capacity of the chip to access the memory is relatively larger. The main feature of the active tag is that it can use its power source to actively send out signals to the reader. Compared with the other two, although it has the best performance, this type of tag has a life limit, and the tag cannot work when the battery is exhausted. Due to the built-in power supply, active tags are usually larger and costly to manufacture.
- b) Semi-passive tags: Compared with the passive type, the semi-passive tag has an additional small battery to drive the chip. The purpose is to prevent the tag from still having enough energy to transmit data back to the reader when the reader signal is weak. This means that semi-passive tags will not be unable to work due to the insufficient strength of the electromagnetic signal from the reader. When the reader is stably transmitting the signal, the semi-passive tag has a better reading distance and transmission efficiency than the passive tag.
- c) Passive tags: The tag is only composed of an antenna and a chip. The power of the excitation chip and the backscattered signal to be transmitted is obtained from the electromagnetic wave signal transmitted by the reader. The antenna radiation efficiency is very important in the passive tag, making the design of the antenna structure to become a critical factor affecting the read performance. Passive tags need to consume part of the energy of the signal received from the reader to power up the chip, so the

reading distance is shorter than those of active and semi-passive tags. Moreover, in certain environments, the transmission performance is more likely to get deteriorated, such as multipath interference (Bekkali et al., 2014) on metal, water, and other interfaces. Although the read distance is not as good as the above two, the simple structure, small size, cheap manufacturing cost, long life, and many advantages make the passive antenna the first choice in the market.

1.4 Spectrum of RFID Systems

Generally, three frequency bands mainly used by RFID systems are low frequency (LF, 120 – 140 kHz), high frequency (HF, 13.56 MHz), and ultra-high frequency (UHF, 860 – 960 MHz), as shown in Figure 1.4. The LF frequency tag communicates through inductive coupling. Since the RF power comes from the induced current from the reader, the antenna is usually a coil design, so the size of the antenna can be reduced. Typical applications include animal identification and access control. Similar to the working principle of the low-frequency tags, the operating frequency band of the HF tags is 13.56 MHz, which is currently the most widely used radio frequency passband in the market, such as by electronic ID cards and contactless payments.

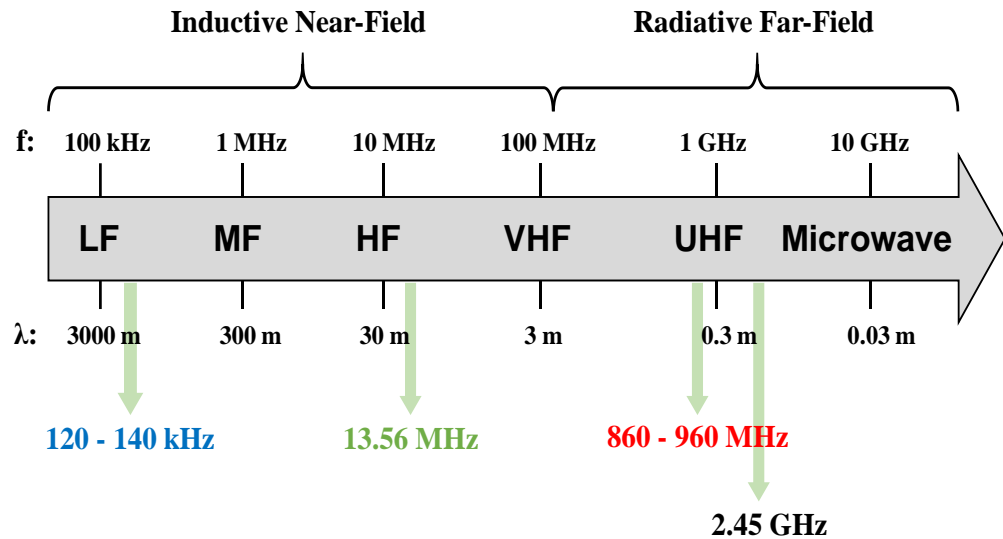


Figure 1.4: Operating spectrum of the RFID system.

The UHF RFID system communicates the reader and the tag through backscattered coupling technology. Operating in this frequency band, the data transmission rate and the amount of information entrained can be higher than the low- and high-frequency RFID systems, while having a longer reading distance. With the aforementioned excellent characteristics, UHF tags are used in logistics management, vehicle identification, and automatic toll collection systems. Figure 1.5 shows the regulated spectra of the UHF RFID systems around the world. Despite each country has its own operating spectrum, the most common specifications nowadays are the EU and US passbands, which are 865 – 868 MHz and 902 – 928 MHz, respectively. In general, the two standards cover the UHF band specifications of all countries. Besides, the common three RFID systems operating in different frequency bands are also sorted out in Table 1.2. The comparison includes read distance, communication mechanism, and applications.

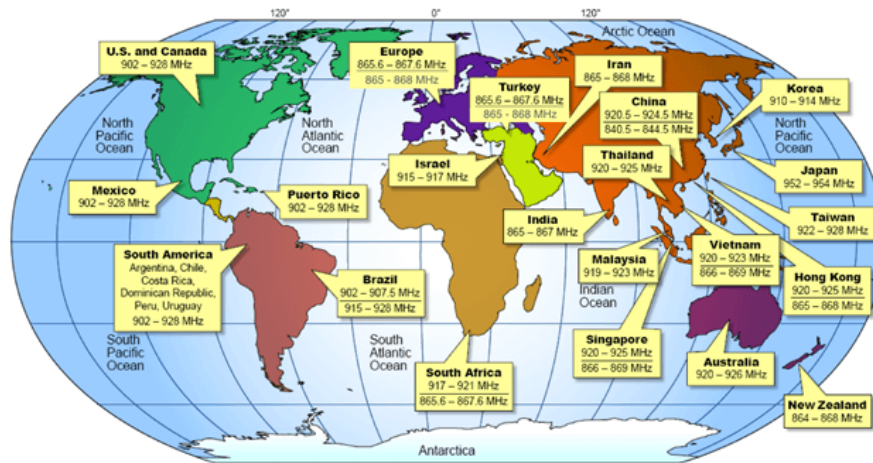


Figure 1.5: Spectrum distribution map of the world.

Table 1.2: Comparison of radio frequency ranges and characteristics of different RFID systems.

Items	Low Frequency (LF)	High Frequency (HF)	Ultra-High Frequency (UHF)
Spectrum	120 to 140 kHz	13.65 MHz	860 to 960 MHz
Read Distance	~ 10 cm	10 cm to 1 m	~ 10 m
Communication Mechanism	Inductive Coupling	Inductive Coupling	Radiative Backscattering
Data Transfer Rate	Low	Moderate	Fast
Sensitivity of Environmental Interference	Low	Moderate	High
Applications	-Animals tagging -Access control	-Smart card -Contactless payment	- Toll collection -Asset Management -Manufacturing

1.5 Problem Statements

Compared with the RFID tags that operate at low and high frequencies, the UHF tag antennas have better read performance, but there are always many issues in the passive UHF RFID tag design. First of all, the UHF tags are quite sensitive to metal and liquid environments. For example, when the tag approaches liquid, the radiated waves may be interfered and absorbed, causing the read performance will jeopardize. The EM wave may be reflected or even blocked by the metal. Some objects with a high dielectric coefficient may also detune the resonance frequency. Furthermore, the radiation performance, antenna size, and manufactured cost have to be considered for the UHF tag design. Generally, tags are expected to have small size, high radiation performance, and low manufacturing costs. However, there is always a trade-off between the three. Additional manufacturing processes or new materials may be required to miniaturize a tag antenna, which can increase the cost. Although a small-sized tag is designed, it can also sacrifice the integrity of the radiator, resulting in poor antenna radiation efficiency.

To reduce the electromagnetic interference from the backing metal object, an additional layer of ground plane can be introduced at the bottom of the antenna. To isolate the radiator, the Artificial Magnetic Conductor (AMC) and electromagnetic bandgap (EBG) (Goussetis et al., 2006) structures can also be embedded between the tag and the metal platform. The drawback is that the overall size of the tag antenna will increase. Besides, the AMC/EBG is only effective for specific frequencies, so a lot of time and costs may be spent on the

design and optimization. The miniaturization of tag antennas can be achieved through the following technologies, such as the use of meandering arms, the introduction of slots, notches, and slits on the radiator, and the use of materials with high dielectric constant as the substrate. However, these methods may deteriorate the radiation performance of the antenna. The usage of vias/pins can also increase the reactance of the tag antenna, and they can control the current flows for adjusting the resonance frequency. However, there are additional procedures in manufacturing that may increase the cost. Besides, if the positions of vias/pins fluctuate, the operating frequency may get detuned as well.

1.6 Objectives

The research motivation of this dissertation is to design passive UHF RFID metal-mountable tag antennas by incorporating lumped elements without changing the antennas structures. The proposed antenna structure must several requirements. First, the tag must have a small size and simple structure. It is lightweight and flexible. Also, it can be mounted on various metal objects with different curvatures. To achieve the above characteristics, the research objectives are organized into the following three items:

- a) The designed flexible planar antenna is electrically small in size, and its simple antenna structure can be mounted on various objects.
- b) To use lumped components to increase the reactance of the antenna impedance greatly for miniaturizing the tag size and maintaining the structure of the radiator, so that the antenna has good radiation efficiency.

- c) The read distance must reach at least five meters when the proposed tag is mounted on various metal objects for testing (3.28 W EIRP reader is used).

To make the design meeting the required objectives, the substrate being used is a soft polyethylene foam. The antenna circuit is printed on a flexible PET film by using the PCB etching technology. Besides, the two proposed projects have both used lumped elements to introduce reactance to make the antenna structure compact and maintain the integrity of the antenna radiator.

1.7 Dissertation Outline

This dissertation is composed of 5 chapters. The first chapter briefly introduces the background of AIDC and the systems it covers. Among them, barcode and RFID systems were proposed for performance comparison to emphasize the advantages of RFID. Next, the operating principle of the RFID system and the mechanism of the two different communication fields are explained in detail. The types of tags and their operating frequency bands will also be discussed and compared. Finally, the current challenges faced by the RFID technologies are stated. Also discussed in this chapter are the research objectives and problem statements.

The second chapter is the introduction of relevant literature and research methodology. The composition and crucial part of the design for passive tags will be mentioned, and various types of metal tags and their applications will be

discussed. Later, several common techniques for miniaturizing antennas and impedance matching will be elaborated. Here, the research method that is explained by a flowchart is presented for explanation. The measurement methods will be explained in detail at the end.

In chapter 3, a high inductive channel is introduced into the top -loading layer of a bowtie-shaped dipolar patch antenna for applying metal surfaces. The narrow inductive channel, which has an embedded external lumped inductor, is loaded on the top of the dipolar antenna to achieve arbitrary tuning capability over a wide range. The top-loading patch can enhance the field of dipolar, and the inductive channel can adjust the current on the top-loading patch. By adjusting the channel width and external inductance, the resonant frequency can be effectively adjusted without greatly deteriorate the reading performance of the tag. Furthermore, the equivalent circuit model is proposed to analyze the impedance characteristics of the antenna. At the end of the chapter, the antenna prototype was mounted on various metal objects for testing.

In chapter 4, a pair of lumped capacitors are inserted in the narrow gap between dipolar patches for introducing extra capacitance to reduce the resonance frequency and minimize the antenna size. The proposed tag antenna has a simple structure and it can be made on the two-dimensional surface of a flexible PET substrate. Likewise, the tag frequency can be easily tuned by adjusting the lumped capacitance. The tag prototype was also attached to various sizes of aluminum plates and metal containers for testing.

The last chapter concludes the research results from chapter 3 to 4, and briefly discusses the future works.

CHAPTER 2

LITERATURE REVIEW AND METHODOLOGY

2.1 Introduction

The passive UHF RFID tags consist of two main components, namely a microchip and an antenna. The tag antenna activates the chip through the EM waves emitted by the reader and then it utilizes the principle of backscattering to transmit data back to the reader. Excluding the choice of reader power and chip sensitivity, the main factor that affects the performance of the tag is the radiation efficiency of the antenna. Another important factor is the impedance matching level between the chip and the antenna.

- a) Radiation performance: Generally, the most important parameter for evaluating the radiation capability of a tag antenna is its radiation efficiency. The larger the antenna size and the more complete the radiator, the better the radiation efficiency is. However, the passive RFID tags used in the UHF band are always required to have a small size. As a result, with the limited tag size, their radiation is usually weaker than the active and semi-passive ones.
- b) Impedance matching: The passive tag is equipped with a chip, which is used to read and write related information to be recorded. Commercially available microchips usually have capacitive impedance characteristics. To obtain the maximum transmission power between the antenna and the chip, the antenna reactance must be able to eliminate the reactance of the chip.

At the same time, the antenna and the chip are to have the same resistance for achieving conjugate match.

The purpose of the dissertation is to propose passive UHF RFID tags that can be used for metal-mountable applications. Therefore, the development of the metal-mountable tag antennas in recent years will be reviewed here.

2.2 Passive Metal-Mountable UHF RFID Tag Antennas

The development of UHF tag antennas has never stopped, and the rapid advancements of automatic identification and fast-tracking have made it widely used by many fields. However, it is always a challenge for the passive UHF tag antennas to work well on metal surfaces. When a passive tag is placed in adjacent to metal, it produces an induced image current with the opposite phase, causing the antenna radiation power to drop significantly and the tag resonant frequency to detune. Different types of antennas that are commonly used for designing the UHF RFID tags are reviewed here.

2.2.1 Conventional Dipole Antenna

Dipole antennas are composed of a set of conductive radiating arms (Rouse et al., 2012). Despite their simple structure, they have good radiation efficiency. However, the total length of the dipole antenna is half of the operating

wavelength, making the antenna size too bulky for the RFID tag design. For the UHF US band of 915 Hz, the antenna length can be as long as 16.4 cm. This footprint is definitely too large. For reducing the size, folded dipole arms (Genovesi and Monorchio, 2010, Erman et al., 2019), as shown in Figure 2.1, and meandered radiating arms (Marrocco, 2003) have come out one after another. These types of tag antennas are also the most popular structures on the market. Although the footprint of the tag antenna is effectively reduced, winding too many wires may cause crowding effect (Shen et al., 2011), which can narrow the antenna bandwidth and deteriorate the radiation efficiency.

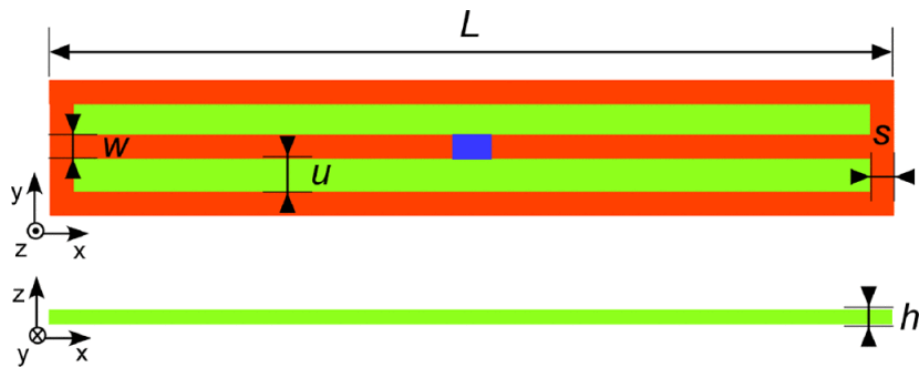


Figure 2.1: Low-profile three-arm folded dipole antenna.

2.2.2 Separation of Antennas by Air Layers

When a dipole tag antenna is directly placed on the metal surface, it will generate induced currents which are opposite in phase to the currents on the antenna, which can weaken the antenna's radiation efficiency. To reduce the interaction between the metal and the antenna, two layers of FR4 are used as the substrates in Figure 2.2 (Hamani et al., 2016), and the distance between the two substrates

is increased to form an air layer for isolating the antenna from the metallic surface, where the antenna gain can be improved through this method. Although the method is simple and effective, with the resonance at 905 MHz and a maximum reading distance of 14.6 m, the too-large antenna size of $104 \text{ mm} \times 31 \text{ mm} \times 7.6 \text{ mm}$ ($0.314\lambda \times 0.094\lambda \times 0.023\lambda$) is not suitable for application on small metal objects.

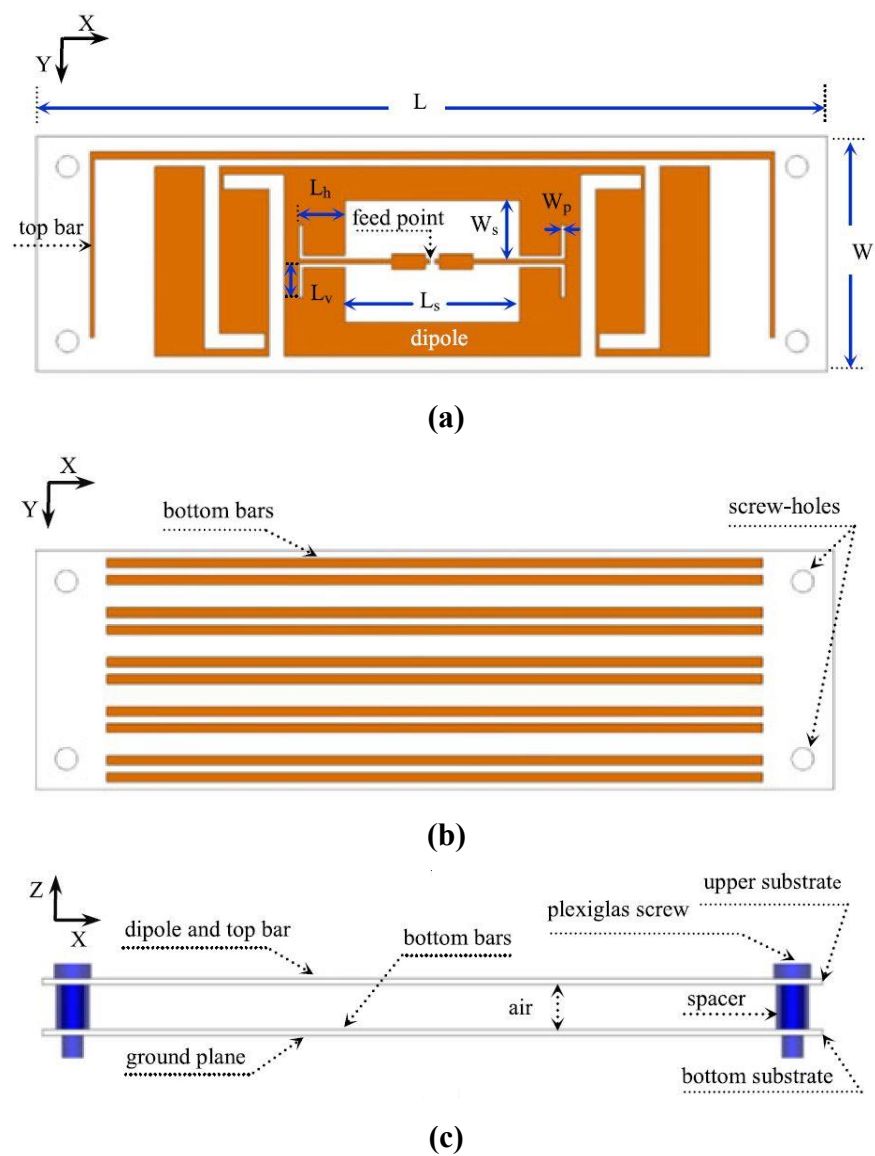


Figure 2.2: (a) Top layer, (b) bottom layer, (c) lateral view of the broadband tag antenna with an air layer.

2.2.3 Planar Antenna with FSS/AMC/EBG Structure

To accurately control the operation of electromagnetic waves, scientists have introduced the concept of metamaterials into the field of microwave engineering. Human-engineered materials such as AMC and EBG are applied to manipulate the amplitude and phase of the electromagnetic waves for the purpose to achieve high antenna gain and special radiation characteristic. Frequency Selective Surface (FSS) (Chakravarty and Mittra, 2003) is an earlier concept that is applied to reflect and transmit electromagnetic waves of a specific frequency through the periodic array pattern of the FSS structure, which can be regarded as a selective filter.

The characteristics of the Perfect Magnetic Conductor (PMC) can be imitated by the Artificial Magnetic Conductor (AMC) (Feresidis et al., 2005) periodic structures. When such engineered structure is introduced into the antenna design, the image current can be made to have the same phase as the incident wave at a specific frequency to enhance the radiated fields. Figure 2.3 (Kim and Yeo, 2008) shows that a dipole that is placed on an AMC structure with a ground plane can significantly improve the performance of the antenna on metal without changing the antenna structure. Similarly, the same technology applications are also shown in (Kim and Yeo, 2012) and (Sarkar and Gupta, 2020).

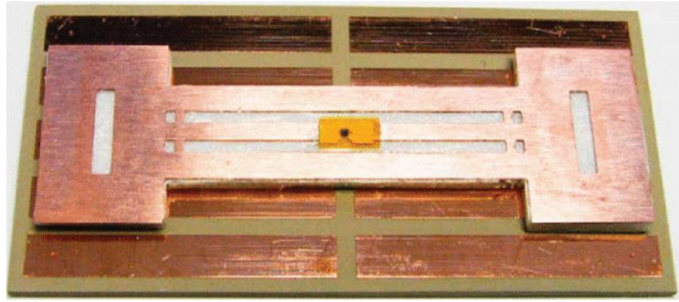


Figure 2.3: Dipole antenna with AMC patch.

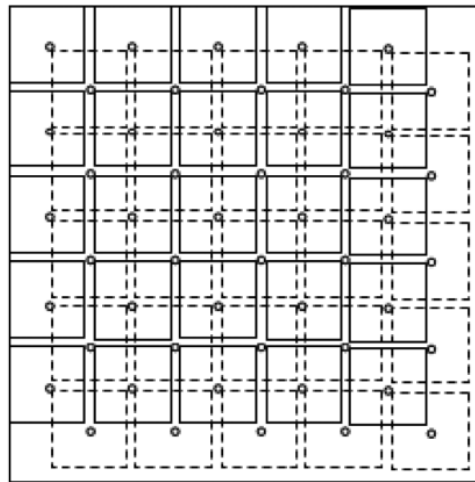


Figure 2.4: The lateral and top view of the EBG structure.

Electromagnetic bandgap (EBG) is developed from a high impedance surface (HIS) (Sievenpiper et al., 1999), and its periodic structure is similar with AMC. However, these arrayed conductive patches can exhibit high impedance characteristics to prohibit the passage of electromagnetic waves of specific frequencies. The conventional EBG structure is formed by connecting square patches to the ground plane through vias to form mushroom-like units, which are arranged in a geometric periodic array, as shown in Figure 2.4 (Gao and Yuen, 2011). The relative phase of the electromagnetic wave reflected by the EBG can change from -180° to 180° . Generally, when the resonance of the tag antenna

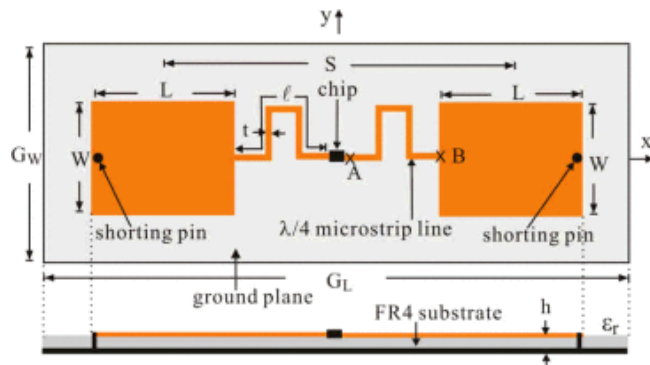
coincides with the operating frequency of the EBG, the electromagnetic waves can be blocked and attenuated, so that the antenna can be made to achieve radiation performance.

Although the combination of the tag antenna and the FSS/AMC/EBG structure can improve the radiation performance, the resulted structure occupies too much area and it is not easy to be mounted on small objects. Besides, they are only working in some specific frequency bands and such human-engineered structures may be very complicated. These reasons make their applications not economical.

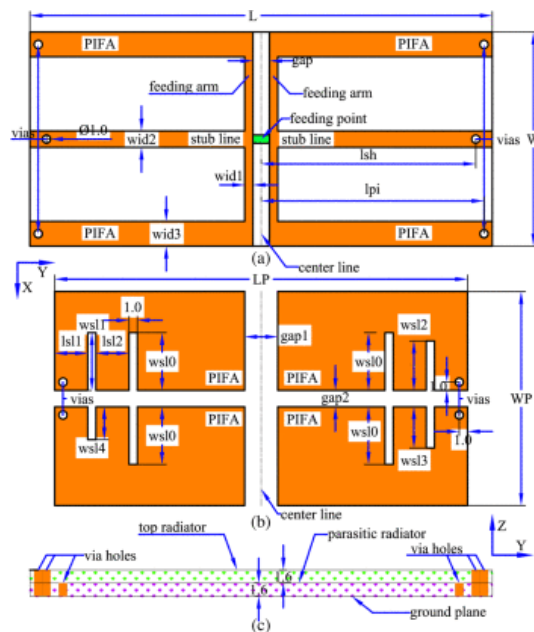
2.2.4 Planar Inverted Antenna

Most dipole antennas have excellent radiation performances, but the half-wavelength antenna size is difficult to be used for designing metal-mountable UHF tag antennas. To reduce the antenna profile, the concept of small hidden antennas (Chang and Wong, 2009) was introduced for mobile communications. Here, quarter-wave monopoles such as planar inverted-L (PILA) and inverted-F (PIFA) antennas were applied. In Figures 2.5, (Chen and Tsao, 2010b, Zhang and Long, 2013a) demonstrated the application of the dual PIFA structure. From the figure, it can be observed that one end of the radiator is connected to the ground plane through inductive vias to reduce the size. In addition, the structure of planar inverted antenna has its own ground plane, which can isolate electromagnetic interferences from metal and maintain its radiation performance.

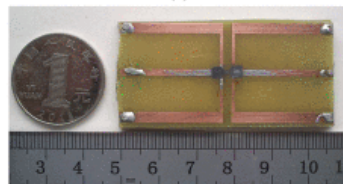
Instead of shorting vias, in (Hirvonen et al., 2004), a simple shorting plate, without need of drilling holes, is used by the structure. By applying the concept of planar inverted antenna, a number of UHF passive tags were also designed using the planar inverted-S antenna (Ng et al., 2019) and E-shaped patch (Ng et al., 2018) structures.



(a)



(b)



(d)

Figure 2.5: Structure of the dual PIFA array shown in (a) and (b).

2.2.5 Folded-patch Antenna

Generally, ordinary microstrip patch UHF antennas are manufactured on rigid substrates such as FR4, which are not easy to be mounted on objects with curved surfaces. Therefore, a folded-patch antenna that can be printed on a flexible polyethylene terephthalate (PET) has been developed. Referring to the tag antenna structure in Figure 2.6 (Lee et al., 2018c), it can be found that the radiation patch, shorting stubs, as well as the ground plane can all be printed on one side of a flexible substrate by using PCB printing technology. Here, the polyethylene foam is used as the structural support of the folded patch antenna. The semi-rigid physical structure allows it to be attached to curved objects.

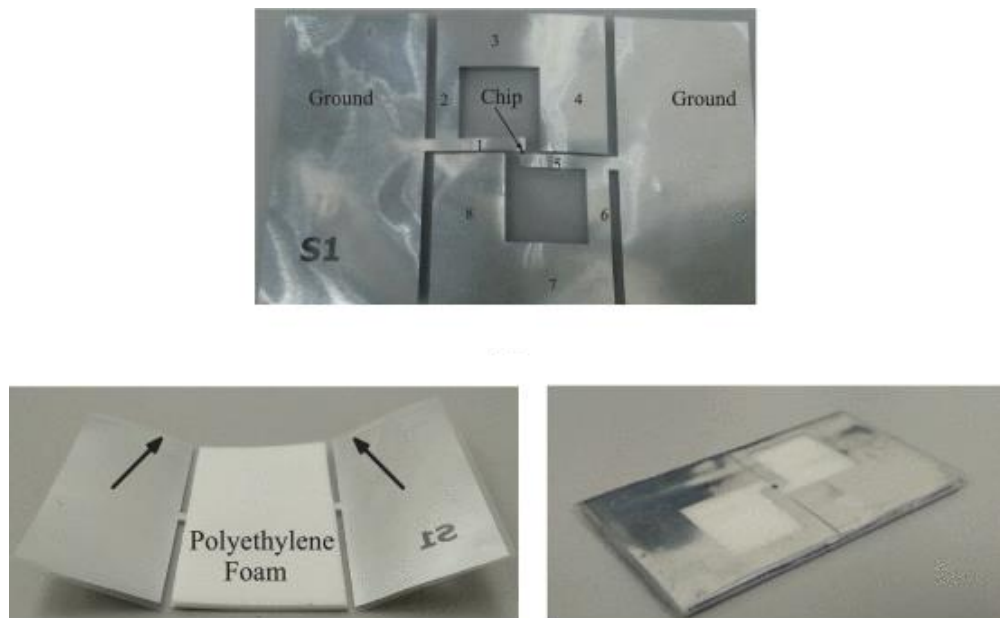


Figure 2.6: Inlay and prototype of the folded-patch antenna.

2.3 Miniaturization Techniques for UHF RFID Tag Antenna

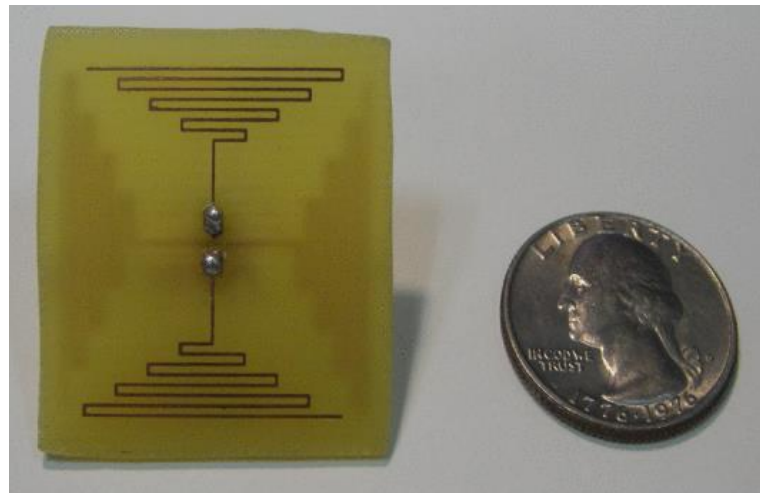
In response to market demand, tags are required to have a low-profile antenna size. However, when the resonance is operated in the UHF band, the electrical size of the antenna is usually too large, which is not conducive to the application on small objects. Therefore, scientists have developed many techniques for miniaturizing antennas efficiently. In this section, several common miniaturization techniques in recent years will be presented for analysis and review.

2.3.1 Meandering

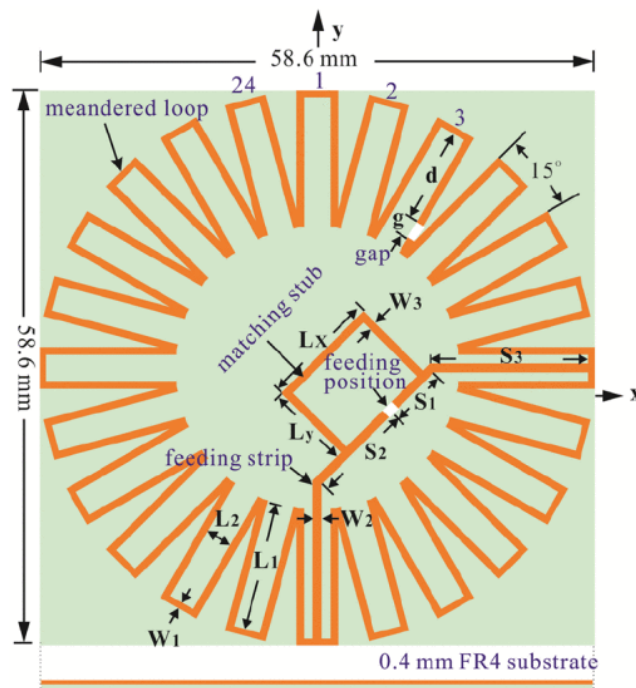
The meandering technique is commonly used for miniaturizing dipole antennas. Since the electrical size of the half-wavelength antenna is usually too larger, the antenna area can be greatly reduced after densely folding the feedlines, as shown in Figure 2.7 (Bhaskar and Singh, 2017). Referring to Figure 2.8 (Chen et al., 2011, Chen et al., 2016), the meandered lines can also be used directly as the radiator. The two concepts mentioned above are working in the same principle, which is to extend the current path through meandering a line. It has been confirmed in (Warnagiris and Minardo, 1998) that bending the microstrip line into a meandering structure can simultaneously generate capacitive and inductive reactance, causing the tag resonant frequency to become much lower. However, under the influence of the crowding effect, the cost is to have narrower bandwidth and lower antenna gain.



Figure 2.7: Fabricated prototype of a meandered dipole.



(a)



(b)

Figure 2.8: (a) Configuration of the meandered dipole. (b) Geometry of the meandered-loop antenna.

2.3.2 Meandered Slotlines/Slotting on Radiator

Incorporating slots, slits, or notches into the antenna patch can change the antenna impedance characteristics. Referring to Figure 2.9, the dipole patches are separated by the symmetric meandered slotline (Bong et al., 2017) instead of a single vertical slotline. This approach can introduce inductive reactance, and there is a capacitive coupling between the two patches that can be used to enhance the electric fields. The tag size is significantly reduced to only $23 \text{ mm} \times 16 \text{ mm} \times 1.6 \text{ mm}$ ($0.07\lambda \times 0.05\lambda \times 0.005\lambda$) with a resonant frequency of 915 MHz. Although the antenna profile can be greatly reduced, the usage of meandered slotline on the patch causes the radiator structure to become incomplete and the antenna radiation efficiency to deteriorate. As a result, its reading distance on the metal is only 4.5 meters (at EIRP of 4 W).

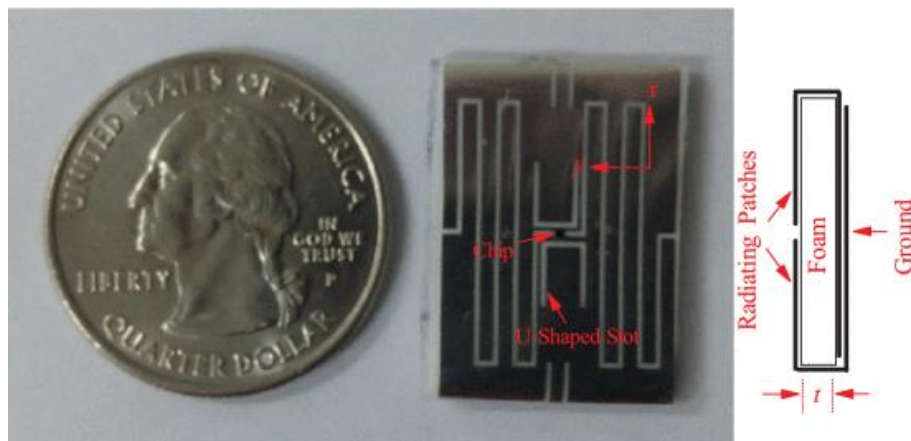


Figure 2.9: Dipole patch antenna with meandered slotline.

In (Reed et al., 2001), by loading a microstrip patch with inductive slits on both sides, the antenna size can be reduced by 50%. This method has been used as a miniaturization technique for many years. Similarly, by referring to Figure 2.10 (Michel et al., 2018), several arrays of narrow slits are introduced on both sides of the radiator and with combination with shorting vias to increase the inductive reactance for reducing the antenna size. The radiator of the folded-patch structure in Figure 2.11 (Bong et al., 2016) is slotted to form a serration on the edge of the patch, which extends the current path and brings high inductance to reduce the resonant frequency. Despite slotting on the antenna radiator can effectively reduce the tag resonant frequency for achieving the purpose of miniaturization, these techniques can cause the antenna radiator to change, which can greatly deteriorate the radiation efficiency.

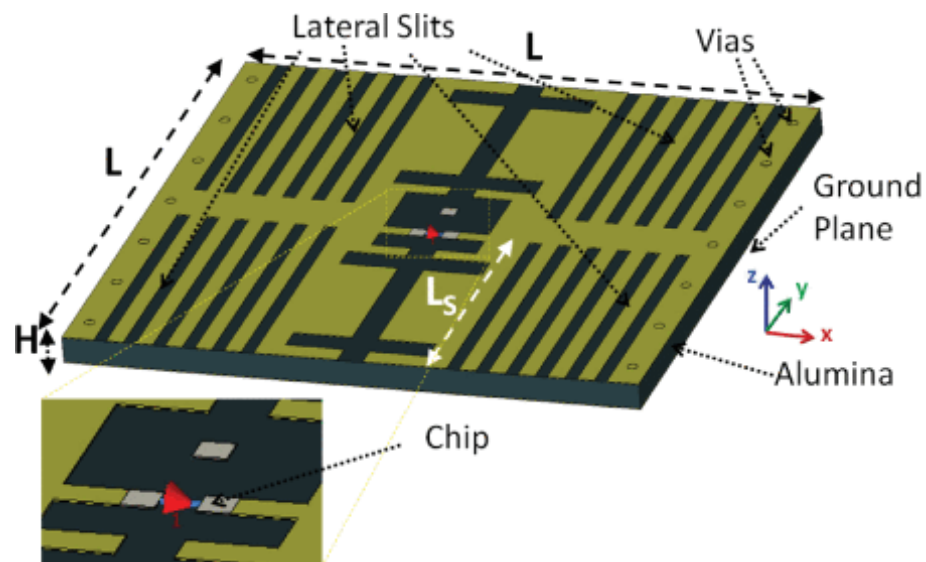


Figure 2.10: Dipole patch antenna with inductive slits and shorting vias.

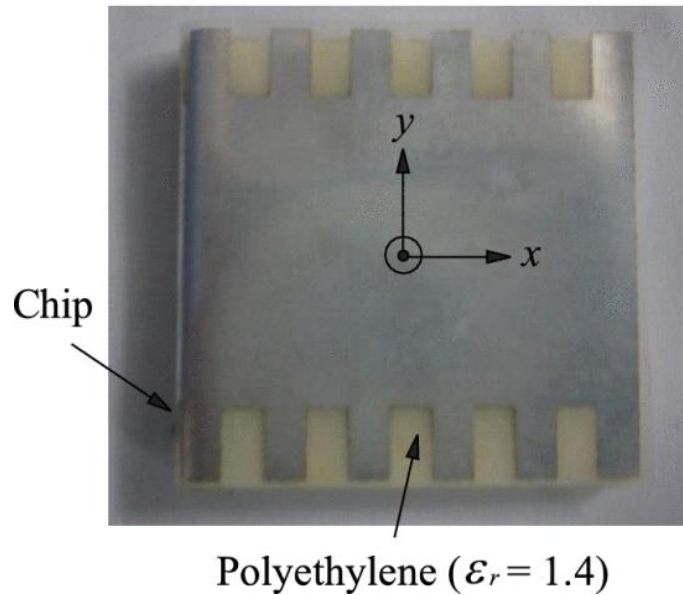


Figure 2.11: Flexible folded-patch antenna with serrated edges.

2.3.3 Shorting Elements

When a half-wave patch antenna is incorporated with shorting elements, its electrical length becomes a quarter-wavelength, which means that the physical size of the antenna can be reduced where the antenna is still operating at the same frequency (Sanad, 1994). Because of this, shorting elements such as shorting vias/pins are also commonly used to miniaturize tag antennas. As shown in Figure 2.12 and Figure 2.13 (Lin et al., 2012, Zhang and Long, 2013b), the patch is connected to the ground plane by vias, and the current flow can be controlled by adjusting the aperture, amount, and positions of the vias to tune the resonance. Generally, the narrower the aperture, the higher the inductance is, causing the tag resonance to become lower. However, such antennas are usually very sensitive to the positions of the shorting vias/pins. A slight offset may cause the operating frequency to fluctuate significantly. As a result, additional procedures

are required for the optimization and production processes.

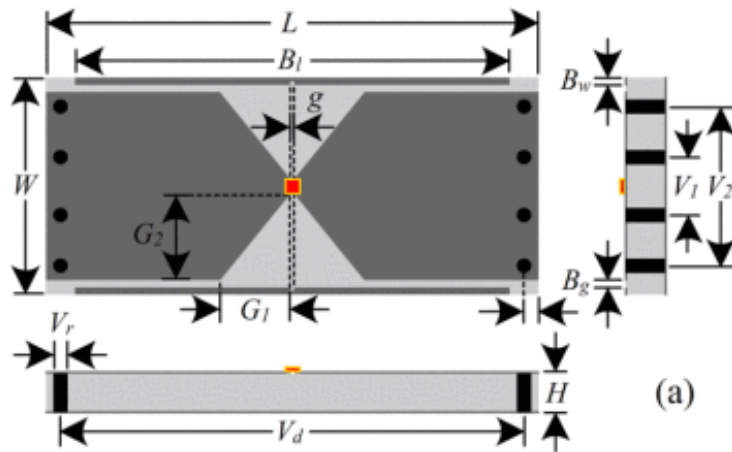


Figure 2.12: Configuration of the RFID metal tag antenna with shorting vias.

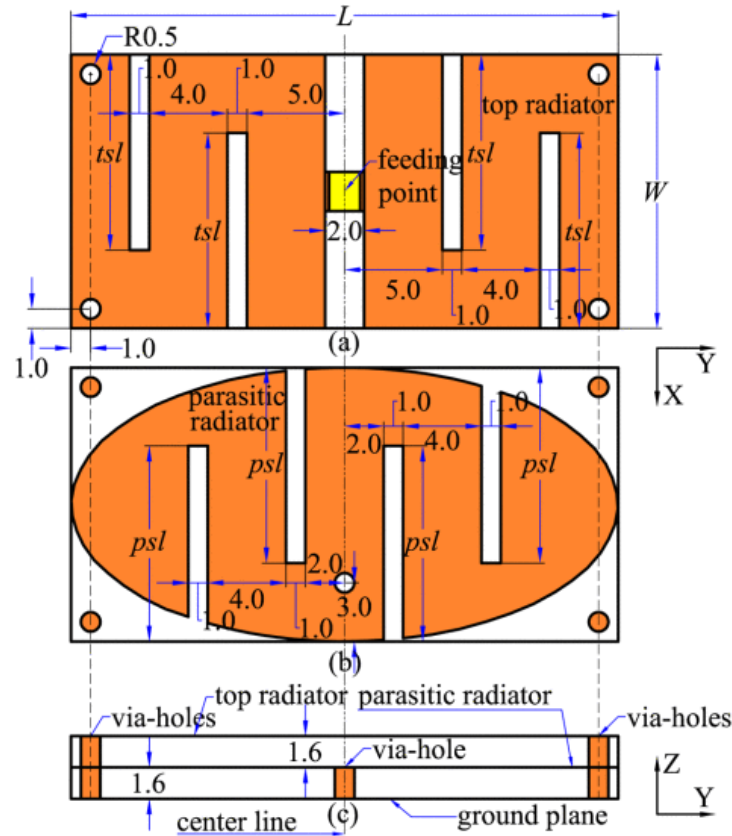
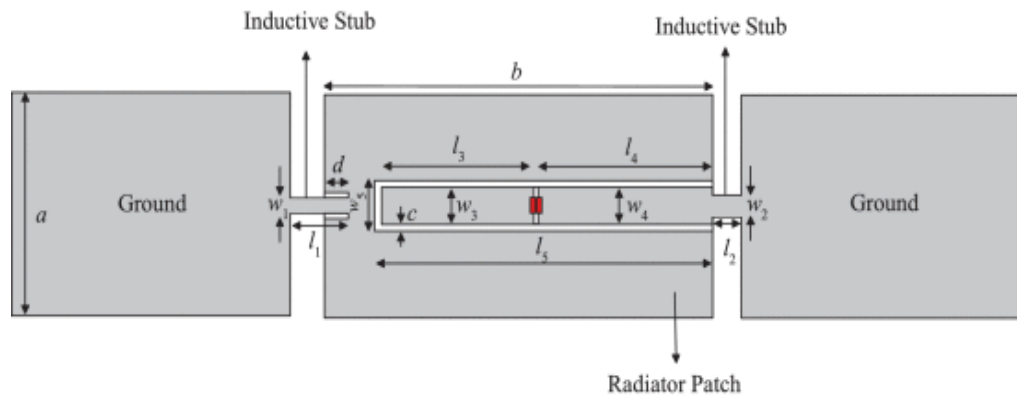


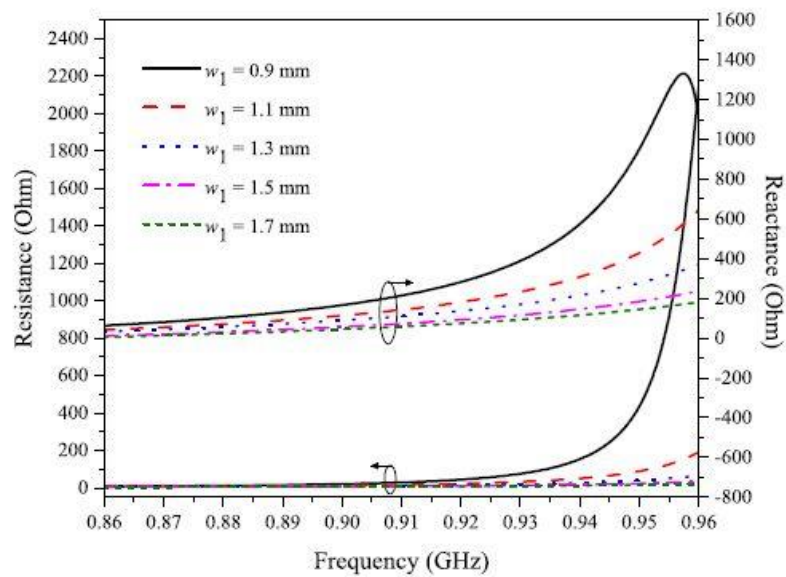
Figure 2.13: Structural configuration of the dual-layer antenna.

With the increasing popularity of the semi-rigid folded patch antennas, shorting vias/pins have been replaced by shorting stubs, as can be seen in Figure 2.14(a) (Moh et al., 2018). Here, frequency tuning can be achieved by adjusting

the widths of the stubs to change the inductance, as depicted in Figure 2.14(b).



(a)



(b)

Figure 2.14: (a) Configuration of the miniature coplanar-fed folded patch antenna, (b) Effects of stub width w_1 on resistance and reactance.

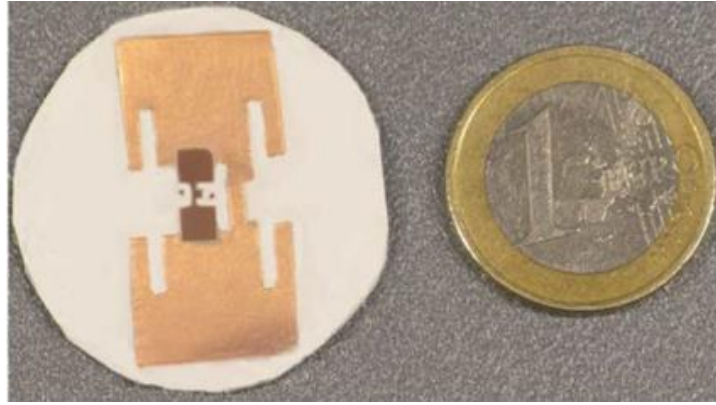
2.3.4 High Dielectric Substrate

Due to the technical limitations in the past, tag substrates mostly used low-dielectric materials such as FR4 laminates. However, these low-dielectric materials can limit tag miniaturization. With the evolution of manufacturing

technology, high-dielectric substrates have been used to increase the Q -factor (Sharma and Shrivastava, 2008), reducing the tag resonant frequency, and decreasing the antenna size. With reference to Figure 2.15(a) (Kim et al., 2008), a ceramic material with a dielectric constant of 22 is used for designing a tag. Figure 2.15(b) (Babar et al., 2012) is a tag antenna with flexible ceramic (BaTiO_3) polymer and polydimethylsiloxane (PDMS) composite substrate, which has a dielectric constant of around 12 and a loss tangent of 0.01. The read distances of the two antennas are designed to be no more than 4.5 meters. This is because high-dielectric materials usually have high dielectric loss (Rowe and Waterhouse, 2003), causing the tag antennas to have narrow bandwidth and weak radiation efficiency. Undoubtedly, there are also high-dielectric materials with low tangent loss, such as Duroid[®] 6010 laminate with a dielectric constant of 10.2, which has a dielectric loss of only 0.0023. Although this type of material can realize miniaturized tags, the material itself is very expensive and it is not economical for mass manufacturing.



(a)



(b)

Figure 2.15: (a) Prototype of the tag with a diameter of 34 mm and a thickness of 5 mm, (b) Prototype of the tag with a diameter of 32 mm and a thickness of 1.5 mm.

2.4 Impedance Matching

The tag antenna is composed of a microchip and an antenna unit. The RFID microchip is used to store data. The commercial chip exhibits high capacitance characteristics, which can be represented by the series circuit as $Z_c = R_c - jX_c$. Generally, the resistance value is about 5 to 20 ohms, and the capacitive reactance is in the range of -100 to -400 ohms (Marrocco, 2008). To have a good impedance match between the antenna and the chip means that the antenna must be designed to be inductive.

The basic equivalent circuit of the RFID antenna is depicted in Figure 2.16 (Rao et al., 2005b). The antenna is regarded as a conventional *RLC* series resonant circuit. When the inductance of the antenna and the capacitance of the chip are completely cancelling out, which is called conjugated matching $Z_a = Z_c^*$, there will be an ideal maximum power transmission $\tau = 1$, meaning that the

antenna power is totally transferred to the chip.

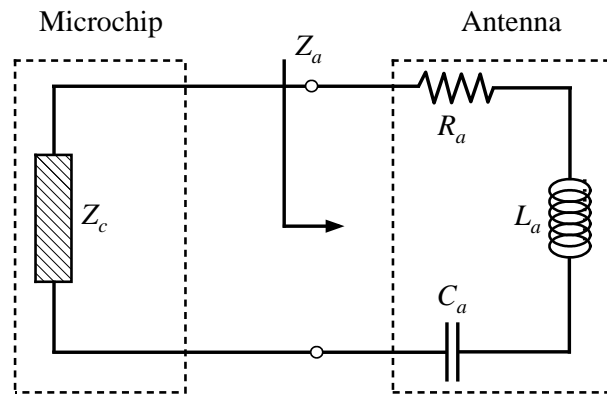


Figure 2.16: Equivalent circuit model of the RFID tag antenna.

However, in the preliminary antenna design process, it is often difficult to find an antenna impedance that can match well to the chip impedance. Therefore, several simple matching networks can be introduced between the chip and the antenna to improve the impedance matching, such as T-match circuit, inductively-coupled technique, and nested-slot matching methods without modifying the antenna structure much (Marrocco, 2008). The transmission power between the chip and the antenna can be improved through these matching networks.

2.5 Research Methodology

Figure 2.17 shows the flowchart of the tag antenna design process. First of all, the first factor to be considered at the beginning of antenna design is the environment in which the tag antenna is mounted. If the tag is to be used on a

material with a non-specific dielectric constant, the tag resonant frequency may become very uncertain. The absorption and reflection characteristics of different materials are actually quite different, which can affect the reading performance significantly (Girbau et al., 2010). In this project, the backing interface is metal.

For designing a tag antenna, the first step is to select the right material and antenna structure. Generally, the dielectric constants of the materials may directly affect the size of the tag. The materials of the substrate and the patch must be determined first. The next step is to choose the main structure of the antenna and select the correct antenna type to achieve the required polarization pattern. Besides, it must also be able to achieve good radiation performance in a compact size. Finally, it is to select a microchip with high read and write sensitivity, and the antenna impedance must be in conjugate match with the chip impedance to allow maximum power transmission between them.

The design and simulation tool is the CST Microwave Studio Suite, which is used to construct the antenna model and perform simulation in a specific frequency band. Once the tag is optimized, the next step is to make the prototype and do the measurement. In the manufacturing process of the antenna schematic, traditional etching technology is used, instead of carving with an engraving machine, to avoid excessive loss of the substrate that can cause error.

Then, the prototype of the tag will be placed on the backing metal and measured using the Voyantic Tagformance Pro measurement system (anechoic chamber) to obtain the realized gain, reading distance, and radiation pattern. If

the measurement results are in line with the simulation, the proposed UHF RFID antenna design can be used. If the tolerance is too large compared with the simulation result, the factors that are causing the problem must be checked. These may include whether the parameters are set incorrectly in the simulation or the prototype is damaged during the manufacturing process. Next, it is to re-manufacture a new prototype and measure it until the simulation and measurement results are consistent.

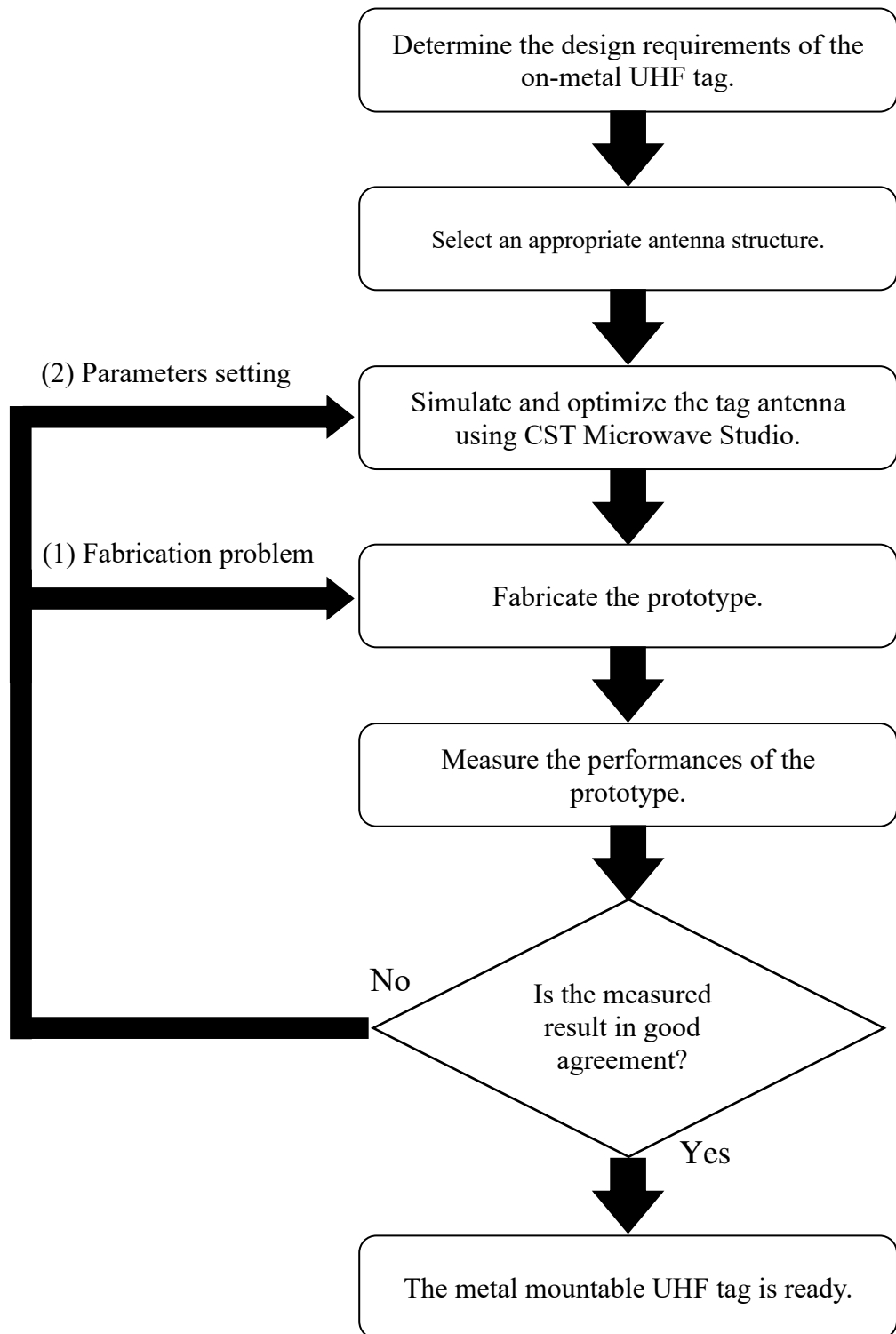


Figure 2.17: Design process of the UHF RFID tag antenna.

2.6 Measurement Process of UHF RFID Tag Antenna

The traditional method of measuring the read distance is to fix the transmitting power (P_{tx}) and change the distance between the reader antenna and the TUT (tag under test) until the tag is activated. This length is recorded as the measured distance. This kind of measurement method requires a big space. However, most of the anechoic cabinet systems are using the method mentioned in (Virtanen et al., 2013). By fixing the distance between the TUT and the reader antenna, the transmitting power is slightly increased until the tag is turned on. Then, the realized gain and the corresponding read distance in the frequency range are calculated. The prototypes of the proposed tag designs are all measured using the commercial RFID measurement cabinet system, Voyantic Tagformance (Voyantic, 2012), for obtaining the read distance (R_{max}), tag sensitivity (P_{tag}), and realized gain (G_r).

The measurement setup including the TUT, is depicted in Figure 2.18. The distance (d) between the reader and the tag is always fixed during the measurement, and the frequency range is set to 800 MHz – 1000 MHz, which can cover the US and Euro bands. Before starting the measurement, a reference tag (a wideband dipole tag) is employed to calibrate the anechoic cabinet to ensure that the noise level can be lower than -60 dB for minimizing the error (Nikitin and Rao, 2006). During calibration, the reference tag should be placed at the center of the platform and aligned with the reading antenna to obtain polarization matching. The path/forward loss from the reader to the tag antenna can be described as:

$$L_{fwd} \text{ (dB)} = L_{cable} \text{ (dB)} - G_{tx} \text{ (dBi)} + FSPL \text{ (dB)} \quad , \quad (2.1)$$

where L_{cable} is the loss of the cable linking reader to the relevant antenna, G_{tx} is the gain of the reader antenna which is 8 dBi, $FSPL$ is the free space loss in the chamber. After calibration, the TUT is mounted on the metal object and placed at the center of the platform for testing the read performances subsequently. During the measurement, the transmitted power P_{tx} is gradually increased until the reader antenna receives the backscattered signal from the TUT. Among them, the minimum power that can turn on the TUT is called the threshold power P_{thr} . Based on the P_{thr} received on the tag antenna, the tag sensitivity P_{tag} can be expressed as:

$$P_{tag} \text{ (dBm)} = P_{thr} \text{ (dBm)} - L_{fwd} \text{ (dB)} \quad , \quad (2.2)$$

Then, the equation (2.1) of L_{fwd} is added to equation (2.2) to become:

$$P_{tag} \text{ (dBm)} = P_{thr} \text{ (dBm)} - L_{cable} \text{ (dB)} + G_{tx} \text{ (dBi)} - FSPL \text{ (dB)} \quad , \quad (2.3)$$

Chip sensitivity is a constant value that can be obtained in the microchip datasheet, which defines the threshold power for chip activation. It can be expressed as:

$$P_{chip} \text{ (dBm)} = P_{tag} \text{ (dBm)} + G_r \text{ (dBi)} \quad , \quad (2.4)$$

where G_r is the realized gain of TUT, and equation (2.4) can be rewritten, where:

$$G_r \text{ (dBi)} = P_{chip} \text{ (dBm)} - P_{tag} \text{ (dBm)} \quad , \quad (2.6)$$

Converting equation (2.5) to linear scale, the realized gain of the TUT can be

expressed as:

$$G_r = \frac{P_{chip}}{P_{tag}} = \frac{P_{chip}}{P_{thr}L_{fwd}} \quad , \quad (2.6)$$

Referring to the Friis transmission equation, the maximum read distance R_{max} of the TUT can be calculated as:

$$R_{max} = \frac{\lambda}{4\pi} \sqrt{\frac{P_{tx}G_{tx}G_r}{P_r}} = \frac{\lambda}{4\pi} \sqrt{\frac{P_{EIRP}G_r}{P_{chip}}} = \frac{\lambda}{4\pi} \sqrt{\frac{P_{EIRP}}{P_{tag}}} \quad , \quad (2.7)$$

where,

$$P_{EIRP} = P_{tx} \cdot G_{tx} \quad , \quad (2.8)$$

where λ is the wavelength corresponding to the operating frequency of the TUT. P_{EIRP} is the regulated equivalent isotropic radiated power (*EIRP*). The Euro standard 3.28 W is used in the Voyantic Tagformance measurement system to calculate the maximum read distance R_{max} . To normalize it with 4 W, an additional 11% should be added to the read distance when $P_{EIRP} = 3.28$ W. Besides, the realized gain G_r (dBi) = G_{tag} (dBi) \times τ , where G_{tag} is the antenna gain, and τ is the power transmission coefficient. When τ equals to 1, it represents a perfect conjugate match between the chip and the antenna, which is mentioned in the previous section. It can be observed from the equation of realized gain G_r that the main factors affecting the antenna are the antenna radiation efficiency and impedance matching. The actual measurement set up in the anechoic cabinet is shown in Figure 2.19.

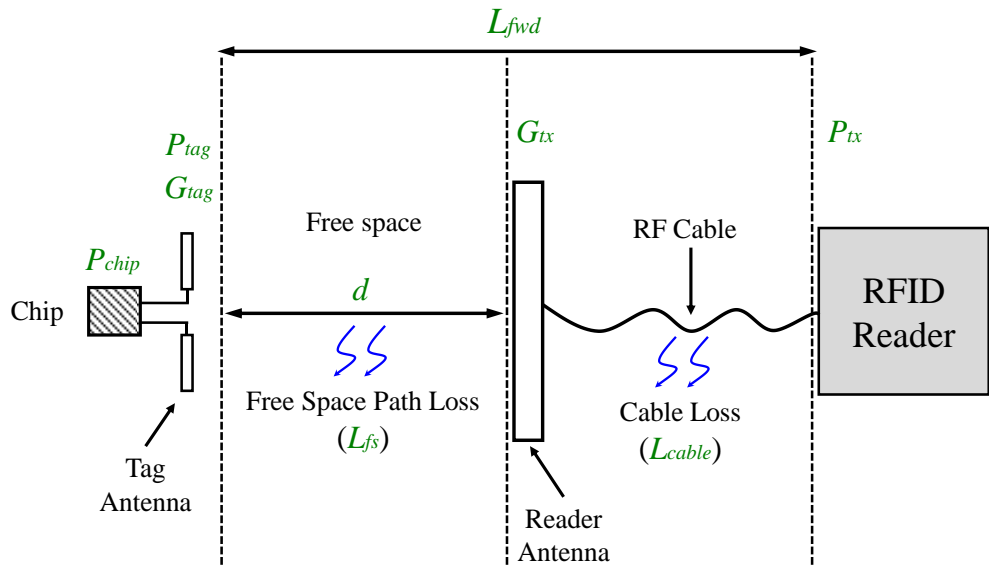


Figure 2.18: Setup of the UHF RFID measurement system.

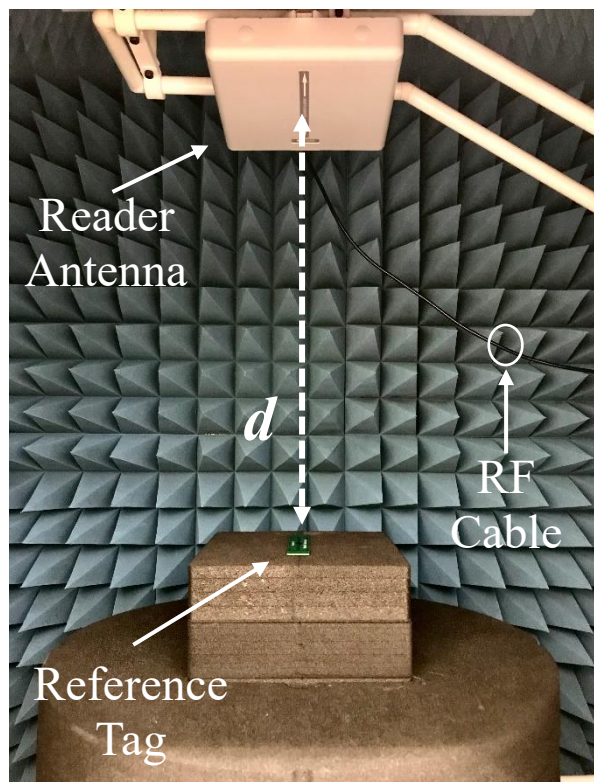


Figure 2.19: Actual measurement setup in anechoic cabinet.

CHAPTER 3

DIPOLAR TAG ANTENNA WITH A TOP-LOADING INDUCTIVE CHANNEL WITH BROADRANGE FREQUENCY TUNING CAPABILITY

3.1 Introduction

Since the structure of a dipolar antenna is simple and easy to design, commercially, various dipolar antennas (Rao et al., 2005a) have been employed for designing passive tags for a long time. However, such antennas have the disadvantage of having a large size, making them not suitable to be mounted on small objects. Furthermore, when a dipole is placed on a metal surface, an opposite image current will be generated, which cancels out the current on the radiator, resulting in significant attenuation of radiation efficiency, fluctuation of antenna impedance, and deviation of operating frequency (Dobkin and Weigand, 2005). To improve, a Perfect Electric Conductor (PEC) is inserted between the dipolar patch and the backing metal for isolation (Best, 2004, Genovesi and Monorchio, 2010). Similarly, the introduction of Artificial Magnetic Conductor (AMC) (Kim and Yeo, 2008) and Electromagnetic Bandgap (EBG) (Li et al., 2020) can also achieve the same effect. Nevertheless, the sizes of AMC and EBG are usually large and not suitable for mounting on small objects. Moreover, the operating frequency of such a tag antenna can't be re-located easily as the phase response of an AMC/EBG structure is only valid in a certain frequency range. Usually, re-locating the tag operating frequency requires a full cycle of re-design

process.

Meandering a radiation arm (Chen and Tsao, 2010a) or folding a patch (Koo et al., 2011) are among the design methods that can be used for reducing the tag antenna profile and tuning the tag resonant frequency. In addition, the introduction of cutting slots and notches on a radiator patch can also increase the antenna inductance for tuning the tag resonance (Michel et al., 2018, Liu et al., 2018). Serrating the edges of the folded patch (Bong et al., 2016) was also found to be an effective method for increasing the current paths for tuning the tag resonant frequency effectively. The abovementioned techniques are commonly applied for tag frequency tuning. However, they require changing the structure of the radiator, causing the radiation performance and antenna bandwidth to have significantly deteriorated. Limited by the antenna structure itself, modifications made to the tag antenna are only able to shift the operating frequency in a pretty narrow range. Embedding shorting elements such as vias/pins (Lin et al., 2012, Zhang and Long, 2014) in the antenna structure can also change the frequency characteristics tunable by moving the positions of the vias/pins, which are commonly applied in high-dielectric substrates, such as ceramic tags (Kim et al., 2008). Shorting vias can also be incorporated with a patch for designing the planar inverted-L antenna (PIFA) (Casula et al., 2016, Lee et al., 2018b) which has quarter-wavelength electrical characteristic and small physical footprint. However, manufacturing vias requires additional printed-circuit-board (PCB) procedures. Tolerances in the positions of the shorting vias can cause the tag resonance to fluctuate significantly. It is almost impossible to re-tune the tag resonant frequency after the vias are made as it

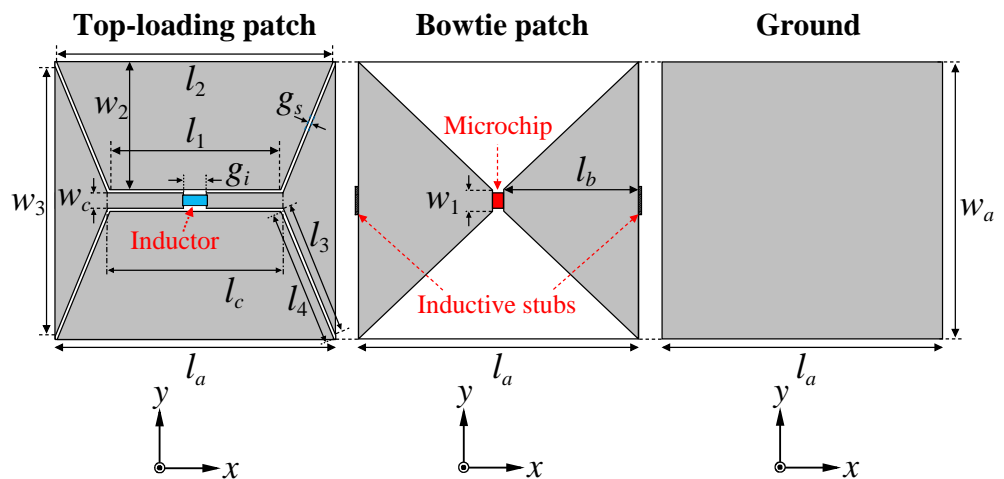
involves changing the internal structure.

In this chapter, for the first time, an inductive channel is incorporated with the top-loading patch of a dipolar tag antenna for achieving arbitrary frequency tuning capability in a broadrange across the UHF passband. The loading patch is composed of an inductive channel and two trapezoidal patches, simultaneously introducing inductive and capacitive loading effects for reducing the resonant frequency to the UHF band. Here, a lumped inductor is tactfully embedded into the channel for introducing arbitrary inductance to the tag structure for adjusting and tuning its resonant frequency, without needing to modify the antenna structure. Although the application of a simple top-loading patch was found to be able to enhance the electric and magnetic fields of a tag antenna (Niew et al., 2019), however, it was usually very difficult to tune the tag resonance without changing the antenna structure and to introduce sufficient reactance to the tag configuration. In this project, we have solved the two problems by introducing an inductive channel to the top-loading patch. With the inclusion of the external lumped inductor into the channel, the possible inductance range has virtually been extended much further. As a result, the tag resonant frequency can be easily tuned in a broadrange without modifying the antenna structure itself. It will be shown that the proposed tag antenna can be easily tuned to any operating frequency, without causing much degradation to its read performance. The structure of the chapter has been organized in the following way. In Section 3.2, the antenna configuration is briefly described. The antenna's structural evolution will be discussed simultaneously along with the impedance and field analysis. An equivalent circuit model will be proposed for describing the antenna

impedance characteristics and the key design parameters will be carefully analyzed in Section 3.3. Finally, the proposed tag antenna is experimentally tested for evaluating its read performances.

3.2 Configuration and Design Procedure

The proposed tag antenna design is shown in Figure 3.1. It comprises three metallic layers: a top-loading patch, the middle bowtie dipole patch, and a bottom ground plane. All the metal patterns are imprinted on the copper foil ($9\ \mu\text{m}$) of a single-layer flexible PET (polyethylene terephthalate, $50\ \mu\text{m}$) substrate through the standard Printed-Circuit-Board (PCB) etching processes. Here, two pieces of polyethylene foams ($\epsilon_r = 1.03$ and loss $\tan \delta \sim 0.0001$), all of which have the dimension of $l_a = 50\ \text{mm}$, $w_a = 50\ \text{mm}$, $h_s = 1.6\ \text{mm}$, are employed to separate the three metallic layers. The foam blocks are also forming the structural support so that the tag structure can hold itself.



(a)

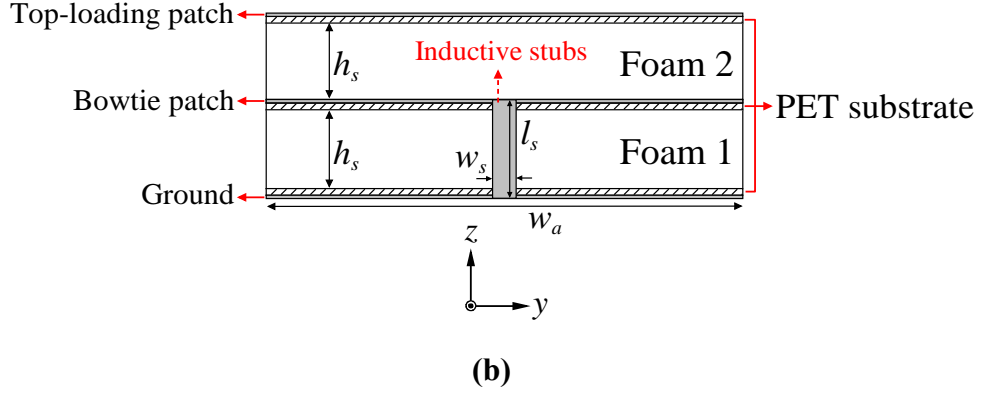


Figure 3.1: Configuration of the proposed tag antenna shown in (a) top view and (b) side view.

The microchip being employed here is a UCODE 8/8m (NXP, 2020) flip chip that is tested with an actual read sensitivity of -20.85 dBm, along with an input impedance of $13 - j191 \Omega$ at 915MHz. With reference to Figure 3.1, the chip is bonded across the center of two flaps of identical triangular patches forming the middle bowtie antenna ($w_1 = 4$ mm, $w_a = 50$ mm, $l_b = 24.385$ mm). Two inductive stubs ($l_s \times w_s$) are then employed to connect the two edges of the bowtie patches to the bottom ground for regulating the current flows. The ground here is also functioning as an isolator for mitigating the impact of the backing metallic object. The construction process of the tag antenna is now briefly described. First, the middle bowtie, two inductive stubs, and two identical ground patches are made on the single surface of a single piece of PET inlay. Then, the inlay is then folded with reference to the center of each of the inductive stubs and wrapped around the first piece of foam (Foam 1 with $l_a = 50$ mm, $w_a = 50$ mm, $h_s = 1.6$ mm) to form the bowtie patch antenna and its ground. After the formation of the bowtie antenna, subsequently, the second piece of foam block (Foam 2), which has the same footprint and profile as the antenna, is directly attached on top to be used as a support for the loading patch. The loading patch

at the top is mainly composed of a narrow channel and two trapezoidal patches. With reference to Figure 3.1(a), a narrow gap of $g_i = 1.00$ mm is reserved at the middle of the channel to bond surface-mount-device (SMD) inductor ($L_p = 2$ nH, component size = 1.6 mm \times 0.8 mm) for further enhancing the inductance effect. It will be shown later that the lumped inductor can be employed as an effective tuning element. Here, the inductive channel of the top-loading patch is aligned in parallel to the currents of the bowtie patch so that it can regulate the current flows. The two slits formed between the inductive channel and the two trapezoidal patches can also introduce additional capacitance. The design and optimization processes are all conducted using the CST software. The optimized values of the design parameters shown in Table 3.1. The components of the prototype are further illustrated in Figure 3.2.

Table 3.1: Optimized parameters of the proposed design.

Parameter	(mm)	Parameter	(mm)
l_a	50.00	w_a	50.00
l_b	24.385	w_c	1.80
l_c	32.76	w_s	0.50
l_s	1.718	w_1	4.00
l_1	32.36	w_2	23.80
l_2	49.68	w_3	49.12
l_3	25.18	g_s	0.30
l_4	25.33	g_i	1.00
h_s	1.60		

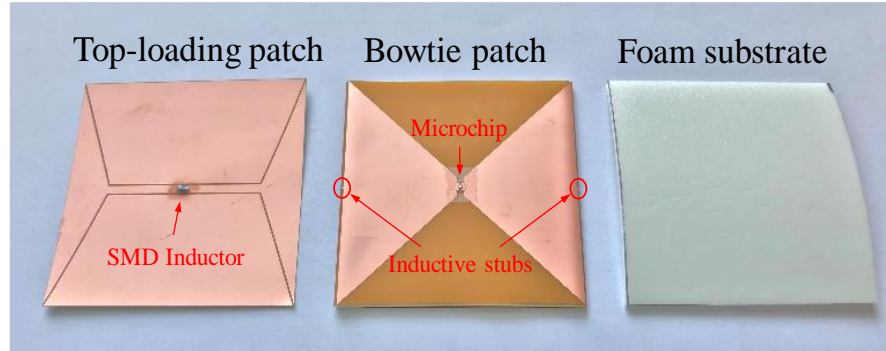
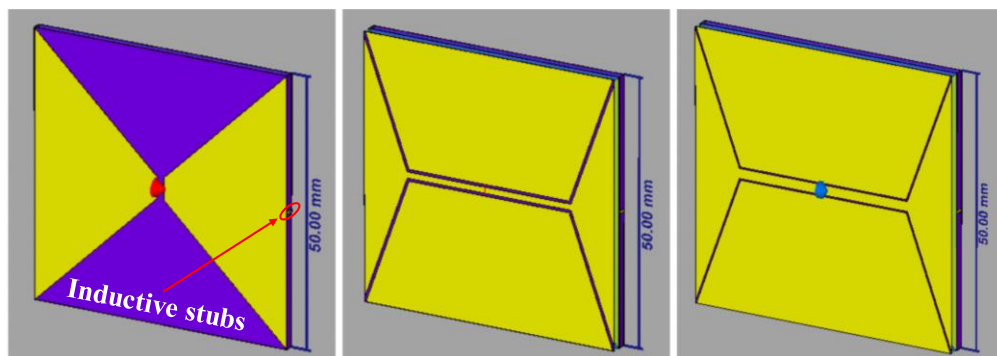


Figure 3.2: Components of the prototype.

The proposed tag antenna is designed to be applied on metal surface. The design process was started with simulation, where the microchip was replaced by an external discrete port, and the impedance value of the port was defined to be the chip impedance. It is placed on a square metal plate with a dimension of 20 cm in both the simulation and measurement. The design was begun by simulating the single-layer bowtie antenna (without loading patch), with the top-loading patch and Foam 2 removed, and this intermediate configuration is named as *Configuration A*, as shown in Figure 3.3(a). The corresponding antenna impedance is further depicted in Figure 3.4(a), which has a tag resonance at 1281 MHz, being far beyond the regulated UHF band. The input impedance and realized gain are found to be $3.36 + j191.7 \Omega$ and -1.278 dBi, respectively, with a poor power transmission coefficient of 0.61. By including a top-loading patch with a narrow channel (without inductor), as can be seen in *Configuration B* in Figure 3.3(b), the tag resonant frequency can be successfully brought down to 914 MHz, shown in Figure 3.4(a), with an input impedance of $6.74 + j191.74 \Omega$. Now, the operating frequency is in the regulated US band with a power transmission coefficient = 0.91. The inclusion of the top-loading patch that has an inductive channel causes the tag to become more inductive, which in turn

increases the reactance significantly. Nevertheless, to drastically reduce the operating frequency, it is essential to continuously decrease the width of the inductive channel. Narrowing the channel width is effective in increasing the tag inductance. However, there is a limit in increasing tag inductance in such a way as a very narrow channel can be very difficult to be implemented physically. Fabrication of narrow lines can be very difficult for the regular printed-circuit board (PCB) etching processes. To further enhance the inductance, a small gap is etched at the center of the inductive channel of the top-loading patch for accommodating a lumped inductor (2 nH), and this structure is named *Configuration C*, which is also our final tag antenna configuration, as depicted in Figure 3.3(c). The simulated impedance in Figure 3.4(b) shows that loading a lumped SMD inductor to the inductive channel can further enhance the tag inductance significantly and it has successfully brought down the tag resonance to 868 MHz, which is usable for the regulated European passband. The corresponding antenna impedance is $7.35 + j191.4 \Omega$ and the power transmission coefficient is 0.92. Loading an external lumped component, obviously, has enabled the channel inductance to be made very large and controllable arbitrarily. In this case, the antenna reactance is quite close to achieve conjugate match, although the antenna resistance is slightly different.

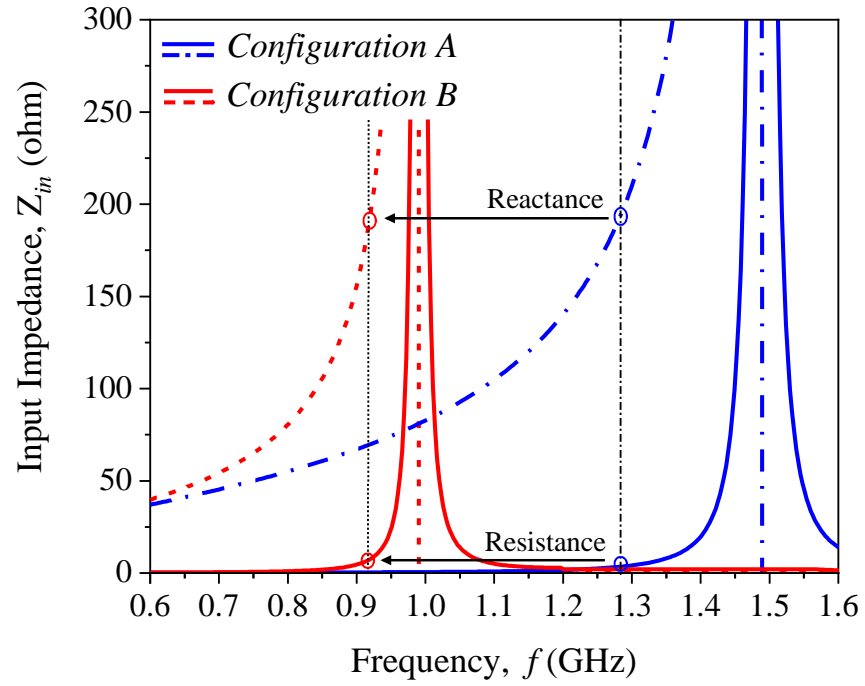


(a)

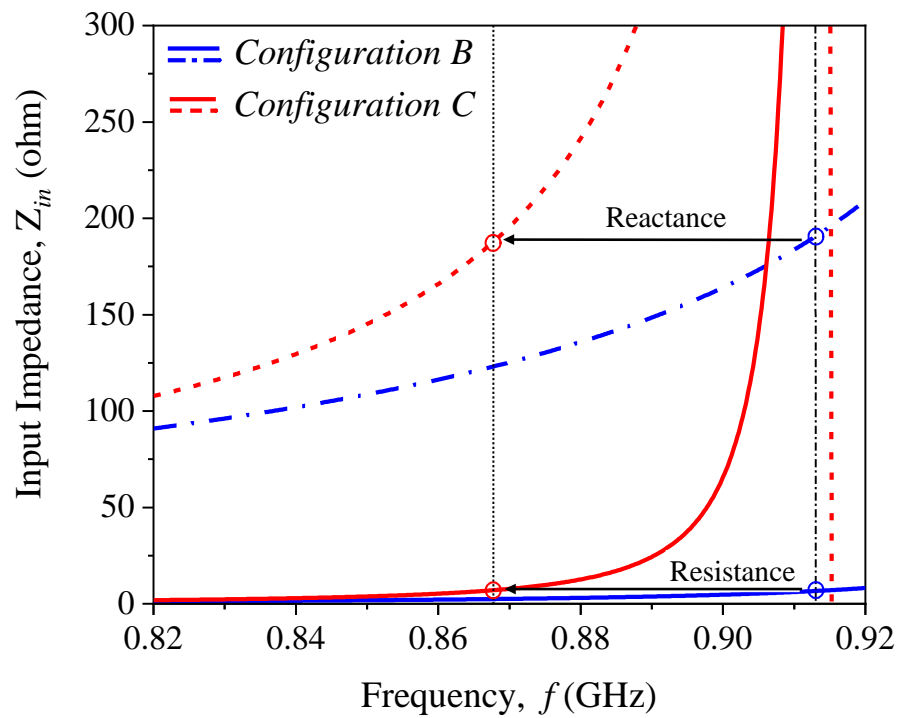
(b)

(c)

Figure 3.3: Structural evolution of the antenna design. (a) *Configuration A*. (b) *Configuration B*. (c) *Configuration C*.



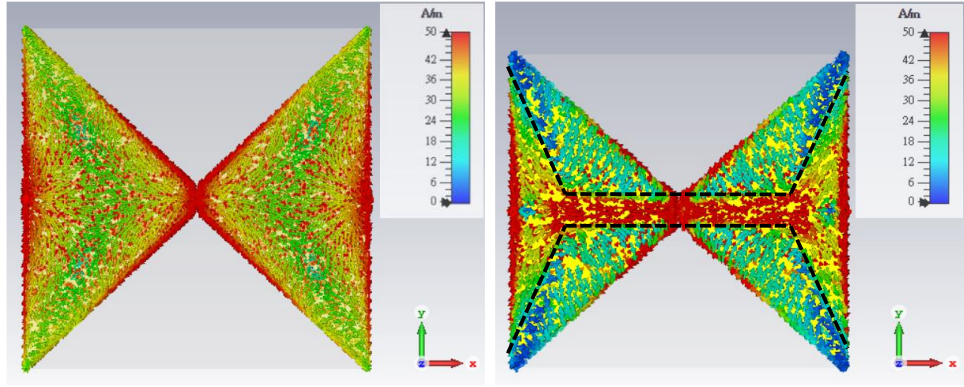
(a)



(b)

Figure 3.4: Comparison of antenna impedances for (a) *Configuration A* and *Configuration B*. (b) *Configuration B* and *Configuration C*.

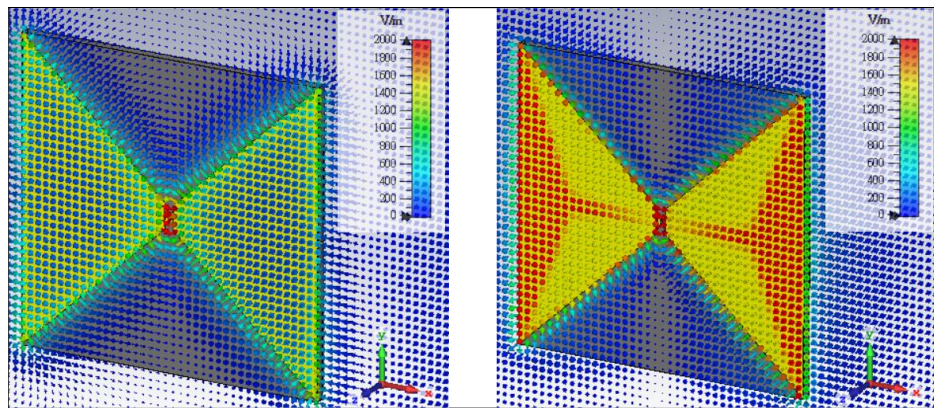
Next, the effects of the top-loading patch and the inductive channel are further investigated. The surface currents, electric field, and magnetic field distributions of *Configuration A* and *Configuration C* are compared in Figures 3.5, 3.6, and 3.7 at their respective tag resonant frequencies. With reference to Figures 3.5(a) and (b), currents are induced on the top-loading patch and high current intensity is observed along the inductive channel, showing that it is effective in introducing inductance to the tag antenna. By justifying from the electric and magnetic field vectors, as can be seen in Figure 3.6 and 3.7, a TM mode has been observed, and the top-loading patch is found to have enhanced the electric and magnetic field intensities significantly. High magnetic field intensity along the channel, as can be seen in Figure 3.7(b), has further confirmed the formation of the highly inductive channel, which can in turn be effectively used for regulating the current flows along the channel. Although the effect of a loading patch was also studied in (Niew et al., 2019), it was very difficult to introduce sufficient inductance in that antenna structure. In our new design here, arbitrarily high inductance value can be easily introduced by the adjusting the channel width w_c and by controlling the external lumped inductor. Design analysis of w_c and L_p will be presented in the next section.



(a)

(b)

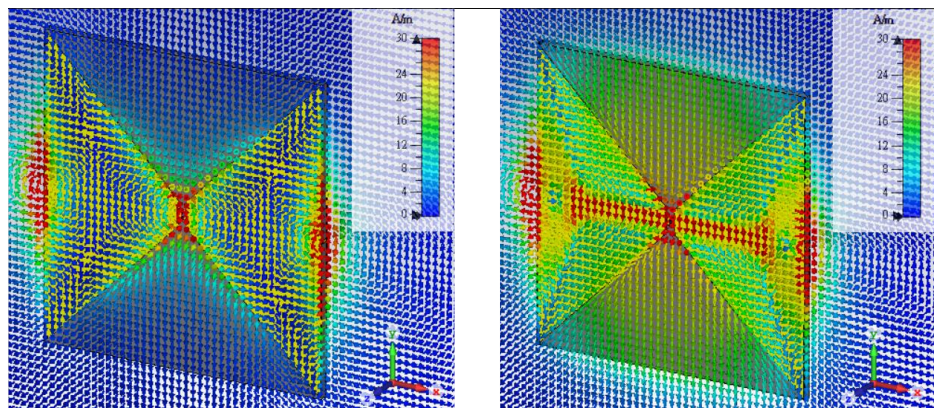
Figure 3.5: Current distributions of (a) *Configuration A* and (b) *Configuration C*.



(a)

(b)

Figure 3.6: Electric field distributions of (a) *Configuration A* and (b) *Configuration C*.



(a)

(b)

Figure 3.7: Magnetic field distributions of (a) *Configuration A* and (b) *Configuration C*.

3.3 Equivalent Circuit Model and Parametric Analysis

The equivalent circuit of the proposed tag antenna is shown in Figure 3.8. It is developed for analyzing the impedance characteristics. Since the middle-layer bowtie antenna is composed of a pair of triangular patches, each of them can be represented by an RLC parallel resonant circuit labelled as R_b , L_b , and C_b . The loading inductance L_b (in nH) can be calculated by using $L_b = 200l_b \{ \ln [2l_b / (0.5(w_1 + w_a) + t_c)] + 0.50049 + [(0.5(w_1 + w_a) + t_c) / 3l_b] \}$ (Greenhouse, 1974). In view of the effect of the electric fields, the space between the radiation patch and ground plane can be regarded as a pair of parallel capacitive plates, in which the capacitance (in pF) can be evaluated using the equation $C_b = \epsilon_r \epsilon_o A_e / h_s$ (Yang et al., 2011), where h_s and ϵ_r are the thickness of polyethylene foam and the relative permittivity, respectively. The effective area of the patch is given by $A_e = l_b(w_1 + w_a) / 2$. The resistance of the bowtie patch is obtained using a macro model method (Kim and Yeo, 2010), and the shorting stub is represented by the resistance R_s and the inductance L_s being composed in series. The resistance of the shorting stubs is $R_s = 2[(\rho l_s) / (w_s / h_s)] [K_c / (1 - e^{-x})]$ (Payne, 2017), where $\rho = 1.72 \times 10^{-8} \Omega\text{m}$ is the resistivity of copper, and $K_c = 1.94$ is the current crowding factor. $x = [2(1 + h_s / w_s)] \times (\delta / h_s)$, where $\delta = 2.18 \times 10^{-6}$ m is the skin depth of copper. The stub inductance can be calculated through the equation $L_s = 400l_s \{ \ln [2l_s(t_c + w_s)] + 0.50049 + [(t_c + w_s) / 3l_s] \}$. Subsequently, the equivalent model of the loading patch is discussed. Since the patch is directly stacked on top of the

bowtie antenna, it can be linked to the two ends of the RLC resonator in parallel. The inductive stubs with high inductance can be described by serial connection of a resistor (R_s) and an inductor (L_s). The channel resistance can be approximated $R_c = \{[\rho K_c(l_c - g_i)]/[t_c w_c(1 - \exp(-2\delta/t_c(1 + t_c/w_c)))]\}$. Meanwhile, the channel's equivalent inductance comprises the effective inductance of the microstrip line, which can be described as $L_c = 200(l_c - g_i)\{\ln [2(l_c - g_i)/(t_c + w_c)] + 0.50049 + [(t_c + w_c)/3(l_c - g_i)]\}$, and the lumped inductor $L_p = 2$ nH. The two trapezoidal patches with capacitive loading effect are placed in parallel on both sides of the channel and they can be calculated by $C_p = \epsilon_r \epsilon_o A_p / h_s$, where A_p is the area of each of the trapezoidal patches. The values of the proposed equivalent circuit were calculated by the aforementioned equations, as shown in Table 3.2.

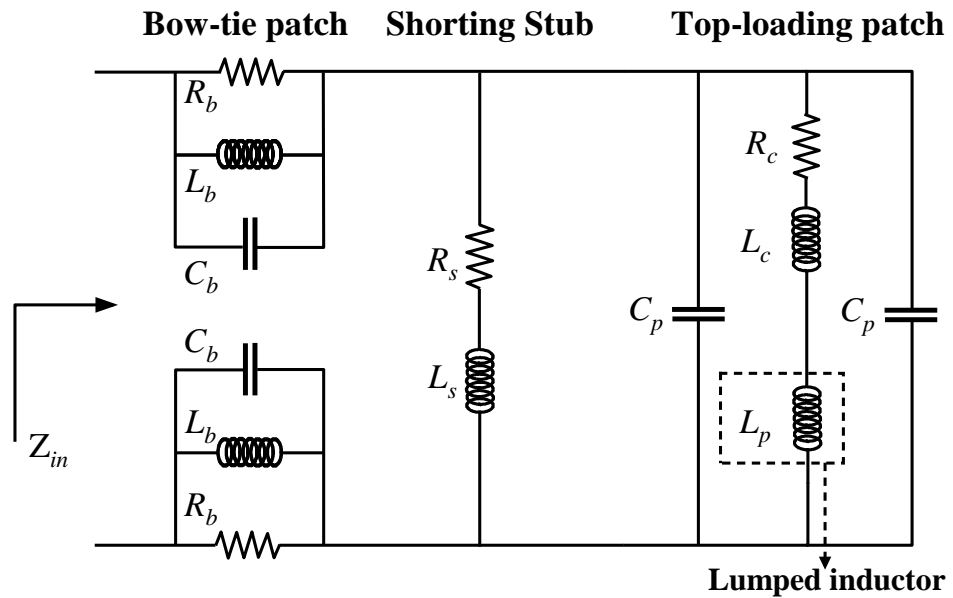


Figure 3.8: Equivalent circuit model for the proposed tag antenna.

Table 3.2: Parameters of the proposed equivalent circuit model.

Component	Value	Component	Value
R_b	0.1 Ω	R_c	92 m Ω
L_b	7.124 nH	L_c	28.02 nH
C_b	3.753 pF	L_p	2.0 nH
R_s	3.0 m Ω	C_p	5.53 pF
L_s	3.128 nH		

With reference to Figure 3.8, the two RLC resonators, where $Z_b = R_b || L_b || C_b$, are connected in series with the loading circuit Z_L , which includes the shorting stub and the top-loading elements. The input impedance of the proposed antenna can be calculated by equation 3.1.

$$Z_{in} = 2Z_b + Z_L \quad , \quad (3.1)$$

where

$$Z_b = \frac{\omega^2 R_b L_b^2 + j\omega R_b^2 L_b (1 - \omega^2 L_b C_b)}{(R_b - \omega^2 R_b L_b C_b)^2 + (\omega L_b)^2} \quad , \quad (3.2)$$

$$Z_L = \frac{j\omega(L_s + L_c + L_p + 2C_p \beta) + R_s + R_c}{\beta} \quad , \quad (3.3)$$

and

$$\beta = (R_s + j\omega L_s)[R_c + j\omega(L_c + L_p)] \quad , \quad (3.4)$$

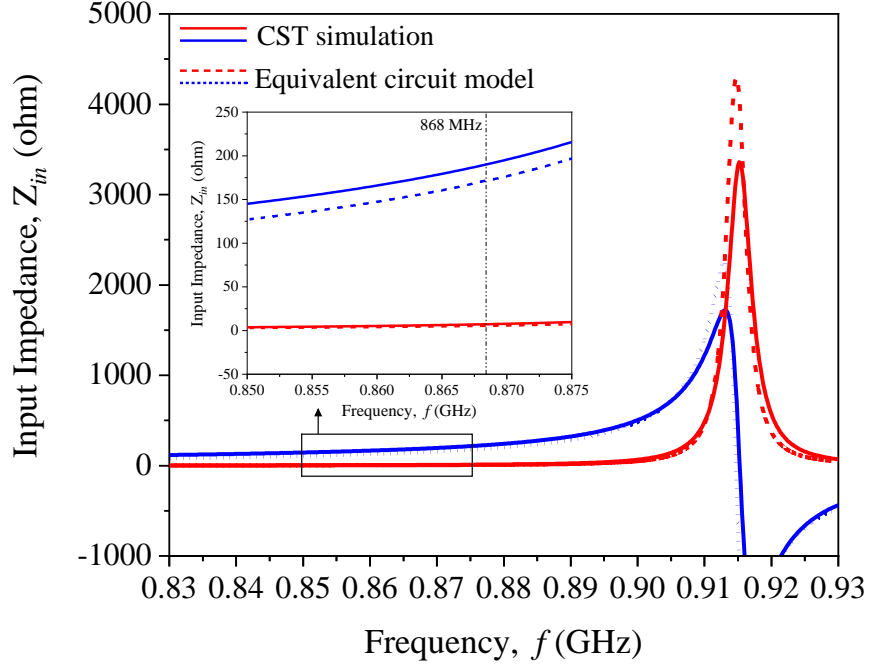
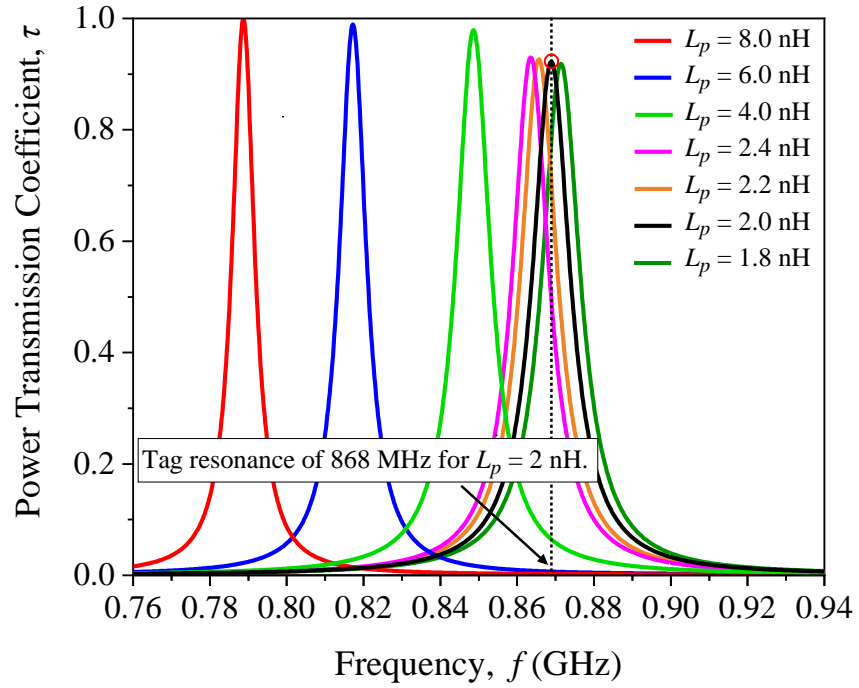


Figure 3.9: Simulated and modeled input impedances of the proposed tag antenna.

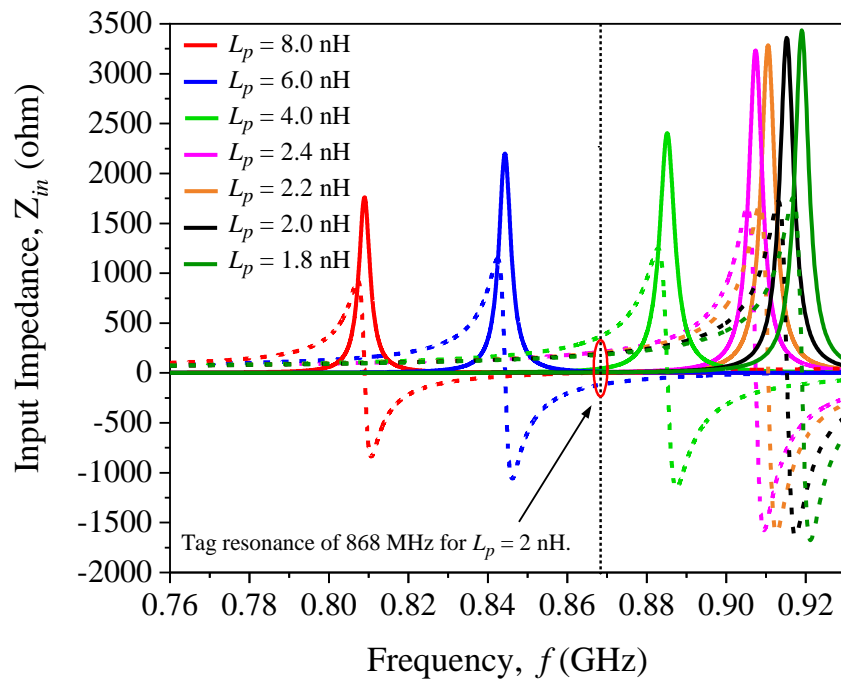
The antenna impedances generated by the CST full-wave simulation (solid curves) and the equivalent circuit model (dashed curves) are compared in Figure 3.9. The dashed curves are both generated by eqn. (1), which is derived from the equivalent circuit model. They are in reasonable agreement with those generated by full-wave simulation. It shows that the equivalent circuit can reasonably describe the impedance characteristics of the antenna. It should be mentioned that mutual coupling effects are not considered in this case.

A design analysis has been performed to further investigate the effects of the top-loading inductive channel. First, to study the influence of the external lumped inductor embedded in the channel, at this time, the channel width w_c is fixed at 1.8 mm. As can be seen in Figure 3.10, when L_p is slightly increased from 1.8 nH to 2.4 nH with an interval of 0.2 nH, the tag resonant frequency

reduces from 871.4 MHz to 863.6 MHz, with a rate of change of 2.6 MHz/nH. Then, the inductance is dramatically increased at a larger interval of 2 nH to observe its effect. When the inductance value is increased from 4 nH to 8 nH, the tag resonant frequency drops from 848.8 MHz to 788.8 MHz with a steady change rate of 30 MHz/nH. To sum up, the value of inductance is inversely proportional to the tag resonant frequency. The loading inductor in the channel is proven to be able to control the tag resonant frequency proportionally. The power transmission coefficient of all the cases of 1.8 nH – 2.4 nH has the similar value of 0.91. It can reach 0.97 when the inductance is in the range of 4 nH – 8 nH. The slight increase in τ is partially contributed by the increase in tag resistance. With reference to the datasheet of the SMD inductors, a larger inductance value has a higher internal resistance, which indirectly causes the antenna resistance to increase, making it match even better with the chip impedance. Next, by fixing L_p at 2 nH, the impact of the channel width w_c is further investigated. Figure 3.11 shows the curves of the power transmission coefficient and input impedance when the proposed channel width is increased and decreased slightly. When w_c is reduced from 2.6 mm to 1.0 mm at an interval of 0.4 mm, the tag resonant frequency decreases from 879.2 MHz to 855.2 MHz with a rate of 6 MHz/mm. This is because a narrower channel is more inductive and it has a higher inductance. Obviously, the tag resonant frequency can be tuned by the inductive channel and the loading inductor. However, the channel width can't be made too narrow as it is difficult to be fabricated using the standard PCB processes in practice. This problem can be easily overcome by engaging the external lumped inductor.

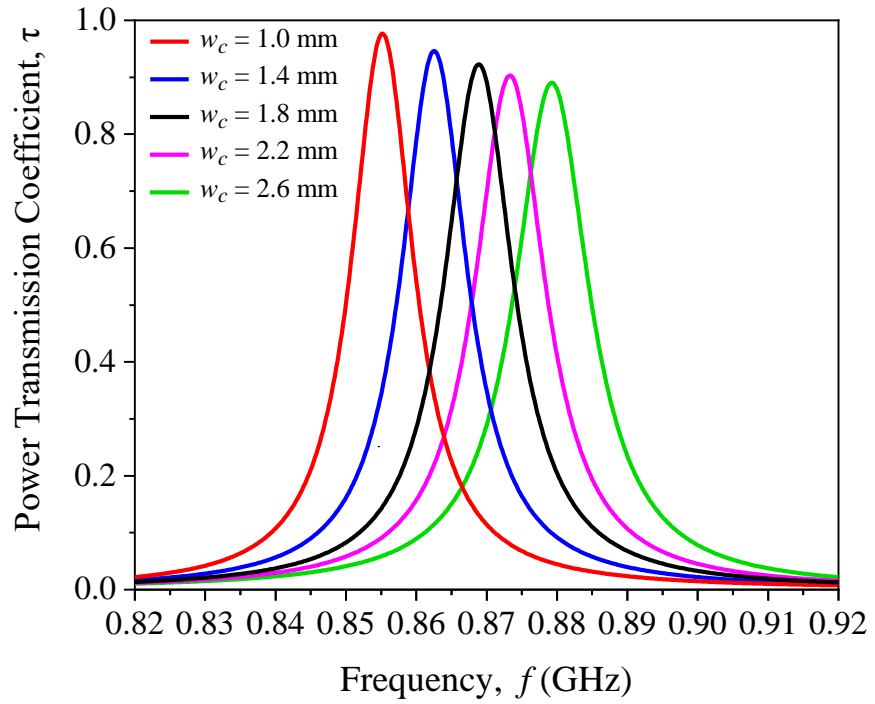


(a)

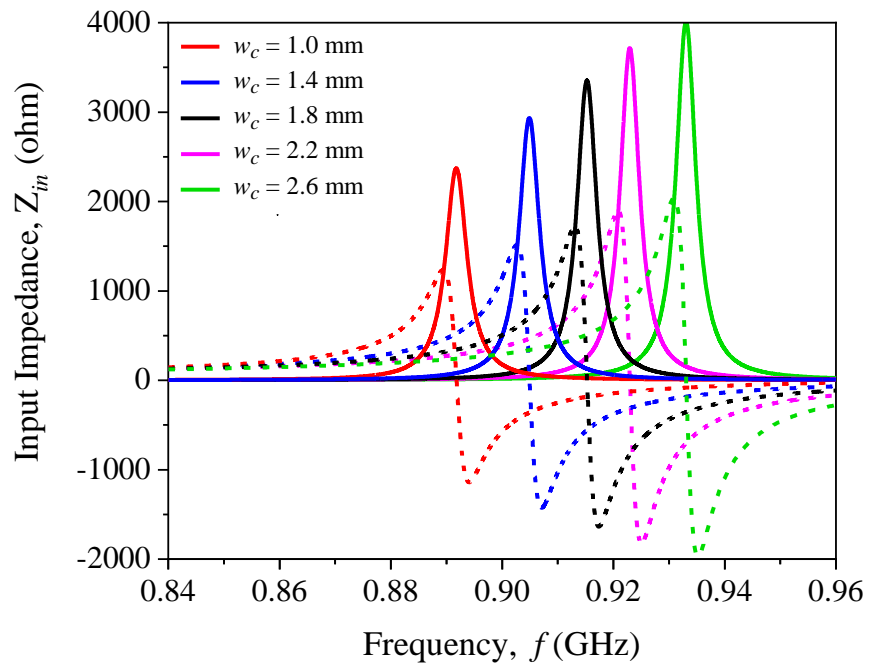


(b)

Figure 3.10: Effects of varying inductance L_p on the (a) power transmission coefficient, (b) input impedance.



(a)

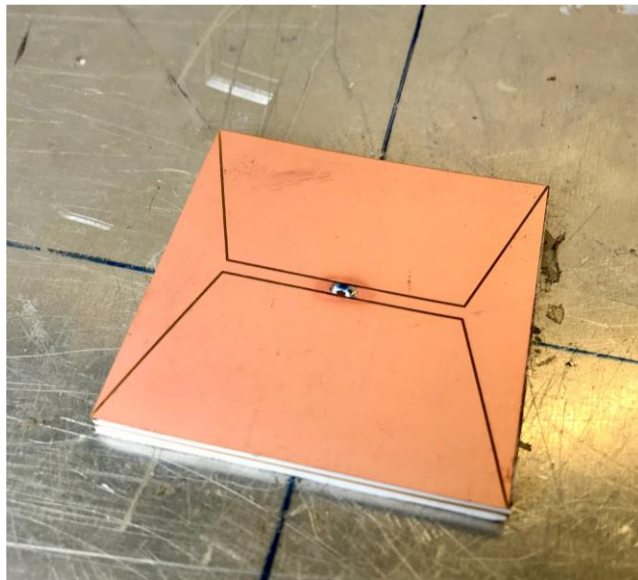


(b)

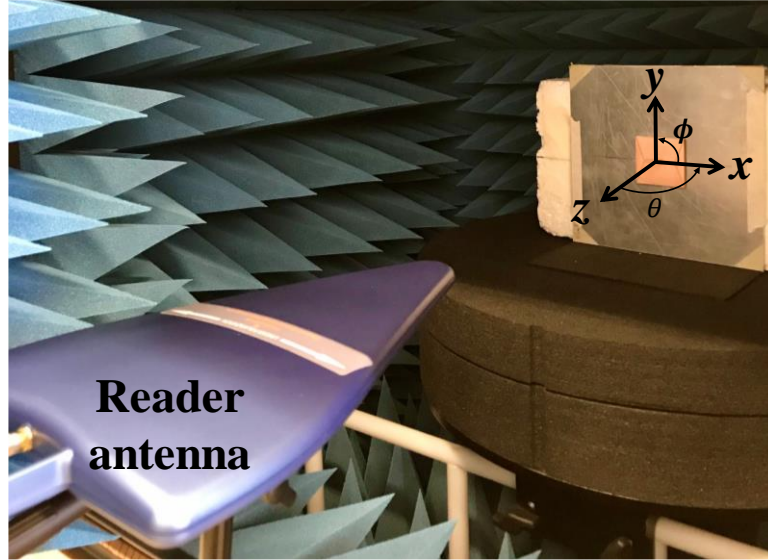
Figure 3.11: Effects of varying channel width w_c on the (a) power transmission coefficient, (b) input impedance.

3.4 Results and Discussion

The performances of the proposed tag antenna were tested using the Voyantic Tagformance measurement system (Voyantic, 2012) to characterize its reading distances (R) and realized gains (G_r). Figure 3.12 shows the experimental setup for measuring the prototype in the anechoic chamber. With reference to Figure 3.12(a), the tag is placed at the center of an aluminum plate with a size of 20 cm \times 20 cm, which is similar to that used by the simulation. The signal power to excite and detect the tag comes from a linearly polarized reader with a gain of 8 dBi, which is always aligned with the tag-under-test and maintained at a fixed distance of 52 cm. Before performing measurements, the system was first calibrated by using a reference broadband tag for calculating the path loss (P_l).



(a)

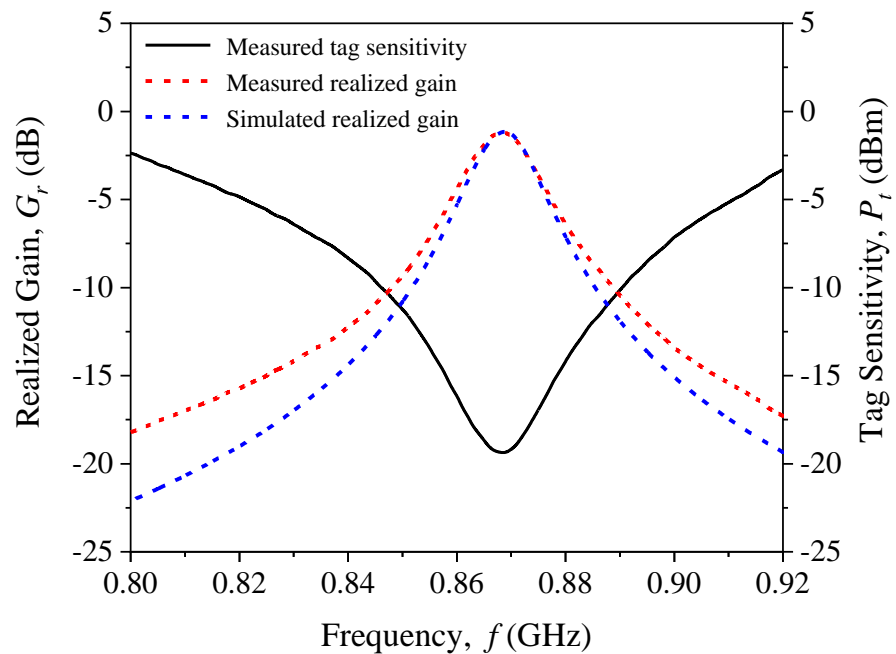


(b)

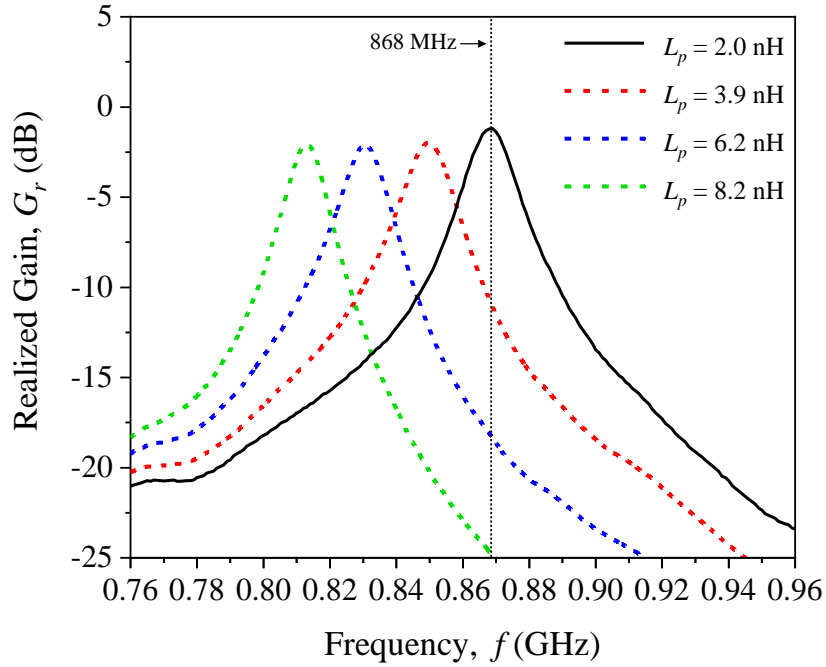
Figure 3.12: (a) The prototype is placed on the center of the metal plate. (b) Measurement setup in the anechoic cabinet.

The realized gain of the antenna can be described as $G_r = P_c/P_l \times P_t$, where P_c is the read sensitivity (-20.85 dBm) of the chip, P_t is the lowest power from reader to activate the tag, and P_l is the path loss including the free space loss and cable loss. First, the measured results of the realized gain and tag sensitivity of the proposed tag are shown in Figure 3.13(a). The maximum achievable tag sensitivity is measured to be $P_t = -19.38$ dBm at 869 MHz, with a measured realized gain is $G_r = -1.2$ dB, which is slightly higher than its simulated counterpart of $G_r = -0.51$ dB at 868 MHz. The proposed tag antenna was also tested when the top-loading inductive channel was soldered with different inductance values, as shown in Figure 3.13(b). Three inductances (3.9 nH, 6.2 nH, and 8.2 nH) were selected for the experiments due to the limitation of the inductance values of inductors kit. For $L_p = 3.9$ nH, the tag resonant frequency is measured to be 0.85 GHz with a realized gain of $G_r = -1.9$ dB. The tag resonance had shifted to 0.83 GHz and 0.814 GHz, respectively, for the

inductances 6.2 nH and 8.2 nH, both of which has a realized gain of -2 dB. The changing trend agrees well with the observation in Figure 3.10. This feature is very useful as the tag resonant frequency can now be adjusted arbitrarily and in a broader range, without compromising the realized gain, by simply employing a lumped inductor. Also, it has been experimentally proven that the top-loading inductive channel can alter the antenna reactance effectively for tuning the tag resonant frequency. Although other tuning mechanisms such as serrations (Bong et al., 2016) and slotlines (Bong et al., 2017) can also be used to tune the tag resonant frequency, they can cause the read performances, particularly the realized gain, to deteriorate significantly due to the decrease in the Q -factor. For a tag antenna, the read distance is directly proportional to the Q -factor.



(a)



(b)

Figure 3.13: (a) Measured and simulated realized gains and the measured tag sensitivity when the tag is placed on a 20 cm \times 20 cm aluminium plate. (b) Measured realized gains when the inductive channel is loaded with a lumped inductor with different values.

Next, the read performances of the proposed tag antenna are characterized. In the measurement processes, the proposed tag prototype is placed at the center of the chamber, as defined by the Cartesian coordinate system in Figure 3.14. Here, the reader antenna is always maintained at a fixed distance along the z -axis from the tag-under-test. Rotating the tag around its own x - and y -axis, respectively, has enabled measuring the read patterns in the yz - and xz -planes, which are shown in the polar plot, Figure 3.15(b). Obviously, the definitions of the xz - and yz -planes are the same as the conventional spherical coordinate system. It should be mentioned that the xy -plane read pattern, which is obtained by spinning the tag around its own z -axis, is different from the

conventional coordinate. It signifies the polarization characteristics of the tag antenna in the boresight direction. The xy -plane read pattern is measured in Figure 3.15(a) at the tag resonance of 868 MHz. With reference to the figure, this tag antenna is found to be linearly polarized along the x -axis ($\theta = 0^\circ$ or 180°) in the boresight direction, achieving a maximum reading distance of 14 m. The polarization appears to be in the same direction as the current flows along the inductive channel on the top-loading patch. From the cutplane polar plots in Figure 3.15(b), the read patterns have broadside feature in both the yz - and xz -planes.

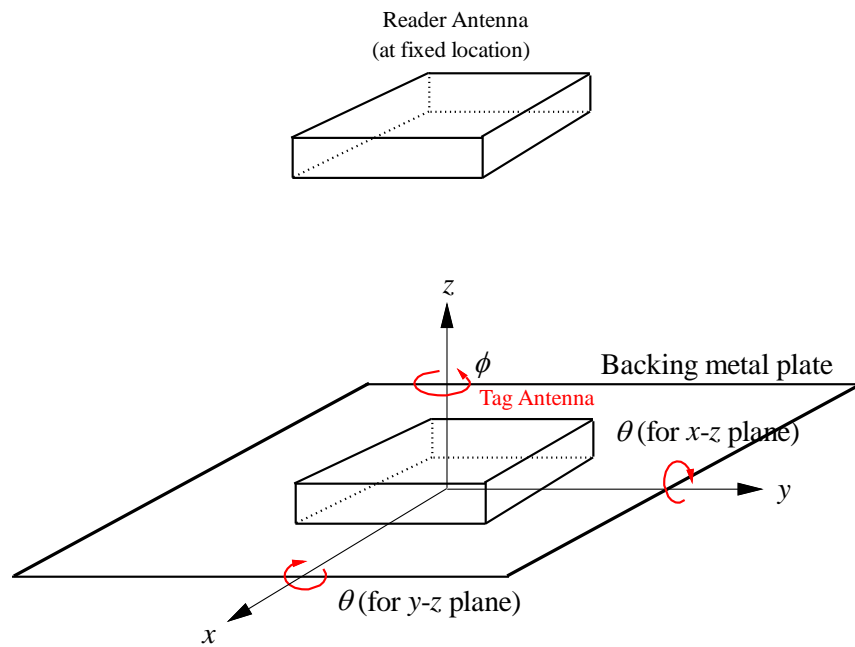
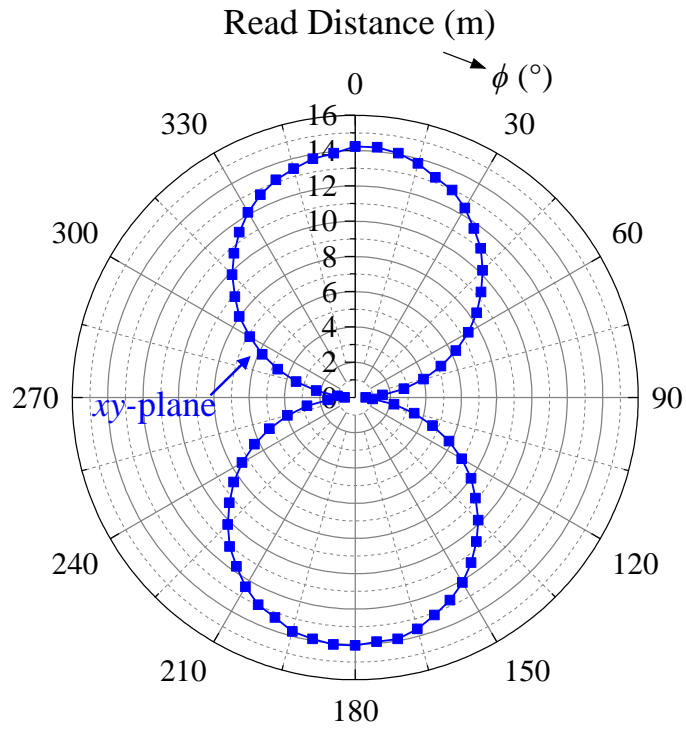
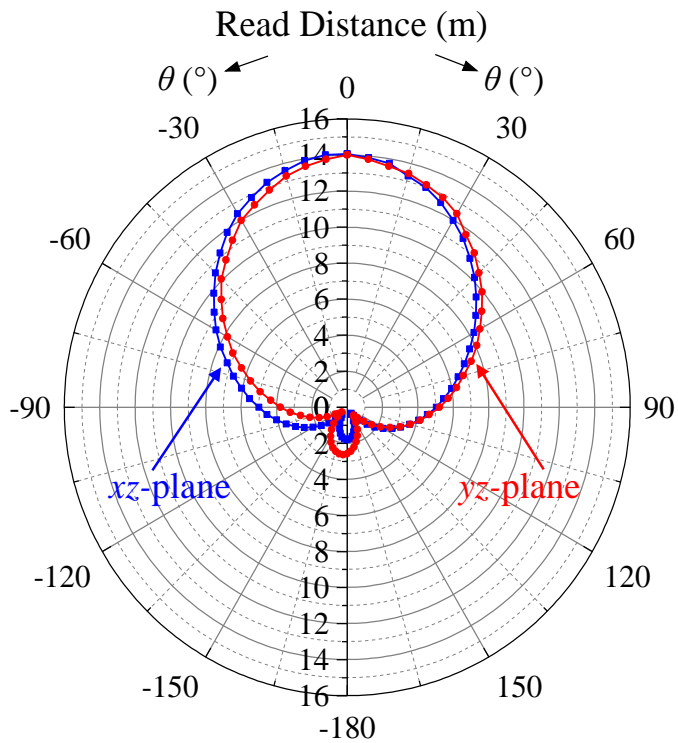


Figure 3.14: Plane definition for measuring the read patterns.



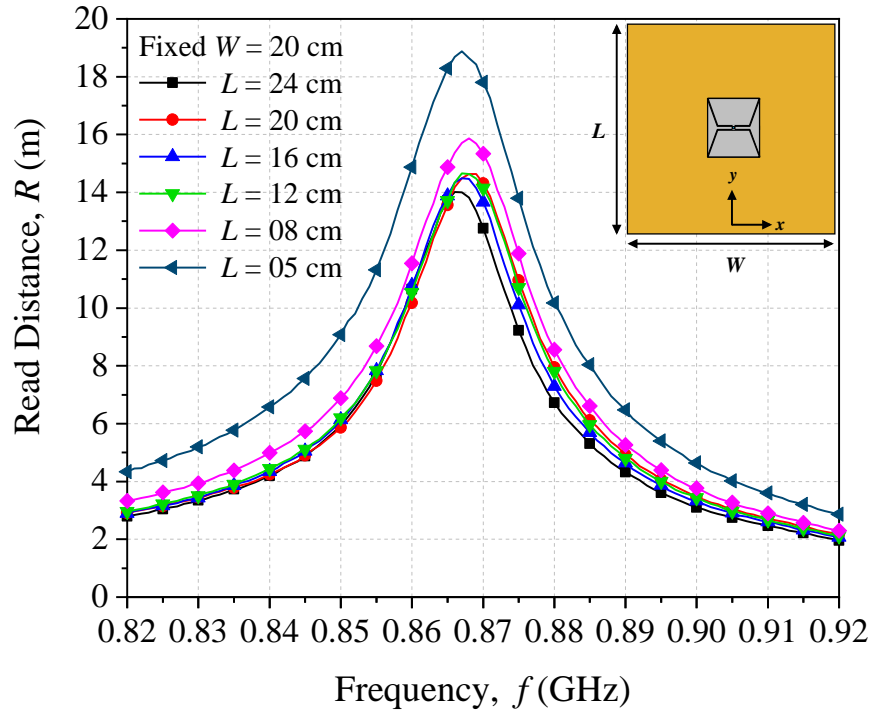
(a)



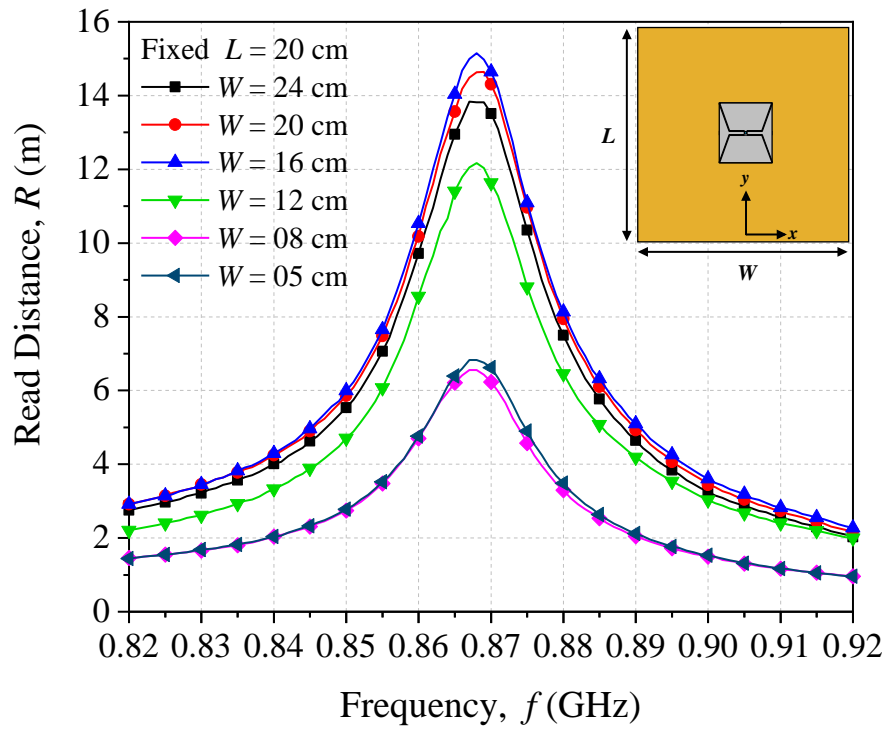
(b)

Figure 3.15: Measured read patterns of the proposed tag antenna in the (a) xy -plane, (b) xz - and yz -planes at 868 MHz.

Since the proposed tag antenna is designed to be applied on metallic surface, it is tested on aluminum plates with different sizes. In experiment, the tag prototype was placed at the center of an aluminum plate ($W \times L$) with a thickness of ~ 5 mm. Maximum read distances for the plates were gradually taken in the boresight ($\theta = 0^\circ$) for comparison. As shown in Figure 3.16(a), when W is fixed at 20 cm, by sequentially increasing L from 5 cm to 24 cm, the reading distance is being able stably maintained at 14 m, especially when L is 5 cm, a distance close to 19 m can be obtained. Next, the plate width W is slightly increased while L is fixed at 20 cm, and the results are shown in Figure 3.16(b). The reading distance is only 7 m when W is in the range of 5 – 8 cm. This is because this tag antenna is linearly polarized in the x -direction, but the plate width is causing the electric fields in the boresight to weaken, which can reduce the reading distance. Then, when W is increased from 12 cm to 24 cm, the read distance is found to have increased from 12 m to 14 m, with a stable reading level.



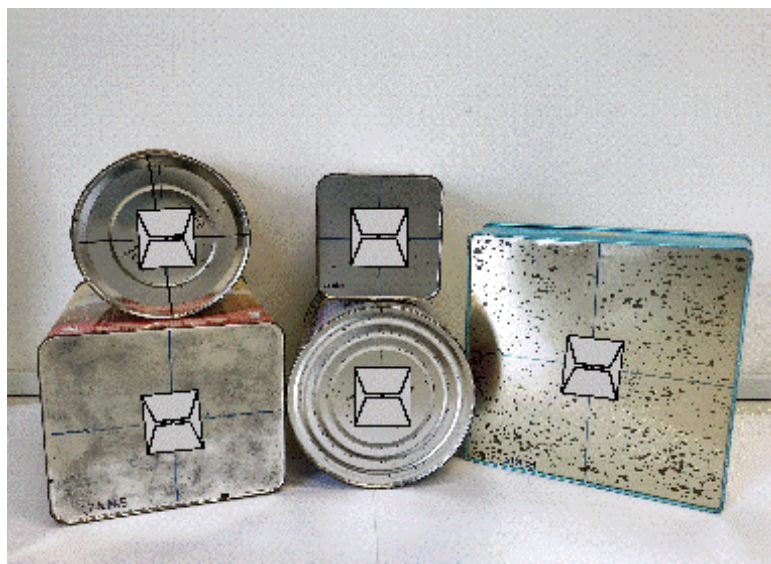
(a)



(b)

Figure 3.16: Measured read distances of the proposed tag antenna on the metal plate with different (a) plate length L and (b) plate width W .

For practical implementation, the proposed tag was also mounted on the metallic containers of several household products for measurement. First, as shown in Figure 3.17(a), the tag antenna was mounted on the bottom and body of several household containers to test their read distances in the boresight ($\theta = 0^\circ$) direction. The results for the tag on the bottom are shown in Figure 3.18(a). Except for the cases “Frishum” and “Oat Krunch”, which are slightly worse due to small surface area, the measured distances of others are more than 15 m. Similarly, when the tag is attached to the body of the containers, as can be seen in Figure 3.18(b), the read distances of all cases are at least 15 m. A far read distance of 18.8 m is obtainable when the tag is mounted on the curved surface of the “Annum” container. It is worth mentioning that no matter the tag antenna is mounted on the bottom or body of the metallic containers with different sizes and materials, the tag resonant frequency does not fluctuate drastically. It can be maintained within a narrow range of 864 – 868 MHz with stable and good reading distance. It shows that the proposed tag design is not sensitive to the curvature of the metal platform.

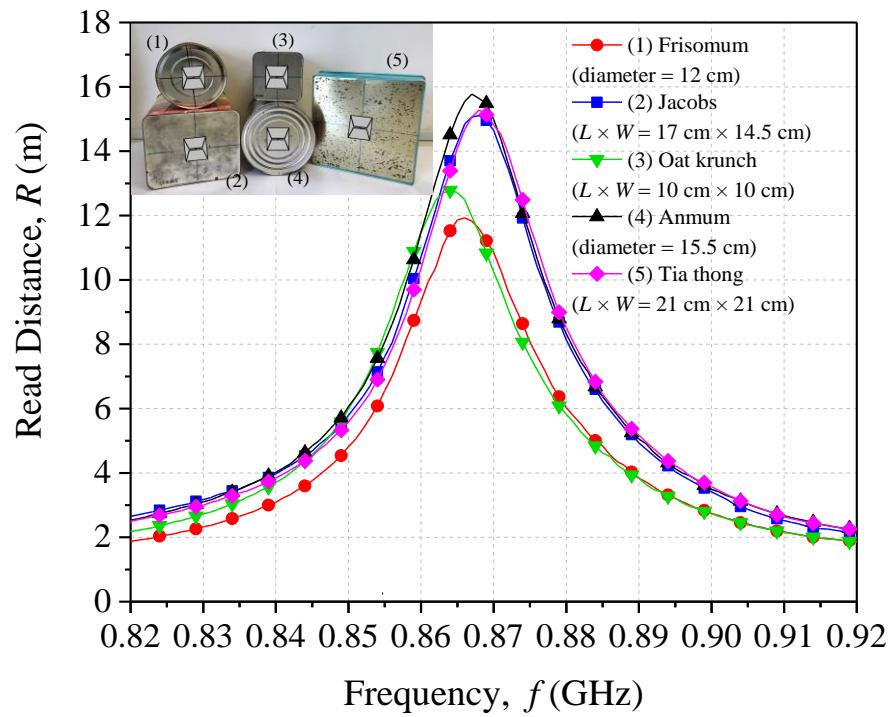


(a)
91

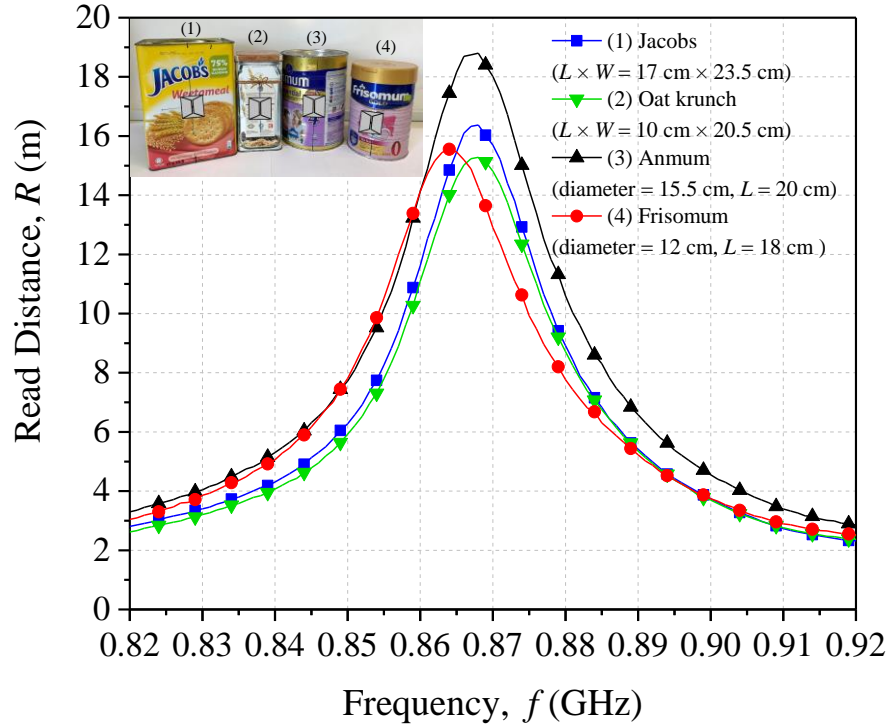


(b)

Figure 3.17: Samples of different household containers (a) with the tag antenna mounted on the bottom, (b) with the tag antenna mounted on the body.



(a)



(b)

Figure 3.18: Measured result of read distances for different household containers (a) with the tag antenna mounted on the bottom, (b) with the tag antenna mounted on the body.

The proposed tag is also compared with other UHF tag antennas, which are designed using the dipolar patches, in Table I. The referenced works are all metal-mountable tag structures published in recent years. To perform a fair comparison, the reading distance of referenced tag antennas are all normalized according to a fixed chip sensitivity ($P_c = -20.85$ dBm) and reader power ($P_r = 4$ W, EIRP). In (Lin et al., 2012), four pairs of vias are interconnected with a resonator and its backplane for designing the tag antenna, but the locations of the vias can change the operating frequency significantly, thus increasing the accuracy and complexity of the fabrication. Our proposed tag has almost the same reading distance as that in (Hamani et al., 2016), however, the rigid tag in this design has a large footprint and a high profile (7.6 mm), making it hard to

apply on small metal objects. The tag antenna in (Bong et al., 2017) has a miniature structure. Although its meandered slotlines can reduce the resonance frequency, they also cause the read distance to deteriorate significantly due to the reduction in the Q -factor. In (Li et al., 2020), an EBG structure is employed for improving the radiation performance of a tag antenna. However, it has inevitably increased the thickness of the antenna, and it requires a lot of time to analyze the EBG phase responses during the design procedure.

Table 3.3: Comparison of UHF tag antennas made of dipolar patch.

Ref.	Power (W)	Chip Sensitivity (dBm)	Substrate Material	Tag Dimension (mm)	Metal Plate Size (cm)	Normalized Read Distance (m)
This work	3.28 (EIRP)	-20.85	Foam $\epsilon_r = 1.03$	$50 \times 50 \times 3.38$	20×20	16.2
(Lin et al., 2012)	4.00 (EIRP)	-18.0	FR4 $\epsilon_r = 4.2$	$68 \times 30 \times 3$	16×16	14.12
(Hamani et al., 2016)	4.00 (EIRP)	-18.5	FR4 $\epsilon_r = 4.4$	$104 \times 31 \times 7.6$	30×25	16.82
(Bong et al., 2017)	4.00 (EIRP)	-18.5	Foam $\epsilon_r = 1.03$	$23 \times 16 \times 1.6$	20×20	5.70
(Li et al., 2020)	4.00 (EIRP)	-16.0	FR4 $\epsilon_r = 4.4$	$72 \times 32 \times 6.8$	30×30	21.19

3.5 Conclusion

For the first time, an inductive channel has been tactfully incorporated with a top-loading patch for achieving broad frequency tuning range in the operating frequency of a dipolar patch for designing a metal-mountable tag. An external lumped inductor has been embedded into the inductive channel for extending the tuning range significantly. The top-loading patch with the current-regulating inductive channel can effectively adjust the tag resonance to any arbitrary frequency in the UHF band by adjusting the channel width and inductor value. Since the tuning capability can be easily performed without damaging the antenna structure, the original tag configuration can be kept intact and its radiation performances do not deteriorate. It has enabled easy frequency tuning by simply replacing the lumped inductor, without the need to re-design the entire tag antenna. Measurements were conducted to verify the simulations. The maximum reading distance was measured to be ~ 14 m when the tag was placed on the center of a $20 \text{ cm} \times 20 \text{ cm}$ metal plate. Simultaneously, when being tested on several practical metal containers, the reading distance can achieve at least 18.8 m.

CHAPTER 4

CAPACITORS-LOADED DIPOLAR PATCH ANTENNA FOR UHF TAG MINIATURIZATION

4.1 Introduction

The RFID system can provide fast access and data visibility, and it has been widely used in the market. Although the active tag has better performance, due to the existence of the interior battery, it is much more expensive than the passive tag. The conventional dipolar tag antenna (Genovesi and Monorchio, 2010), which has half-wavelength electrical characteristics, is widely applied for passive tag design as it has good radiation performance. However, the antenna size of the dipolar patch is usually quite large and it is not suitable for mounting on small objects. When a passive tag antenna is placed on a metal object, the induced current on the metal surface can affect the antenna's radiation mechanism, causing the operating frequency to fluctuate. To avoid the interference from the metal platform, an additional loading layer can be introduced in between the resonating patch and the ground plane for improving the radiation efficiency of the antenna (Hamani et al., 2016). This makes the overall size of the antenna becomes too large and difficult to be applied for practical applications. For the same isolation purpose, the structures of AMC (Park and Kim, 2014) and EBG (Li et al., 2020) have been explored for tag design recently. However, these structures can cause the tag profile to increase

significantly, and such approach is not suitable for designing miniature tags. Several techniques have been proposed for miniaturizing tag antennas. In addition to increase its electrical length, the meandered dipole (Bhaskar and Singh, 2017, Rasilainen et al., 2014) can provide additional inductance that is required for reducing the tag resonant frequency. Introducing meandered slotline (Bong et al., 2017) between dipolar patches can also be used for miniaturization, but this approach can cause the antenna Q -factor to deteriorate, resulting a reduction in the read performance. Inductive vias (Lin et al., 2012) between the resonant patch and the ground plane can disperse currents, also providing additional inductance for reducing the operating frequency. However, additional design procedures and costs are always needed. The location of the vias can affect the resonant frequency. To miniaturize the tag size, for most of the aforementioned techniques, the radiator structure is always modified and the radiator area is often sacrificed, resulting in degradation in the radiation performance.

In this design, without changing the radiator structure, two lumped capacitors are introduced to incorporate with dipolar patches for increasing capacitive loading. The introduction of the pair of capacitors across the dipolar patches can not only miniaturize the antenna size, but it has also successfully reduced the tag resonant frequency to the regulated UHF band. The two patches are fed by a pair of coplanar feedlines. Different from that in (Moh et al., 2018, Lee et al., 2019), the feedline here is made into T shape for increasing tuning freedom. It is worth mentioning that the radiator structure can be kept quite complete, even with the introduction of the pair of lumped capacitors, and it is

able to provide good read performance. The architecture of the project is organized in the following way. The antenna configuration and impedance analysis will be discussed in Section 4.2. The analysis of crucial parameters is illustrated in Section 4.3. Measurement results and discussion will be provided in Section 4.4. Finally, a summary is provided.

4.2 Antenna Configuration and Design Process

The configuration of proposed tag is depicted in Figure 4.1. It is made by laminating a thin layer of copper ($9\ \mu\text{m}$) on a flexible polyethylene terephthalate (PET) film with a thickness of $50\ \mu\text{m}$. As shown in Figure 4.1, the configuration of the tag composes a dipolar patch antenna. It consists of two simple dipole resonant patches ($w_a \times l_a$), each of which is fed by a T-shaped coplanar feedline, providing a two-dimensional tuning freedom. The width of the feedline is fixed at $w_f = 1.20\ \text{mm}$ and the gap is $g_f = 0.30\ \text{mm}$. The microchip being employed here is a UCODE 8/8m (NXP, 2020), a flip chip that is tested with an actual read sensitivity of $-20.85\ \text{dBm}$, along with an input impedance of $13 - j191\ \Omega$ at $915\ \text{MHz}$. With reference to Figure 4.1, the chip is bonded across the center of the two T-shaped feedlines. In this design, a narrow gap ($g_c = 0.35\ \text{mm}$) is inserted between the two resonating patches so that capacitance can be introduced to the antenna structure. To introduce inductive effect to the antenna structure, two lumped capacitors are bonded across the two patches. It will be shown that, when the pair of capacitors are introduced, the size of tag antenna can be further

miniaturized, while maintaining good radiation performance. Both end of resonant patches are connected to the ground through inductive narrow stubs ($s_w \times s_l$) for controlling the current flow between the resonator and the ground plane for the purpose of tuning the operating frequency. To construct the tag, the PET film is wrapped around a rectangular polyethylene foam (with $\epsilon_r = 1.03$, $\tan\delta = 0.0001$) with a size of $w_a \times l_a$ (35 mm \times 30 mm) and a thickness (h) of 3 mm. The ground is for isolating the tag from the metal platform and mitigating its effect on the antenna radiation efficiency. Other design parameters of the proposed design are also described in Table 4.1.

Table 4.1: Optimized parameters of the proposed design.

Parameter	(mm)	Parameter	(mm)
l_a	30.00	w_a	35.00
l_c	0.10	w_f	1.2
l_t	16.00	w_t	12.2
l_1	14.10	w_1	1.8
l_2	7.40	w_2	10.7
l_3	16.60	g_c	0.35
h	3.00	g_f	0.30
s_l	3.118	s_w	0.65

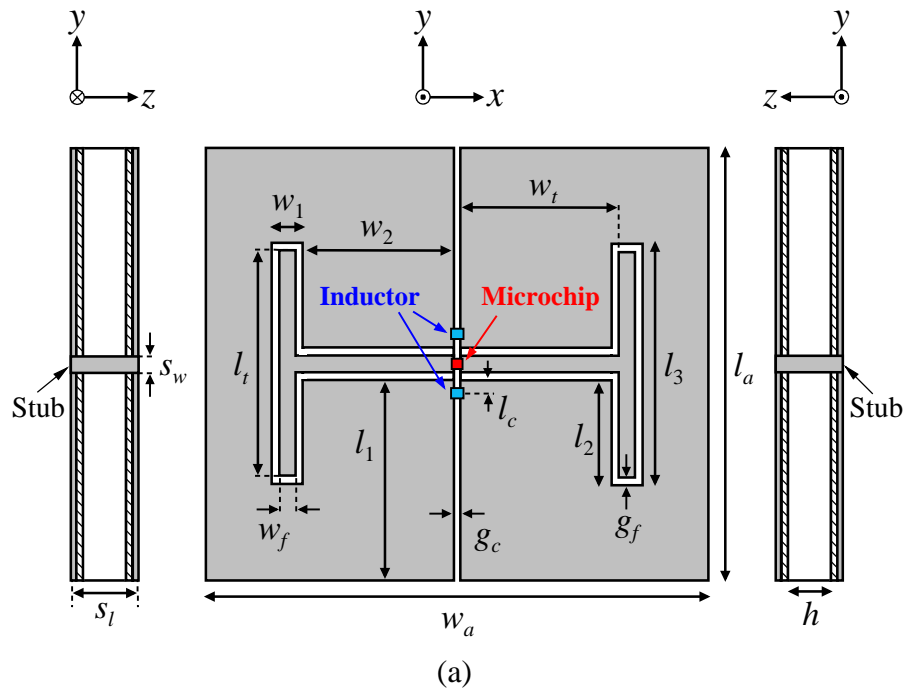


Figure 4.1: (a) Antenna configuration. (b) Prototype of proposed tag antenna.

The proposed tag antenna is designed to be applied on metal surface. Hence, it is placed on a square metal plate with a dimension of 20 cm in both the simulation and measurement. The design and optimization processes are all conducted using the commercial software CST Microwave Studio. The design process was started with simulation, where the microchip was replaced by an

external discrete port, and the impedance value of the port was defined to be the chip impedance. With reference to Figure 4.1, the two resonating dipolar patches are fed by the pair of T-shaped feedlines, where capacitive coupling has been introduced by the narrow gap between the patches. In this new design, a pair of surface-mount-device (SMD) capacitors are bonded across two patches for directly introducing a capacitance of 0.6 pF. Figure 4.2 shows the simulated input impedances for the cases with and without the loading capacitors. For the case without the capacitors, as can be seen from the figure, the tag resonance is located at 1222 MHz with an antenna impedance of $12.55 - j190.97 \Omega$, which is not suitable to be operated in the regulated UHF band at this moment. However, with the introduction of two 0.6 pF capacitors, the tag resonant frequency can be brought down significantly to 915.5MHz, with an antenna impedance of $15.83 - j190.88 \Omega$ and a power transmission coefficient of 0.95.

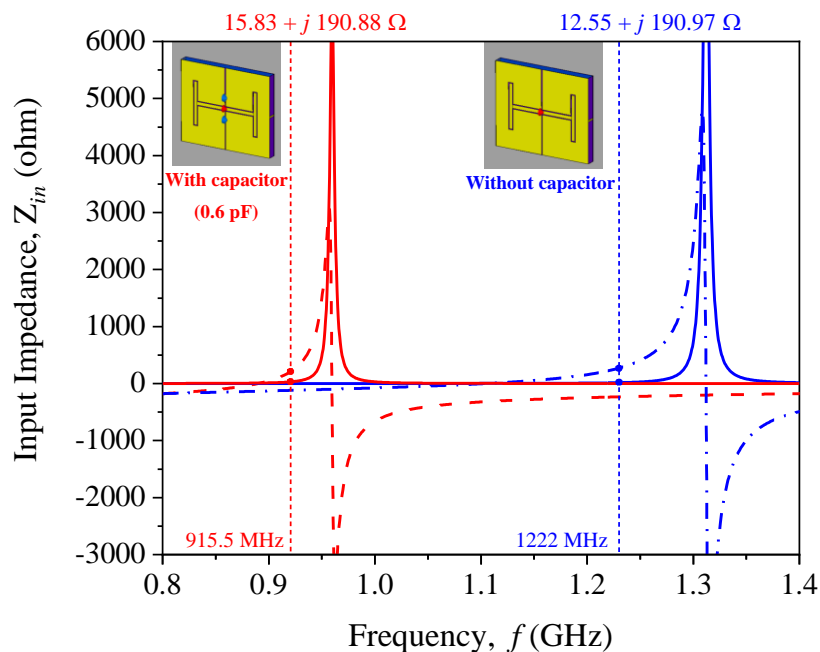
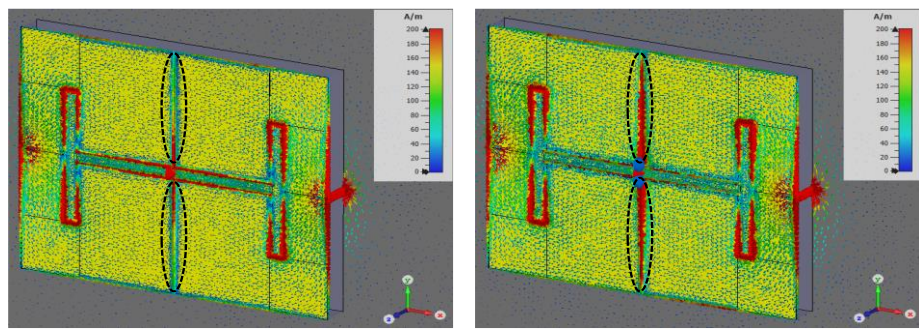


Figure 4.2: Input impedances for the cases with and without the loading lumped capacitors.

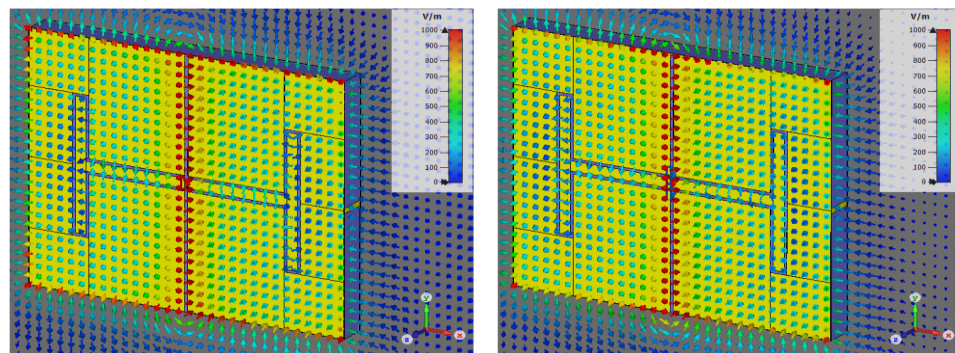
The surface currents, electric field, and magnetic field distributions of the tag for the cases with and without the loading capacitors are compared in Figures 4.3, 4.4, and 4.5. As shown in Figure 4.3, when the tag antenna is bonded with capacitors, the currents around the gap are significantly higher than those without capacitors. The currents and magnetic fields are stronger and intensified around the gap region, as can be observed in Figures 4.3 and 4.5, due to the existence of the capacitors. It has introduced additional reactance that is required to reduce the tag resonant frequency effectively.



(a)

(b)

Figure 4.3: Current distributions for the case (a) without and (b) with the loading capacitors.



(a)

(b)

Figure 4.4: Electric field distributions for the case (a) without and (b) with the loading lumped capacitors.

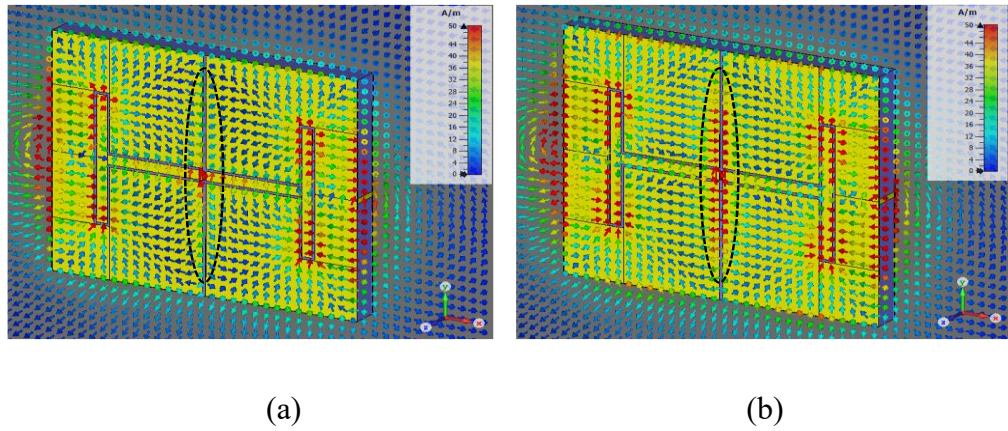


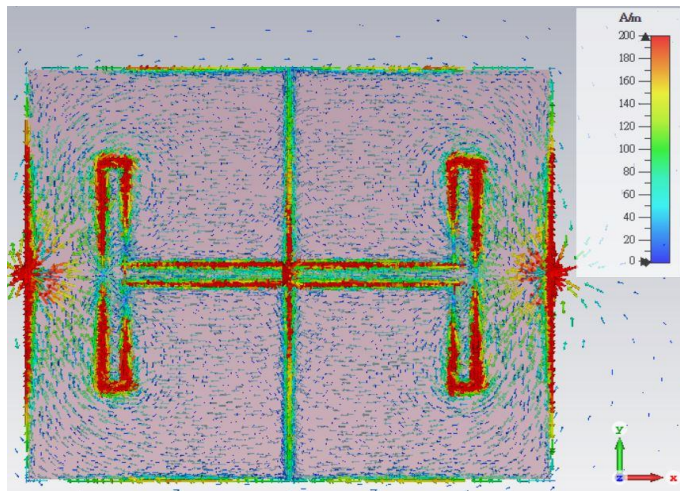
Figure 4.5: Magnetic field distributions for the case (a) without and (b) with the loading lumped capacitors.

4.3 Parametric Analysis

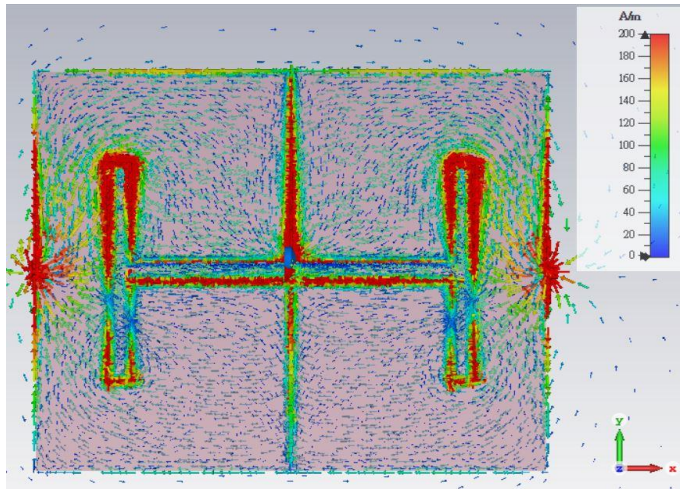
The effects of the capacitor on the magnetic field and antenna impedance were briefly analyzed in the previous section. Parametric analysis has been performed to study the effects of the inductance values of the inductors (C_l), the gap between two dipolar patches (g_c), and the stub width (s_w) on the power transmission coefficient and the input impedance of the proposed tag antenna. Similarly, in all the parametric analyses, the model of the proposed antenna is placed on the center of the $20 \times 20 \text{ cm}^2$ aluminum plate, and it is simulated using the CST Microwave Studio.

To study the capacitive coupling between the two dipolar patches, here, we try to introduce capacitors and observe their effects on the tag antenna.

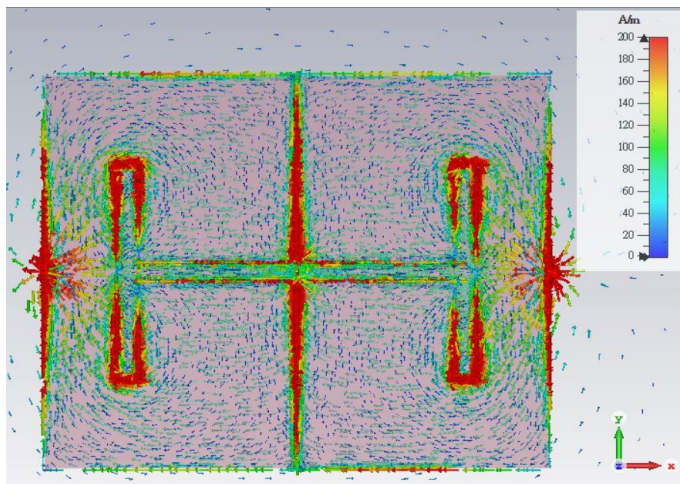
Referring back to Fig. 4.3, it can be seen that the inclusion of the two lumped capacitors causes the current intensity to be enhanced near the central gap. To visualize better, the current flows on the dipolar patches are further amplified in Figs. 4.6(a), 4.6(b), and 4.6(c), respectively, for the cases without any capacitor, with a single capacitor, and with two capacitors. The corresponding antenna impedances are given in Figs. 4.7. By comparing Fig. 4.6(a) and Fig. 4.6(b), it is obvious that incorporating a capacitor near to the upper half of the dipolar patch has made the currents on the upper part of the patch to go for a longer path. It has successfully brought down the tag resonant frequency to 1010.6 MHz, as can be observed in Fig 4.7. With the inclusion of two capacitors, as can be seen in Fig. 4.6(c), the current paths on the top and bottom have become longer at the same time. It has further brought down the tag resonant frequency to 915.5 MHz.



(a)



(b)



(c)

Figure 4.6: Current distribution for the cases (a) without capacitor, (b) with single capacitor, and (c) with two capacitors in simulation.

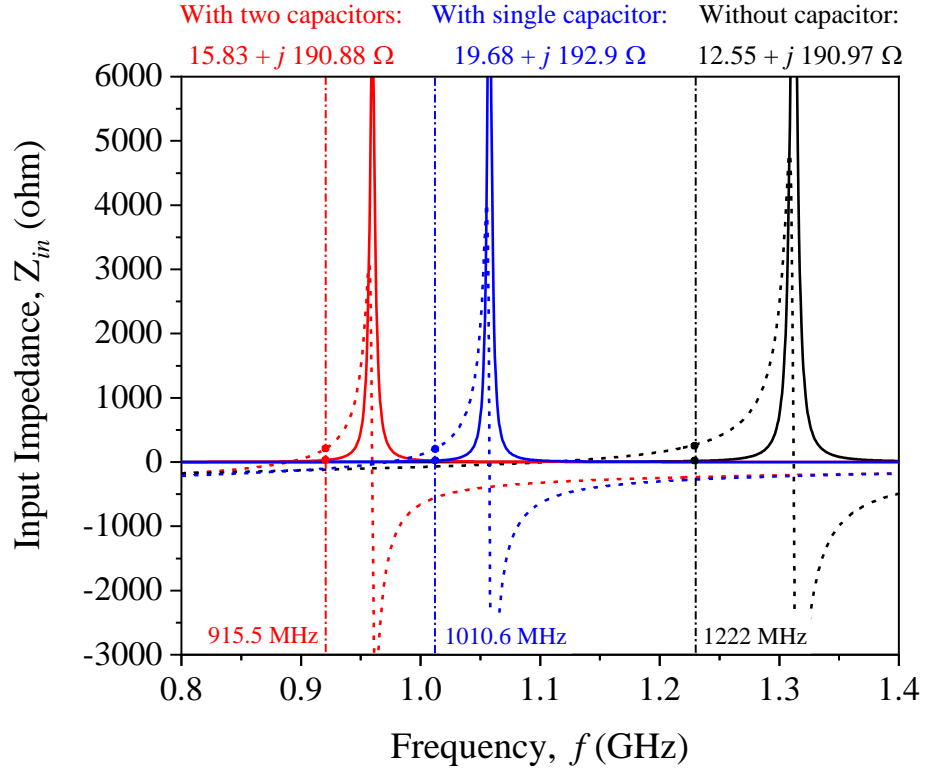
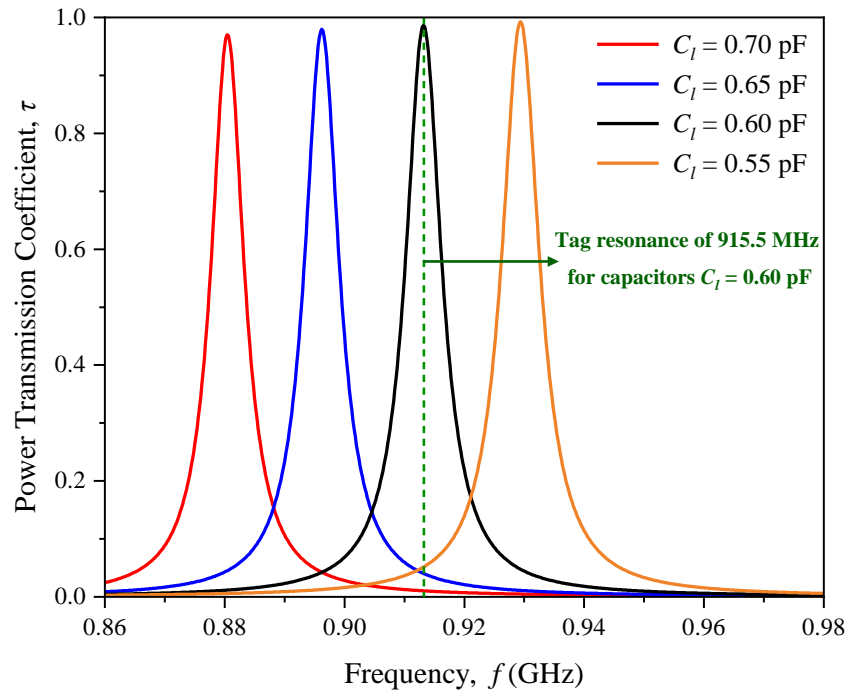
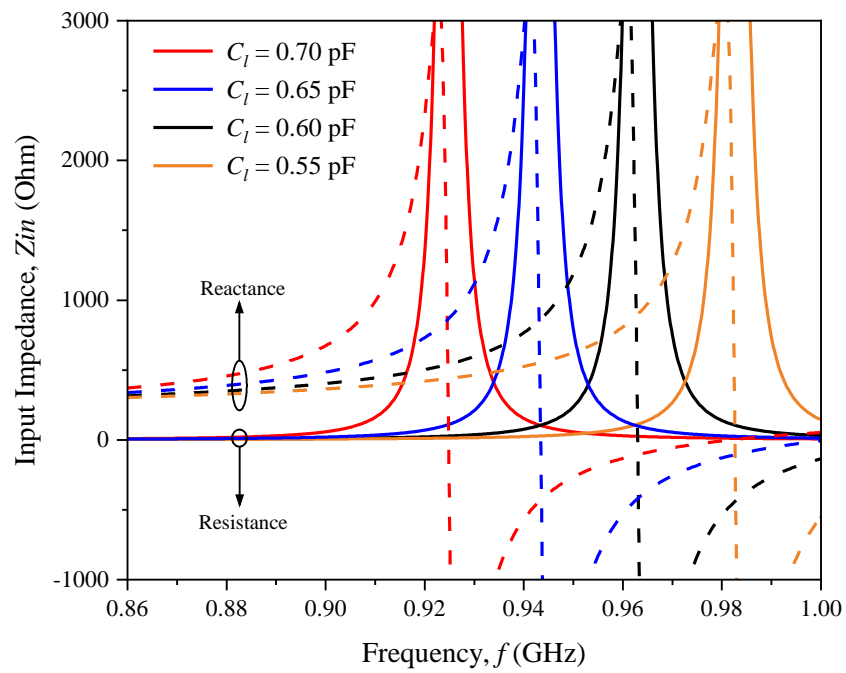


Figure 4.7: Antenna impedances for the cases in Fig. 4.6.

To show that the antenna impedance can be effectively changed by tuning the lumped capacitors on the patches, the first parametric analysis is performed by changing the capacitor value (C_l) from 0.55 to 0.7 pF at an interval of 0.05 pF. As shown in Figure 4.8, when C_l is increased from 0.6 to 0.7 pF, the tag resonant frequency drops from 915.5 MHz to 990.4 MHz at a changing rate of 17.5 MHz per 0.05 pF. Similarly, when C_l is reduced to 0.55 pF, the tag resonant frequency steadily increases to 933 MHz. It is worth mentioning that the value of the power transmission coefficient τ can be maintained beyond 0.97 for all the cases in Figure 4.8(a), meaning that the antenna impedance can match well with the chip impedance for the C_l values.



(a)



(b)

Figure 4.8: Effects of varying capacitance C_l on the (a) power transmission coefficient, (b) input impedance.

In addition to adjusting the values of the capacitors across the patches, the gap formed by the two dipolar patches is like a parallel-plate capacitor, and the gap width can affect the strength of the electric field. As shown in Figure 4.9, when the separation distance between the patches is narrow, the electric fields in the gap are further enhanced due to high capacitance, as can be observed from the red arrows in Fig. 4.9. When the gap becomes wider, the electric field intensity becomes weaker. With reference to the power transmission coefficients in Figure 4.10(a), simulation is conducted for the case when two capacitors are fixed at 0.6 pF, and the gap between the two patches g_c is increased from 0.35 to 0.65 mm at an interval of 0.1 mm. The corresponding simulation results show that the tag resonant frequency increases from 915.5 to 938.4 MHz with a stable changing rate of 7.63 MHz per 0.1 mm. Obviously, this method utilizes the principle of capacitive coupling to adjust the antenna impedance. By adjusting the width between the dipolar patches, the overall antenna impedance can be easily changed, as shown in Figure 4.10(b).

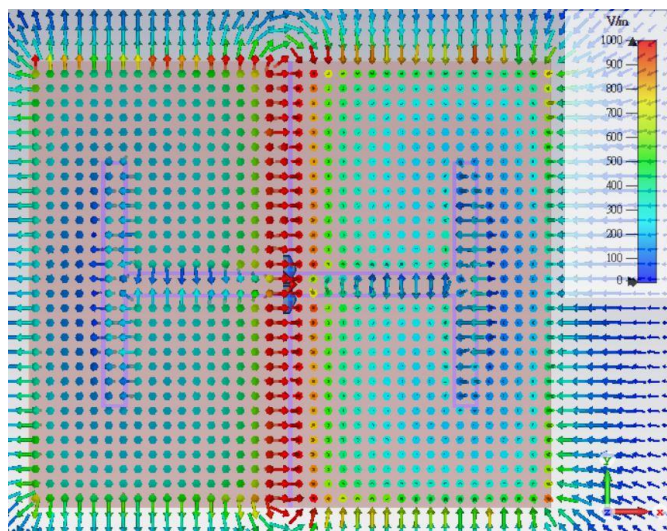
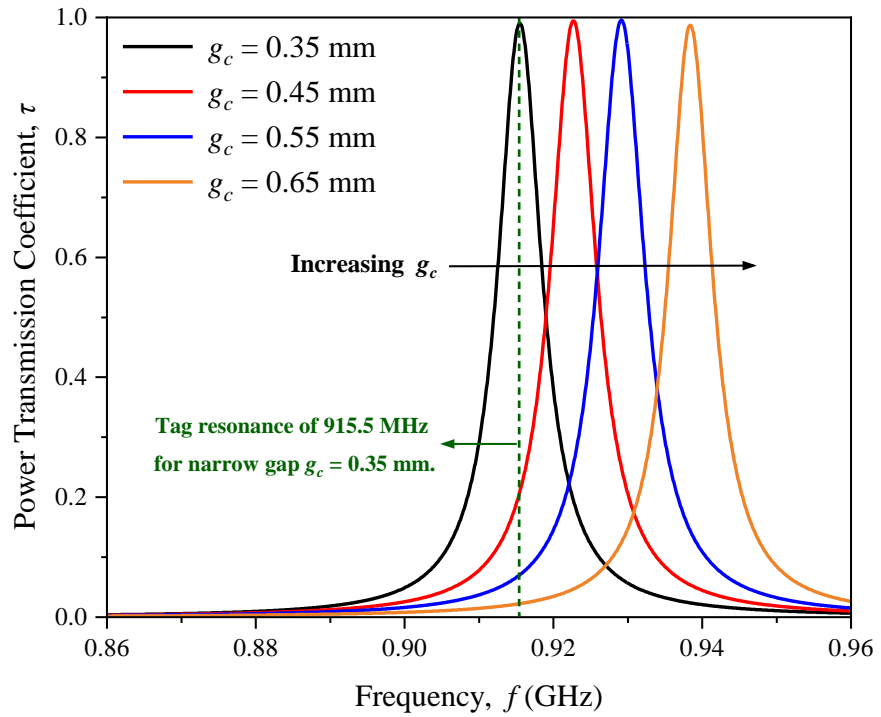
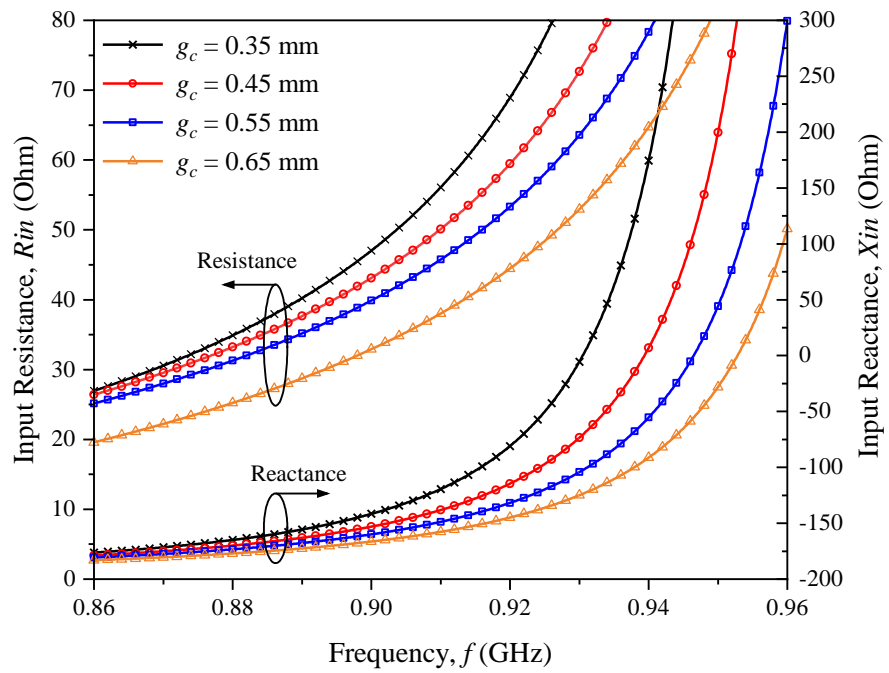


Figure 4.9: Electric field distributions for the case with the loading lumped capacitors.



(a)



(b)

Figure 4.10: Effects of varying the gap width g_c on the (a) power transmission coefficient, (b) input impedance.

The proposed tag antenna has a pair of shorting stubs to interconnect the dipolar patches with the ground plane. The shorting stubs with inductive characteristics can adjust the current flux, as shown in Figure 4.11. When all the parameters are set at the initial value, the width of the stubs is increased and decreased simultaneously from 0.65 mm at intervals of 0.05 mm. The simulation results of stubs width from 0.55 to 0.75 mm are depicted in Figure 4.12. The corresponding resonance frequency is from 902.4 to 923.6 MHz at a changing rate of 5.3 MHz per 0.05 mm. Since narrowing the width of the shorting stub can limit the current flows, it can cause the antenna reactance to increase. This phenomenon introduces inductance effect. And this is the reason why the resonance frequency reduces when the shorting stub is narrowed down, causing the frequency. The same trend is also observed in the power transmission coefficient and input impedance, as shown in Figure 4.12.

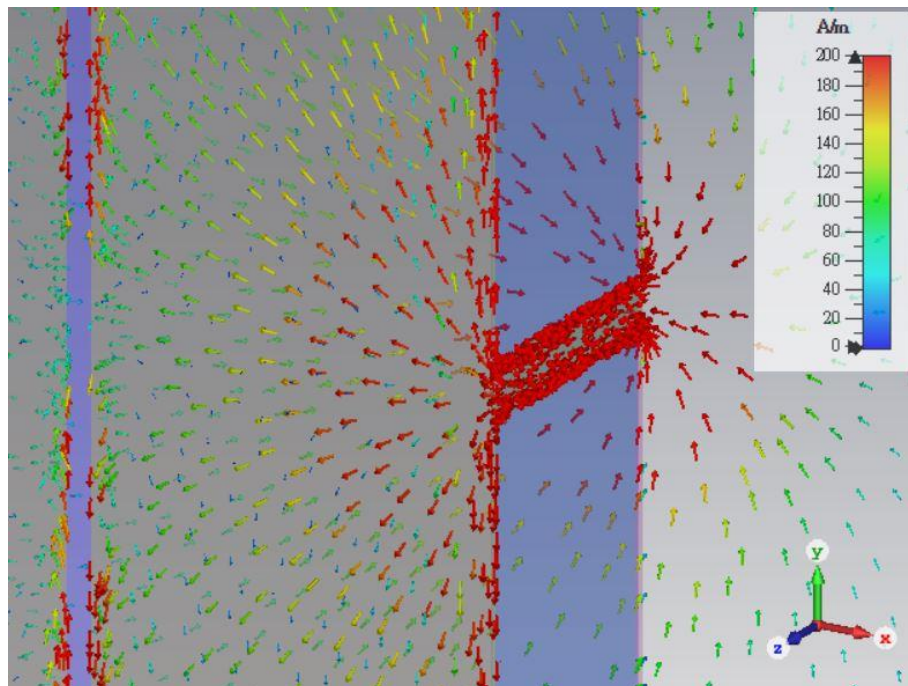
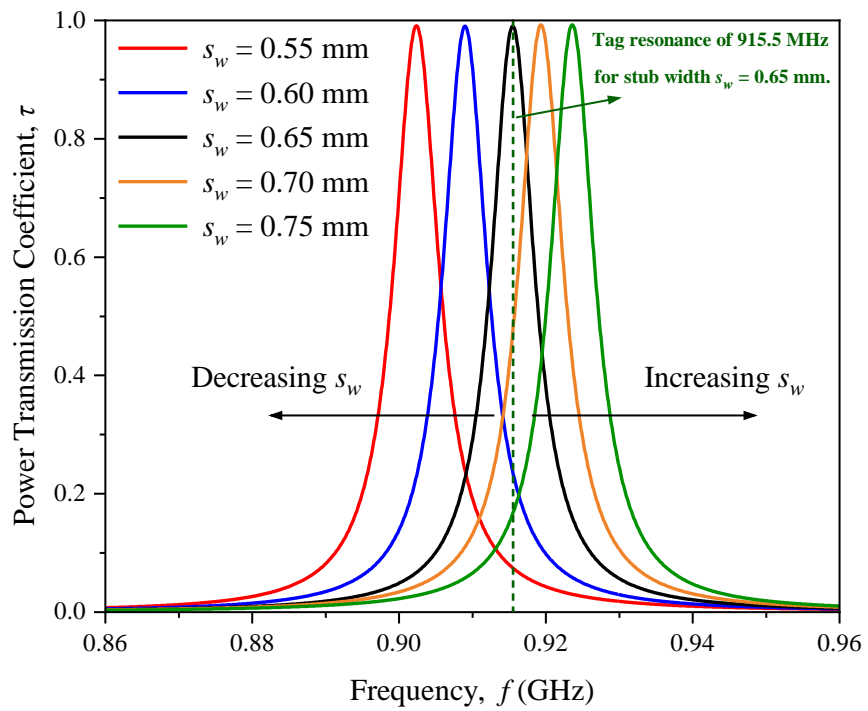
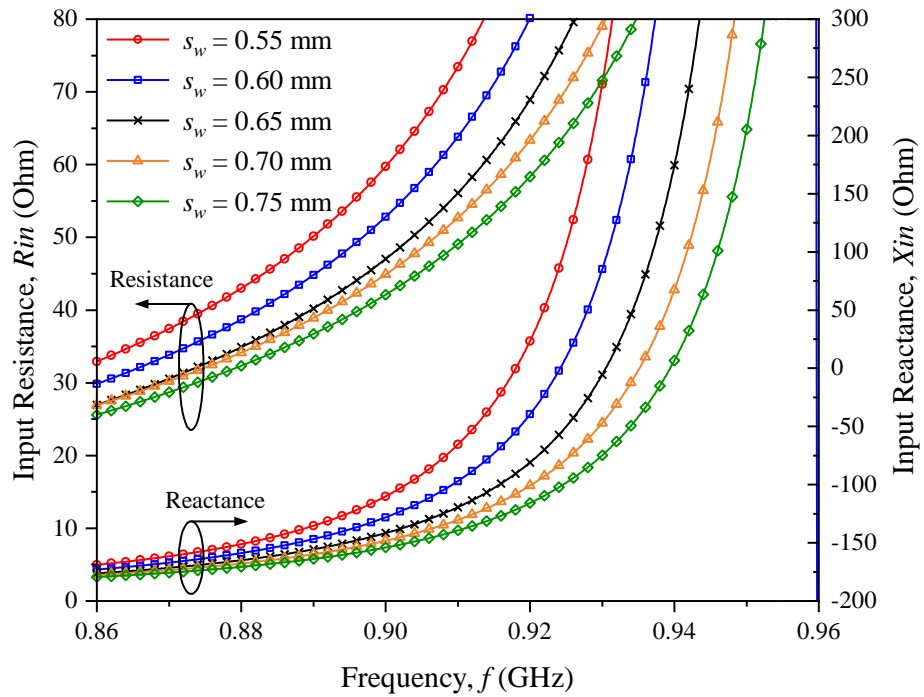


Figure 4.11: Simulated current distribution on the stub.



(a)



(b)

Figure 4.12: Effects of varying width of stubs s_w on the (a) power transmission coefficient, (b) input impedance.

The sensitivities of the design parameters are summarized and shown Table 4.2. Changing C_l has a tuning sensitivity of 350 MHz/pF, and it can be used for coarse-tuning and bringing down the tag resonant frequency to the UHF passband. Changing g_c and s_w can introduce tuning sensitivities of 76.3 MHz/mm and 106 MHz/mm, respectively, and the two parameters can be used for fine-tuning the frequency within a narrow range.

Table 4.2: Tuning sensitivity of the design parameters.

Design Parameter	Tuning Sensitivity, MHz/pF
C_l	350.0
Design Parameter	Tuning Sensitivity, MHz/mm
g_c	76.3
s_w	106.0

4.4 Results and Discussion

The performance of the proposed antenna is verified in an anechoic chamber using the Voyantic Tagformance measurement system (Voyantic, 2012). The measurement setup is shown in Figure 4.13. The tag is mounted on a 20 cm \times 20 cm aluminum plate which is placed on a platform with a far-field distance of 52 cm from the reader. The prototype was tested using a linearly polarized reader with a gain of 8 dBi for measuring the realized gain and read distance. The realized gain can be expressed as $G_r = P_c/P_t \times P_t$, where P_c is the chip sensitivity

of -20.85 dBm. P_l is a path loss which is measured by the calibration system. P_t is the lowest power from reader that is required to power up the tag.

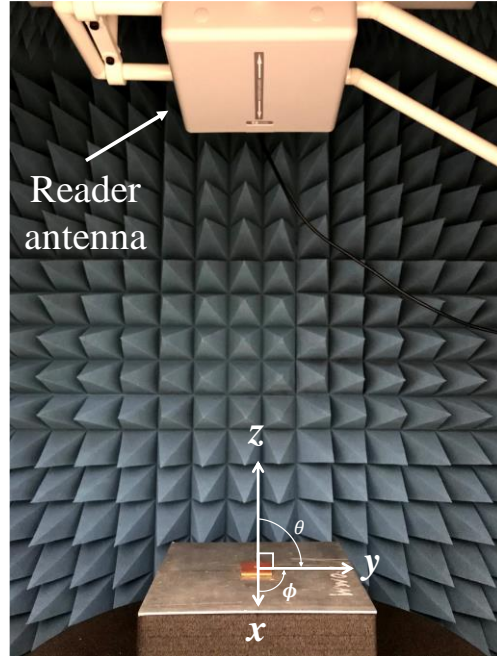


Figure 4.13: Measurement setup in the anechoic chamber.

The measurement results of the realized gain G_r and tag sensitivity P_t are compared with simulation, which is shown in Figure. 4.14. A measured realized gain G_r of -3.255 dBi is obtained at 910 MHz, which is slightly smaller than the simulated -1.368 dBi at 915.5 MHz. Although the measurement result is slightly different from its simulation counterpart, the difference is actual quite small and it is less than 2 dB, which may be caused by manufacturing and experimental tolerances. However, for the proposed miniaturized tag antenna, the measured realized gain is still good. It has proven that the capacitive loading does exist between the dipolar patches, and the size can be easily miniaturized by embedding the lumped capacitors without changing the antenna structure.

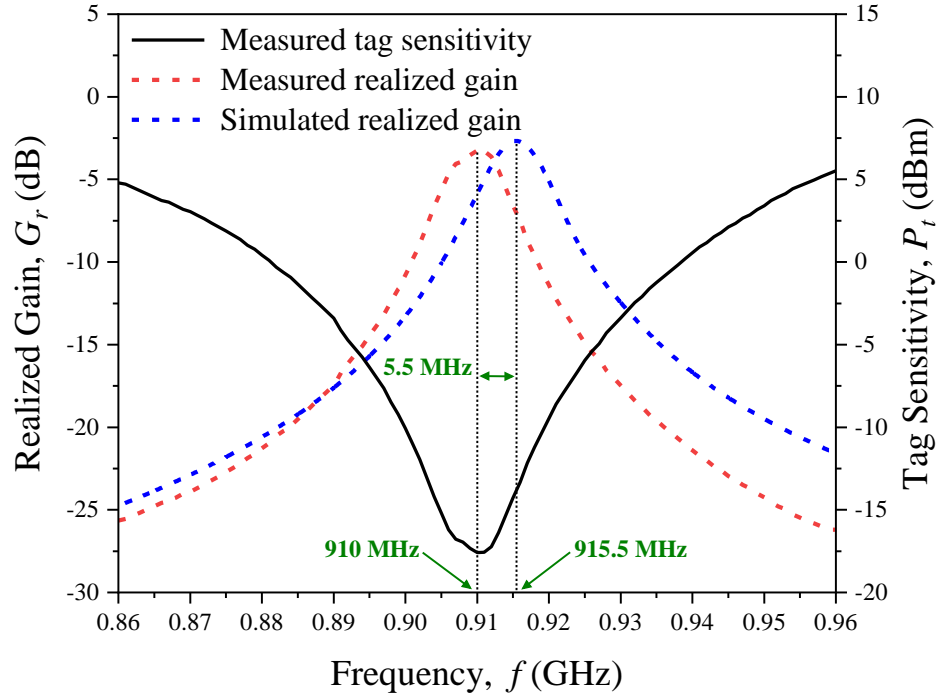


Figure 4.14: Measured and simulated realized gains and the measured tag sensitivity when the tag is placed on a 20 cm \times 20 cm aluminium plate.

Next, the read distance of the prototype was measured. The read patterns are measured following the definition shown in Figure. 4.15. Here, the reader is always maintained at a fixed distance of 52 cm along the z -axis. The xy -plane reading pattern is measured when the tag is rotated around its z -axis, as shown in Figure. 4.16(a). Different from the conventional polarization pattern, the measured pattern is the polarization characteristic of the tag antenna in the boresight axis. It is found that the proposed tag antenna is linearly polarized along the x -axis ($\phi = 0^\circ$ or 180°), and the maximum reading distance is 11.1 m. Similarly, the polarization patterns of the yz - and xz -planes can also be obtained by rotating the tag around its own x - and y -axis, respectively, as shown in Figure. 4.16(b). As can be observed from the cutplanes in Figure. 4.16(b), the read

patterns in the xz and yz planes have a maximum read distance of ~ 11 m in the boresight ($\theta = 0^\circ$). The lobe for $\theta = 90^\circ$ is truncated due to the existence of the metal plate.

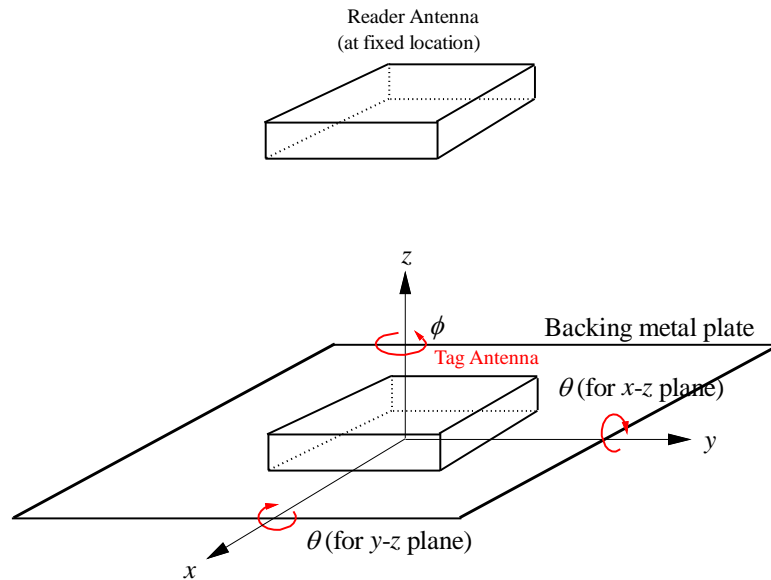
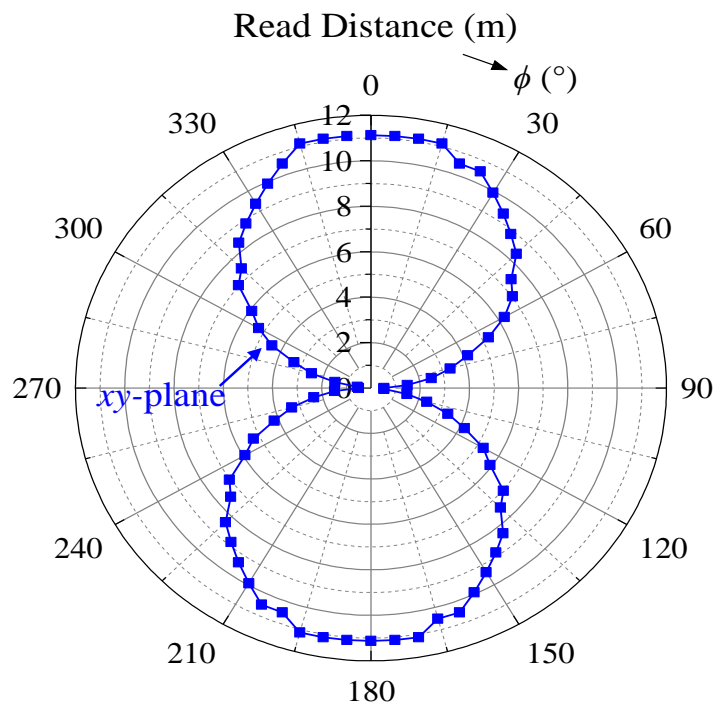


Figure 4.15: Plane definition for measuring the read distance and realized gain in anechoic chamber.



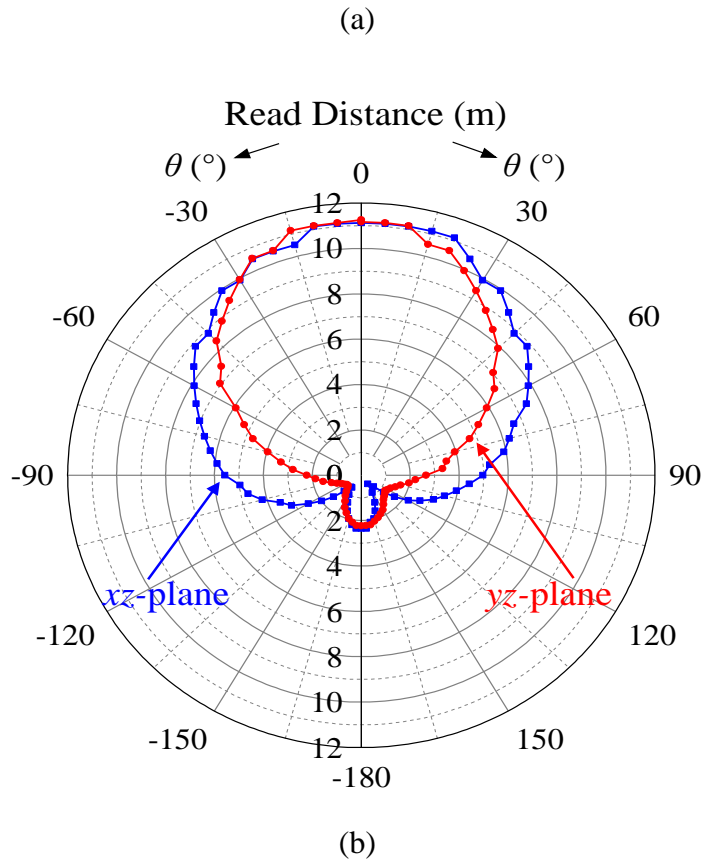
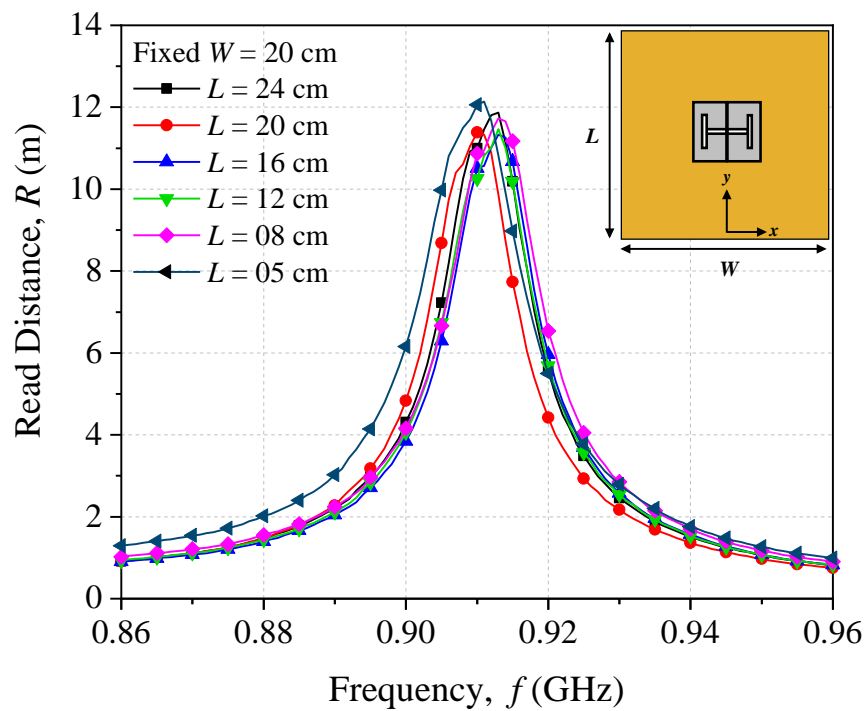


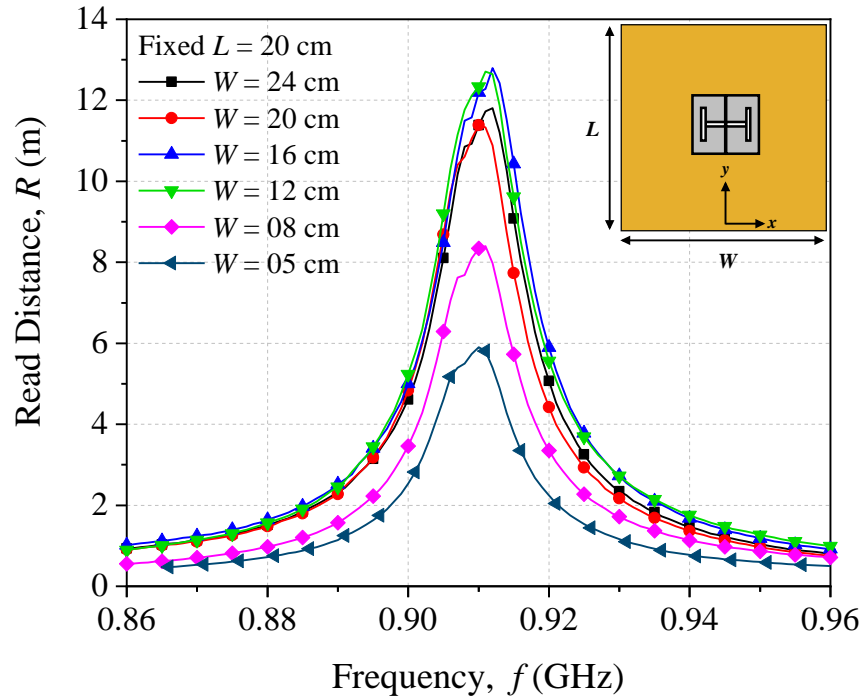
Figure 4.16: Measured read patterns of the proposed tag antenna in the (a) xy -plane, (b) xz - and yz -planes at 910 MHz.

Since the proposed tag antenna is designed for application on metal surfaces, the prototype is placed on the center of aluminum plates ($W \times L$) of different sizes, the maximum reading distance in the boresight ($\theta = 0^\circ$) is measured to evaluate the practical radiation efficiency of the antenna. First, when the width of the metal plate W is fixed at 20 cm, the plate length L is reduced from 24 to 5 cm to perform the read distance test, as shown in Figure. 4.17(a). The results show that in all cases, the read distance can achieve more than 11 meters, with a stable tag resonance that can be maintained in the range of 910 – 913 MHz. Similarly, as shown in Figure. 4.17(b), L is fixed at 20 cm, and the read distance is tested when W is decreased from 24 to 5 cm. It can be found that

when W is reduced from 24 to 12 cm, there is a stable reading level that exceeds 11m. However, when W is 8 cm, the corresponding reading distance drops down to 8.3 meters. The read distance is only 6 meters while W is at 5 cm. This is because the linear polarization of the dipolar patch is in the x -direction. When the width of the metal plate W is truncated, sufficient backscatter cannot be generated, and it makes the reading distance to be significantly reduced. Although the radiation performance has deteriorated, the operating frequency can be maintained at approximately 910MHz, as shown in Figure. 4.17(b).



(a)



(b)

Figure 4.17: Measured read distances of the proposed tag antenna on the metal plate with different (a) plate length L and (b) plate width W .

The prototype of the proposed tag antenna has been mounted on several different household metal containers to test, for evaluating the real implementation scenarios. The containers to be tested include a number of biscuit boxes and powder cans, and the tag antenna is mounted either on the bottom or the body of the container to test the reading distance in the boresight ($\theta = 0^\circ$) direction, as shown in Figure 4.18.



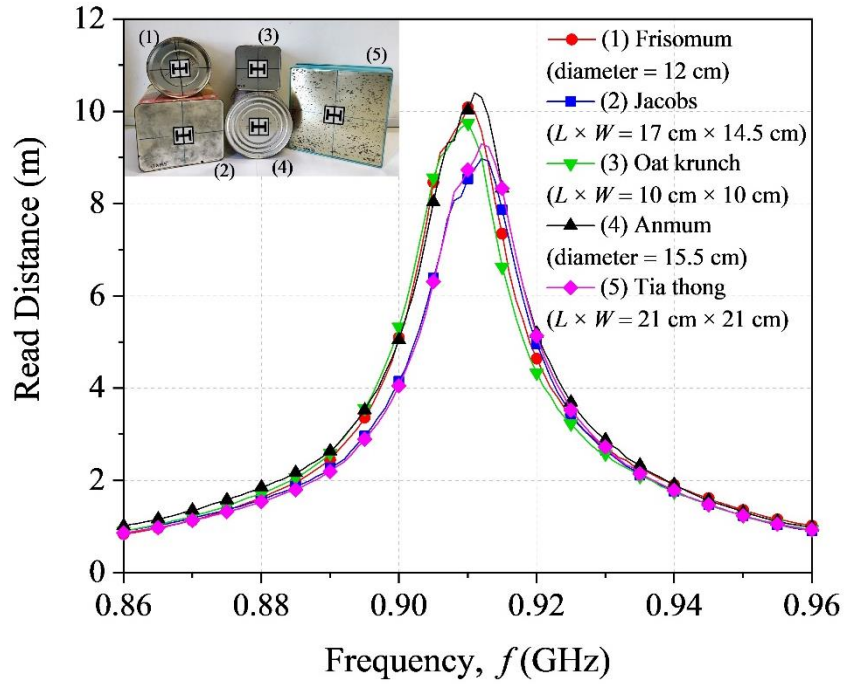
(a)



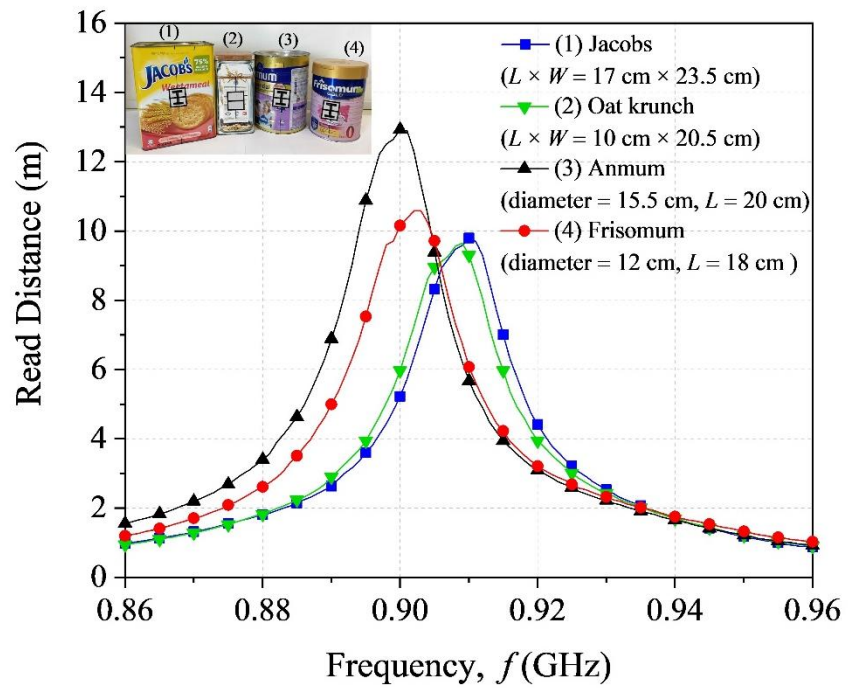
(b)

Figure 4.18: Samples of different household containers (a) with the tag antenna mounted on the bottom, (b) with the tag antenna mounted on the body.

First, Figure 4.19(a) shows the measured reading distances when the tag is mounted on the bottom of the metal container. Except for the cases “Jacobs” and “Tia thong”, cases can achieve at least 10 meters. In general, the tag resonant frequency can be stably maintained at 910 - 912 MHz. The measurement results for the cases when the tag antenna is mounted on the bottom of the container is shown in Figure 4.19(b). It is observed that the read distances can go beyond 10 meters in general.



(a)



(b)

Figure 4.19: Measured read distances for different household containers (a) with the tag antenna mounted on the bottom, (b) with the tag antenna mounted on the body.

The proposed tag design is compared with other UHF RFID tags which are applicable on metal surfaces, as depicted in Table 4.2. To fairly compare the antenna performances, all of the measurement results that are obtained from the literature have been normalized by the reader power and chip sensitivity of 4 W and -20.85 dBm, respectively. The structure of the tag in (Chen and Tsao, 2010b) is simple and the impedance can be tuned by changing the distance between the two PIFAs. However, the tag size is too large to be useful for small metal objects. The worst thing is that the reading distance is very poor. The application of meandered folded dipole as a tag antenna is quite common. In (Koo et al., 2011), a dipole antenna surrounded by an additional loop is used to enhance the antenna gain. This tag design seems to have good reading performance, but it has to be elevated from the metal object by 10 mm. If the separation space is reduced to 1 mm, the estimated reading distance will only be 6.6 m. A bowtie patch is connected to the ground plane through four pairs of inductive vias in (Lin et al., 2012), which can effectively reduce the operating frequency to the desired passband. However, when the positions of the vias fluctuates, the tag resonance will get detuned. And there are additional procedures for manufacturing, so the costs will increase too. Since the material of the antenna substrate is FR4, the tag cannot be mounted on a curved object. Apparently, the volume of the antenna in (Hamani et al., 2016) is too large compared to the proposed design. Although it has good radiation performance, the tag is difficult to be applied on small metal objects. Introducing serrated edges (Bong et al., 2016) on folded patch, causing the current path to increase and the input impedance to reduce, can be used to miniaturize a tag antenna. Since the Q -factor of the radiator has slightly deteriorated, its reading distance is lower than the proposed tag. The dimension

of the tag in (Bong et al., 2017) is quite small with only 589 mm³. The meandered slotlines introduced between the dipolar patches are highly reactive, causing the tag resonant frequency to reduce significantly. However, the radiator has a lower Q -factor, resulting in poorer radiation efficiency with a reading distance of only 5.7 meters. Similarly, in (Lee et al., 2018a), C-shaped slotlines are used to increase the antenna reactance. But the matching network occupies a large part of the patch, which makes the radiation efficiency poor. When the tag was placed on a metal plate for measurement, the read distance was only 5.76 meters. The idea of adding metamaterials such as AMC/EBG to the antenna design has become very popular in recent years. A layer of AMC is embedded in the middle of the folded dipolar patch in (Ripin et al., 2020) to effectively reduce the tag resonant frequency by 200 MHz. The advantage is that the bowtie dipole patch on the top layer is complete, so the radiation efficiency is good. However, the thickness of the label has relatively increased. Besides, the AMC design process is more complicated as it requires the performance of phase analysis.

Table 4.3: Comparison of other metal-mountable UHF tag antennas.

Ref.	Reader Power (W)	Substrate and Flexibility	Tag Dimension (mm)	Metal Plate Size (cm)	Normalized Read Distance (m)
This work	4.00 (EIRP)	Foam Yes	35 × 30 × 3	20 × 20	12.32
(Chen and Tsao, 2010b)	4.00 (EIRP)	FR4 No	130 × 45 × 0.8	20 × 20	3.47

(Koo et al., 2011)	4.00 (EIRP)	PET + Foam Yes	$91 \times 27 \times 10$	20×20	16.1
(Lin et al., 2012)	4.00 (EIRP)	FR4 No	$68 \times 30 \times 3$	16×16	14.12
(Hamani et al., 2016)	4.00 (EIRP)	FR4 No	$104 \times 31 \times 7.6$	30×25	16.82
(Bong et al., 2016)	4.00 (EIRP)	Foam Yes	$30 \times 30 \times 3$	20×20	10.23
(Bong et al., 2017)	4.00 (EIRP)	Foam Yes	$23 \times 16 \times 1.6$	20×20	5.70
(Lee et al., 2018a)	4.00 (EIRP)	Foam Yes	$42 \times 50 \times 1.6$	20×20	5.76
(Ripin et al., 2020)	4.00 (EIRP)	Foam Yes	$30 \times 50 \times 3.35$	20×20	13.60

4.5 Conclusion

Lumped capacitors are combined with a dipolar patch for designing a metal-mountable tag antenna. Embedding the two lumped capacitors across the dipolar patches enables the introduction of additional capacitive loading for adjusting the antenna reactance. Since the capacitors can be of any values, the proposed

tag can achieve a very broad frequency tuning range without modifying the antenna structure. Since the antenna structure is intact, the radiation performance of the proposed tag is not compromised. Besides, the operating frequency can also be effectively tuned by adjusting the width between the dipolar patches or the width of the shorting stubs. The proposed tag antenna is compact. When the tag is tested on a 20 cm × 20 cm aluminum plate, it can achieve a good reading distance of more than 11 m. A maximum reading distance of 13 m is achievable when the proposed tag antenna mounted on different metal objects.

CHAPTER 5

SUMMARY AND DISCUSSION

5.1 Summary

In this project, two compact UHF RFID tag antennas have been proposed for metal mountable application. Both of the tag designs have employed the dipolar patches as the radiator. Additional lumped components were incorporated for reducing the tag resonant frequencies to regulated UHF passband.

In the first design, a conventional bowtie-shaped folded dipolar patch is employed as the radiator and an additional top-loading layer with an inductive channel is employed for tuning the tag resonant frequency. Here, a lumped inductor is embedded into the channel for achieving arbitrary tuning capability in a wide range. Furthermore, it was found that the top-loading patch can enhance the electric fields of the dipolar patch, and the inductive channel can be used to adjust the current flows of the loading patch. The proposed tag antenna with a lumped inductor (2 nH) in the inductive channel of the top-loading patch was fabricated and tested. Results have shown that the operating frequency of the prototype can change steadily with 9 MHz/nH, achieving good realized gain across a very wide bandwidth. This is because the bowtie patch structure can be kept intact without any modification, making the antenna to have good radiation performance. The maximum read distance on metal plate can achieve nearly 19

m at an effective isotropic radiated power of 3.28 W. At the same time, the proposed antenna is found to be insensitive to variation in the backing metal object.

The second tag design is also developed from a dipolar patch. Now, the proposed antenna is fed by two T-shaped coplanar feedlines. One pair of capacitors with 0.6 pF has been inserted across the narrow gap between the patches for introducing additional capacitance. It has successfully brought down the resonant frequency and miniaturized the antenna size. When the capacitors are incorporated into the tag, which has a size of 35 mm × 30 mm × 3 mm, the tag resonant frequency can be drastically reduced from 1220 MHz to 915.5 MHz. Since the radiator of the tag is intact, it has good radiation efficiency. When the prototype is placed on the center of a 20 cm × 20 cm aluminum plate, it can be detected from about 11.1 meters using an effective isotropic radiated power of 3.28 W. Even though the antenna size is small, the tag can still maintain good reading performance.

To conclude, the objectives of my projects have been achieved. First of all, both tag designs have successfully utilized lumped elements to increase their antenna impedance, so that the tag resonant frequency can be effectively brought down to the UHF passband. The tag size is compact and electrically small. Secondly, the tags have been successfully designed using the soft substrates. They can be mounted on curved metal objects. Although the proposed tags are compact, their antenna radiators are intact and frequency tuning can be conducted without modifying the antenna structures. As a result, the radiation

performances are good.

5.2 Future Works

The proposed tag antenna structures can be easily implemented using the low temperature co-fired ceramic (LTCC) technology in the future. With the availability of LTCC materials with high dielectric constant and low loss, the tag footprint can be scaled down significantly. The LTCC technology will also enable easy integration with other sensors. This will make the tag antenna to become a useful multi-functional device.

REFERENCES

- Babar, A. A., Bjorninen, T., Bhagavati, V., Sydanheimo, L., Kallio, P. & Ukkonen, L. 2012. Small and flexible metal mountable passive UHF RFID tag on high-dielectric polymer-ceramic composite substrate. *IEEE Antennas and Wireless Propagation Letters*, 11, 1319-1322.
- Bekkali, A., Zou, S., Kadri, A., Crisp, M. & Pentty, R. V. 2014. Performance analysis of passive UHF RFID systems under cascaded fading channels and interference effects. *IEEE Transactions on Wireless communications*, 14, 1421-1433.
- Best, S. R. 2004. Improving the performance properties of a dipole element closely spaced to a PEC ground plane. *IEEE Antennas and Wireless Propagation Letters*, 3, 359-363.
- Bhaskar, S. & Singh, A. K. Capacitive tip loaded linearly tapered meander line antenna for UHF RFID tag applications. 2017 IEEE Applied Electromagnetics Conference (AEMC), 2017. IEEE, 1-2.
- Bong, F.-L., Lim, E.-H. & Lo, F.-L. 2016. Flexible folded-patch antenna with serrated edges for metal-mountable UHF RFID tag. *IEEE Transactions on Antennas and Propagation*, 65, 873-877.
- Bong, F.-L., Lim, E.-H. & Lo, F.-L. 2017. Miniaturized dipolar patch antenna with narrow meandered slotline for UHF tag. *IEEE Transactions on Antennas and Propagation*, 65, 4435-4442.
- Casula, G. A., Michel, A., Nepa, P., Montisci, G. & Mazzarella, G. 2016. Robustness of wearable UHF-band PIFAs to human-body proximity. *IEEE Transactions on Antennas and Propagation*, 64, 2050-2055.
- Chakravarty, S. & Mitra, R. 2003. Design of a frequency selective surface (FSS) with very low cross-polarization discrimination via the parallel micro-genetic algorithm (PMGA). *IEEE Transactions on Antennas and Propagation*, 51, 1664-1668.
- Chang, C.-H. & Wong, K.-L. 2009. Printed $\lambda/8$ -PIFA for Penta-Band WWAN Operation in the Mobile Phone. *IEEE Transactions on Antennas and Propagation*, 57, 1373-1381.
- Chawla, V. & Ha, D. S. 2007. An overview of passive RFID. *IEEE Communications Magazine*, 45, 11-17.
- Chen, H.-D., Tsai, C.-H. & Kuo, C. 2016. Compact circularly polarized meandered-loop antenna for UHF-band RFID tag. *IEEE Antennas and Wireless Propagation Letters*, 15, 1602-1605.

- Chen, H.-D. & Tsao, Y.-H. 2010a. Low-profile meandered patch antennas for RFID tags mountable on metallic objects. *IEEE Antennas and Wireless Propagation Letters*, 9, 118-121.
- Chen, H.-D. & Tsao, Y.-H. 2010b. Low-profile PIFA array antennas for UHF band RFID tags mountable on metallic objects. *IEEE Transactions on Antennas and Propagation*, 58, 1087-1092.
- Chen, Y.-S., Chen, S.-Y. & Li, H.-J. 2011. A novel dual-antenna structure for UHF RFID tags. *IEEE Transactions on Antennas and Propagation*, 59, 3950-3960.
- Dobkin, D. M. & Weigand, S. M. Environmental effects on RFID tag antennas. *IEEE MTT-S International Microwave Symposium Digest*, 2005. 135-138.
- Erman, F., Hanafi, E., Lim, E.-H., Wan Mohd Mahyiddin, W. A., Harun, S. W., Umair, H., Soboh, R. & Makmud, M. Z. H. 2019. Miniature compact folded dipole for metal mountable UHF RFID tag antenna. *Electronics*, 8, 713.
- Feresidis, A. P., Goussetis, G., Wang, S. & Vardaxoglou, J. C. 2005. Artificial magnetic conductor surfaces and their application to low-profile high-gain planar antennas. *IEEE Transactions on Antennas and Propagation*, 53, 209-215.
- Gao, B. & Yuen, M. M. 2011. Passive UHF RFID packaging with electromagnetic band gap (EBG) material for metallic objects tracking. *IEEE Transactions on Components, Packaging and Manufacturing Technology*, 1, 1140-1146.
- Genovesi, S. & Monorchio, A. 2010. Low-profile three-arm folded dipole antenna for UHF band RFID tags mountable on metallic objects. *IEEE Antennas and Wireless Propagation Letters*, 9, 1225-1228.
- Girbau, D., Lorenzo, J., Lazaro, A. & Villarino, R. Effects of antenna detuning and gain penalty on the read range of UHF RFID. *European Workshop on Smart Objects: Systems, Technologies and Applications*, 2010. VDE, 1-7.
- Goussetis, G., Feresidis, A. P. & Vardaxoglou, J. C. 2006. Tailoring the AMC and EBG characteristics of periodic metallic arrays printed on grounded dielectric substrate. *IEEE Transactions on Antennas and Propagation*, 54, 82-89.
- Greenhouse, H. 1974. Design of planar rectangular microelectronic inductors. *IEEE Transactions on parts, hybrids, and packaging*, 10, 101-109.
- Hamani, A., Yagoub, M. C., Vuong, T.-P. & Touhami, R. 2016. A novel broadband antenna design for UHF RFID tags on metallic surface environments. *IEEE Antennas and Wireless Propagation Letters*, 16, 91-94.
- Hirvonen, M., Pursula, P., Jaakkola, K. & Laukkanen, K. 2004. Planar inverted-F antenna for radio frequency identification. *Electronics Letters*, 40, 848-850.

Jain, A. K., Flynn, P. & Ross, A. A. 2007. *Handbook of biometrics*, Springer Science & Business Media.

Kim, D. & Yeo, J. 2008. Low-profile RFID tag antenna using compact AMC substrate for metallic objects. *IEEE Antennas and Wireless Propagation Letters*, 7, 718-720.

Kim, D. & Yeo, J. 2010. A passive RFID tag antenna installed in a recessed cavity in a metallic platform. *IEEE Transactions on Antennas and Propagation*, 58, 3814-3820.

Kim, D. & Yeo, J. 2012. Dual-band long-range passive RFID tag antenna using an AMC ground plane. *IEEE Transactions on Antennas and Propagation*, 60, 2620-2626.

Kim, J.-S., Choi, W. & Choi, G.-Y. 2008. UHF RFID tag antenna using two PIFAs embedded in metallic objects. *Electronics Letters*, 44, 1181-1182.

Koo, T.-W., Kim, D., Ryu, J.-I., Seo, H.-M., Yook, J.-G. & Kim, J.-C. 2011. Design of a label-typed UHF RFID tag antenna for metallic objects. *IEEE Antennas and wireless propagation letters*, 10, 1010-1014.

Kopyt, P., Salski, B., Olszewska-Placha, M., Janczak, D., Sloma, M., Kurkus, T., Jakubowska, M. & Gwarek, W. 2016. Graphene-based dipole antenna for a UHF RFID tag. *IEEE Transactions on Antennas and Propagation*, 64, 2862-2868.

Lee, S.-R., Lim, E.-H., Bong, F.-L. & Chung, B.-K. 2018a. Slotted folded patch antenna with double-T-slots for platform-insensitive UHF tag design. *IEEE Transactions on Antennas and Propagation*, 67, 670-675.

Lee, Y.-H., Lim, E.-H., Bong, F.-L. & Chung, B.-K. 2018b. Compact folded C-shaped antenna for metal-mountable UHF RFID applications. *IEEE Transactions on Antennas and Propagation*, 67, 765-773.

Lee, Y.-H., Lim, E.-H., Bong, F.-L. & Chung, B.-K. 2018c. Folded antipodal dipole for metal-mountable UHF tag design. *IEEE Transactions on Antennas and Propagation*, 66, 5698-5705.

Lee, Y.-H., Moh, C.-W., Lim, E.-H., Bong, F.-L. & Chung, B.-K. 2019. Miniature folded patch with differential coplanar feedline for metal mountable UHF RFID tag. *IEEE Journal of Radio Frequency Identification*, 4, 93-100.

Li, X., Gao, G., Zhu, H., Li, Q., Zhang, N. & Qi, Z. 2020. UHF RFID tag antenna based on the DLS-EBG structure for metallic objects. *IET Microwaves, Antennas & Propagation*, 14, 567-572.

Lin, K.-H., Chen, S.-L. & Mittra, R. 2012. A looped-bowtie RFID tag antenna design for metallic objects. *IEEE Transactions on Antennas and Propagation*,

61, 499-505.

Liu, L., Liu, C., Li, Z., Yin, X. & Chen, Z. N. 2018. Slit-slot line and its application to low cross-polarization slot antenna and mutual-coupling suppressed tripolarized MIMO antenna. *IEEE Transactions on Antennas and Propagation*, 67, 4-15.

Marrocco, G. 2003. Gain-optimized self-resonant meander line antennas for RFID applications. *IEEE Antennas and Wireless propagation letters*, 2, 302-305.

Marrocco, G. 2008. The art of UHF RFID antenna design: Impedance-matching and size-reduction techniques. *IEEE antennas and propagation magazine*, 50, 66-79.

Michel, A., Franchina, V., Nepa, P. & Salvatore, A. 2018. A UHF RFID tag embeddable in small metal cavities. *IEEE Transactions on Antennas and Propagation*, 67, 1374-1379.

Moh, C.-W., Lim, E.-H., Bong, F.-L. & Chung, B.-K. 2018. Miniature coplanar-fed folded patch for metal mountable UHF RFID tag. *IEEE Transactions on Antennas and Propagation*, 66, 2245-2253.

Ng, W.-H., Lim, E.-H., Bong, F.-L. & Chung, B.-K. 2018. E-shaped folded-patch antenna with multiple tuning parameters for on-metal UHF RFID tag. *IEEE Transactions on Antennas and Propagation*, 67, 56-64.

Ng, W.-H., Lim, E.-H., Bong, F.-L. & Chung, B.-K. 2019. Compact planar inverted-S antenna with embedded tuning arm for on-metal UHF RFID tag design. *IEEE Transactions on Antennas and Propagation*, 67, 4247-4252.

Niew, Y.-H., Lee, K.-Y., Lim, E.-H., Bong, F.-L. & Chung, B.-K. 2019. Patch-loaded semicircular dipolar antenna for metal-mountable UHF RFID tag design. *IEEE Transactions on Antennas and Propagation*, 67, 4330-4338.

Nikitin, P. V. & Rao, K. S. 2006. Theory and measurement of backscattering from RFID tags. *IEEE Antennas and Propagation Magazine*, 48, 212-218.

NXP. 2020. *UCODE 8/8m* [Online]. Available: <https://www.nxp.com/docs/en/data-sheet/SL3S1205-15-DS.pdf>. [Accessed Jan 2020].

Park, I.-Y. & Kim, D. 2014. Artificial magnetic conductor loaded long-range passive RFID tag antenna mountable on metallic objects. *Electronics letters*, 50, 335-336.

Payne, A. 2017. *The ac Resistance of Rectangular Conductors* [Online]. Available: <http://g3rbj.co.uk/wp-content/uploads/2017/06/Theac-Resistance-of-Rectangular-Conductors-Payne-Issue-3.pdf>. [Accessed].

- Rao, K. S., Nikitin, P. V. & Lam, S. F. 2005a. Antenna design for UHF RFID tags: A review and a practical application. *IEEE Transactions on antennas and propagation*, 53, 3870-3876.
- Rao, K. S., Nikitin, P. V. & Lam, S. F. Impedance matching concepts in RFID transponder design. Fourth IEEE Workshop on Automatic Identification Advanced Technologies (AutoID'05), 2005b. IEEE, 39-42.
- Rasilainen, K., Ilvonen, J. & Viikari, V. 2014. Antenna matching at harmonic frequencies to complex load impedance. *IEEE Antennas and Wireless Propagation Letters*, 14, 535-538.
- Reed, S., Desclos, L., Terret, C. & Toutain, S. 2001. Patch antenna size reduction by means of inductive slots. *Microwave and Optical Technology Letters*, 29, 79-81.
- Ripin, N., Lim, E.-H., Bong, F.-L. & Chung, B.-K. 2020. Miniature folded dipolar patch with embedded AMC for metal mountable tag design. *IEEE Transactions on Antennas and Propagation*, 68, 3525-3533.
- Rouse, C. D., Kurz, M. R., Petersen, B. R. & Colpitts, B. G. 2012. Performance evaluation of conductive-paper dipole antennas. *IEEE transactions on antennas and propagation*, 61, 1427-1430.
- Rowe, W. S. & Waterhouse, R. B. 2003. Theoretical investigation on the use of high permittivity materials in microstrip aperture stacked patch antennas. *IEEE Transactions on Antennas and Propagation*, 51, 2484-2486.
- Sanad, H. Effect of the shorting posts on short circuit microstrip antennas. Proceedings of IEEE Antennas and Propagation Society International Symposium and URSI National Radio Science Meeting, 1994. IEEE, 794-797.
- Sarkar, S. & Gupta, B. 2020. A dual-band circularly polarized antenna with a dual-band AMC reflector for RFID readers. *IEEE Antennas and Wireless Propagation Letters*, 19, 796-800.
- Sharma, A. & Shrivastava, S. Analysis of resonant frequency & quality factor of dielectric resonator at different dielectric constant materials. 2008 International Conference on Recent Advances in Microwave Theory and Applications, 2008. IEEE, 593-595.
- Shen, P., Zhang, W., Huang, L., Jin, D. & Xie, H. 2011. Improving the quality factor of an RF spiral inductor with non-uniform metal width and non-uniform coil spacing. *Journal of Semiconductors*, 32, 064011.
- Sievenpiper, D., Zhang, L., Broas, R. F., Alexopolous, N. G. & Yablonovitch, E. 1999. High-impedance electromagnetic surfaces with a forbidden frequency band. *IEEE Transactions on Microwave Theory and techniques*, 47, 2059-2074.

- Smith, A. D. & Offodile, F. 2002. Information management of automatic data capture: an overview of technical developments. *Information Management & Computer Security*.
- Virtanen, J., Björninen, T., Ukkonen, L. & Sydänheimo, L. 2010. Passive UHF inkjet-printed narrow-line RFID tags. *IEEE Antennas and Wireless Propagation Letters*, 9, 440-443.
- Virtanen, J., Virkki, J., Sydänheimo, L., Tentzeris, M. & Ukkonen, L. 2013. Automated identification of plywood using embedded inkjet-printed passive UHF RFID tags. *IEEE Transactions on Automation Science and Engineering*, 10, 796-806.
- Voyantic. 2012. *Tagformance Measurement System Manual 5* [Online]. Available: <https://voyantic.com/products/tagformance-pro> [Accessed 23 Feb. 2021].
- Warnagiris, T. J. & Minardo, T. J. 1998. Performance of a meandered line as an electrically small transmitting antenna. *IEEE Transactions on Antennas and Propagation*, 46, 1797-1801.
- White, G. R., Gardiner, G., Prabhakar, G. & Razak, A. A. 2007. A Comparison of Barcoding and RFID Technologies in Practice. *Journal of Information, Information Technology & Organizations*, 2.
- Yang, P. H., Li, Y., Jiang, L., Chew, W. & Ye, T. T. 2011. Compact metallic RFID tag antennas with a loop-fed method. *IEEE Transactions on Antennas and Propagation*, 59, 4454-4462.
- Zhang, J. & Long, Y. 2013a. A dual-layer broadband compact UHF RFID tag antenna for platform tolerant application. *IEEE Transactions on Antennas and Propagation*, 61, 4447-4455.
- Zhang, J. & Long, Y. 2013b. A miniaturized via-patch loaded dual-layer RFID tag antenna for metallic object applications. *IEEE Antennas and Wireless Propagation Letters*, 12, 1184-1187.
- Zhang, J. & Long, Y. 2014. A novel metal-mountable electrically small antenna for RFID tag applications with practical guidelines for the antenna design. *IEEE Transactions on Antennas and Propagation*, 62, 5820-5829.